SOLAR INFLUENCES ON CLIMATE

L. J. Gray,[1,2] J. Beer,[3] M. Geller,[4] J. D. Haigh,[5] M. Lockwood,[6,7] K. Matthes,[8,9] U. Cubasch,[8] D. Fleitmann,[10,11] G. Harrison,[12] L. Hood,[13] J. Luterbacher,[14] G. A. Meehl,[15] D. Shindell,[16] B. van Geel,[17] and W. White[18]

Received 5 January 2009; revised 23 April 2010; accepted 24 May 2010; published 30 October 2010.

[1] Understanding the influence of solar variability on the Earth's climate requires knowledge of solar variability, solar-terrestrial interactions, and the mechanisms determining the response of the Earth's climate system. We provide a summary of our current understanding in each of these three areas. Observations and mechanisms for the Sun's variability are described, including solar irradiance variations on both decadal and centennial time scales and their relation to galactic cosmic rays. Corresponding observations of variations of the Earth's climate on associated time scales are described, including variations in ozone, temperatures, winds, clouds, precipitation, and regional modes of variability such as the monsoons and the North Atlantic Oscillation. A discussion of the available solar and climate proxies is provided. Mechanisms proposed to explain these climate observations are described, including the effects of variations in solar irradiance and of charged particles. Finally, the contributions of solar variations to recent observations of global climate change are discussed.

Citation: Gray, L. J., et al. (2010), Solar influences on climate, *Rev. Geophys.*, *48*, RG4001, doi:10.1029/2009RG000282.

1. INTRODUCTION

[2] The Sun is the source of energy for the Earth's climate system, and observations show it to be a variable star. The term "solar variability" is used to describe a number of different processes occurring mostly in the Sun's convection zone, surface (photosphere), and atmosphere. A full understanding of the influence of solar variability on the Earth's climate requires knowledge of (1) the short- and long-term solar variability, (2) solar-terrestrial interactions, and (3) the mechanisms determining the response of the Earth's climate system to these interactions [*Rind*, 2002]. There have been substantial increases in our knowledge of each of these areas in recent years and renewed interest because of the importance of understanding and characterizing natural variability and its contribution to the observed climate change [*World Meteorological Organization*, 2007; *Intergovernmental Panel on Climate Change* (*IPCC*), 2007]. Correct attribution of past changes is key to the prediction of future change.

[3] *Herschel* [1801] was the first to speculate that the Sun's variations may play a role in the variability of the Earth's climate. This has been followed by a great number of papers that presented evidence [see, e.g., *Herman and Goldberg*, 1978; *National Research Council* (*NRC*), 1994; *Hoyt and Schatten*, 1997, and references therein], although many of the early investigations have been criticized on statistical grounds [*Pittock*, 1978]. Notwithstanding issues of statistical significance, many of these solar-climate

[1]National Centre for Atmospheric Science, Meteorology Department, University of Reading, Reading, UK.
[2]Now at National Centre for Atmospheric Sciences, Department of Atmospheric, Oceanic and Planetary Physics, University of Oxford, Oxford, UK.
[3]Swiss Federal Institute for Environmental Science and Technology, Dubendorf, Switzerland.
[4]Institute for Terrestrial and Planetary Atmosphere, State University of New York at Stony Brook, Stony Brook, New York, USA.
[5]Physics Department, Imperial College London, London, UK.
[6]Meteorology Department, University of Reading, Reading, UK.
[7]Also at Space Science Department, Rutherford Appleton Laboratory, Didcot, UK.
[8]Institut für Meteorologie, Freie Universität Berlin, Berlin, Germany.
[9]Now at Section 1.3: Earth System Modeling, Deutsches GeoForschungsZentrum Potsdam, Potsdam, Germany.
[10]Department of Geosciences, University of Massachusetts Amherst, Amherst, Massachusetts, USA.
[11]Now at Oeschger Centre for Climate Change Research and Institute of Geological Sciences, University of Bern, Bern, Switzerland.
[12]Department of Meteorology, University of Reading, Reading, UK.
[13]Lunar and Planetary Laboratory, University of Arizona, Tucson, Arizona, USA.
[14]Department of Geography, Justus Liebig University Giessen, Giessen, Germany.
[15]National Center for Atmospheric Research, Boulder, Colorado, USA.
[16]NASA Goddard Institute for Space Studies, New York, New York, USA.
[17]Institute for Biodiversity and Ecosystem Dynamics, Research Group Paleoecology and Landscape Ecology, Faculty of Science, Universiteit van Amsterdam, Amsterdam, Netherlands.
[18]Scripps Institution of Oceanography, University of California, San Diego, La Jolla, California, USA.

8755-1209/10/2009RG000282
Paper number 2009RG000282

associations also seemed highly improbable simply on the basis of quantitative energetic considerations. On average the Earth absorbs solar energy at the rate of $(1 - A)I_{TS}/4$, where A is the Earth's albedo and I_{TS} is the total solar irradiance (TSI), i.e., the total electromagnetic power per unit area of cross section arriving at the mean distance of Earth from the Sun (149,597,890 km). The factor of 4 arises since the Earth intercepts $\pi R_E^2 I_{TS}$ solar energy per unit time (where R_E is a mean Earth radius), but this is averaged over the surface area of the Earth sphere, $4\pi R_E^2$. TSI monitors show a clear 11 year solar cycle (SC) variation between sunspot minimum (S_{min}) and sunspot maximum (S_{max}) of about 1 W m^{-2} [*Fröhlich*, 2006]. Taking I_{TS} = 1366 W m^{-2} and A = 0.3, the solar power available to the Earth system is $(1 - A)I_{TS}/4$ = 239 W m^{-2} with an 11 year SC variation of ~0.17 W m^{-2}, or ~0.07%, a very small percentage of the total. Of greater importance to climate change issues are longer-term drifts in this radiative forcing. Recent estimates suggest a radiative forcing drift over the past 30 years associated with solar irradiance changes of 0.017 W m^{-2} decade^{-1} (see section 2). In comparison, the current rate of increase in trace greenhouse gas radiative forcing is about 0.30 W m^{-2} decade^{-1} [*Hofmann et al.*, 2008].

[4] We can estimate the impact at the surface of the 11 year SC variation in total solar radiation at the top of the atmosphere using the climate sensitivity parameter λ. This is defined by $\Delta T_S = \lambda \Delta F$, where ΔF is the change in forcing at the top of the atmosphere (in this case ~0.17 W m^{-2}) and T_S is the globally averaged surface temperature. Using a value of 0.5 K (W m^{-2})$^{-1}$ for λ [*IPCC*, 2007], we would expect the Earth's global temperature to vary by a mere 0.07 K. However, observations indicate, at least regionally, larger solar-induced climate variations than would be expected from this simple calculation, suggesting that more complicated mechanisms are required to explain them.

[5] Figure 1b shows a time series of sunspot number for the last three solar cycles, together with various other indicators of solar variation and a composite of satellite measurements of TSI. Sunspots appear as dark spots on the surface of the Sun and have temperatures as low as ~4200 K (in the central umbra) and ~5700 K (in the surrounding penumbra), compared to ~6050 K for the surrounding quiet photosphere. Sunspots typically last between several days and several weeks. They are regions with magnetic strengths thousands of times stronger than the Earth's magnetic field. Figure 1c shows a commonly used indicator of solar activity, the flux of 10.7 cm radio emissions from the Sun ($F_{10.7}$), which is highly correlated with the number of sunspots. This also correlates very highly with the core-wing ratio of the Mg ii line (Figure 1d), which is often taken as an index of solar UV variability. Additional indices include the open solar magnetic flux, F_S (Figure 1e), dragged out of the Sun because it is "frozen" into the solar wind; the galactic cosmic ray (GCR) count (Figure 1f); satellite-measured irradiance (Figure 1g); and the geomagnetic *Ap* index (Figure 1h). The flux of neutrons generated in the Earth's atmosphere by galactic cosmic rays (Figure 1f) is reduced by the cosmic ray effect of F_S and therefore varies in the opposite sense to the other indices. Despite the dark obscuring effect of sunspots, comparison of Figures 1b and 1g shows that the TSI (and its components, including the UV) is a maximum around the time when the number of sunspots is at its maximum. This is because the number of compensating smaller, much more numerous, brighter regions, called faculae, also peaks around sunspot maximum. These are less readily visible than sunspots because they are smaller, but they have a high surface temperature of ~6200 K near the edge of the solar disk (where they are brightest).

[6] Going back farther in time, various other proxy solar information is available [*Beer et al.*, 2006], as shown in Figure 2. The *aa* index is a measure of geomagnetic disturbance. It correlates well with both the neutron count rate and the irradiance and also shows good correspondence with the incidence of aurorae, as recorded by observers at middle magnetic latitudes [*Pulkkinen et al.*, 2001]. Higher solar irradiance, lower cosmic ray fluxes, greater geomagnetic activity, and higher incidence of lower-latitude aurorae all occur when solar activity is greater. Cosmogenic isotopes such as ^{10}Be are spallation products of GCRs impacting on atmospheric oxygen, nitrogen, and argon. The time series of ^{10}Be abundance stored in reservoirs such as ice sheets and ocean sediments and of ^{14}C from tree trunks show the 11 year cycle of the sunspot number. This makes sense physically since high sunspot numbers correspond to a strong solar magnetic field, which is the source of the field in the heliosphere that (by virtue of both its strength and its structure) shields the Earth from GCRs. However, geomagnetic activity, low-latitude aurorae, and cosmogenic isotopes all show additional variations that are not reflected by sunspot numbers. The reason for this is that at all minima of the solar cycle the sunspot number R returns close to zero, but the other indicators show that this does not mean the Sun returns to the same base level condition. As a result, there are drifts in solar activity on time scales of decades to centuries that, although reflected in the sunspot numbers at maxima of the solar cycle, are hardly seen in S_{min} sunspot numbers.

[7] These relationships have three important implications for Sun-climate relationships. One is that proxies for solar irradiance can be used to look for Sun-climate relationships in the period before direct observations of solar irradiance. Second, if we can get a good enough understanding of how the Sun's magnetic activity is related to solar irradiance, we can reconstruct the historical variations of the solar irradiance with confidence. Third, as we gain an increasing ability to simulate and predict solar magnetic behavior, we may gain an increasing ability to predict solar irradiance behavior and its effects on the Earth's climate. These reconstructions of solar variability are discussed in more detail in section 2.

[8] A great number of papers have reported correlations between solar variability and climate parameters. One relatively early association was presented by *Eddy* [1976], who examined historical evidence of weather conditions in Europe back to the Middle Ages, including the severity of winters in London and Paris, and suggested that during

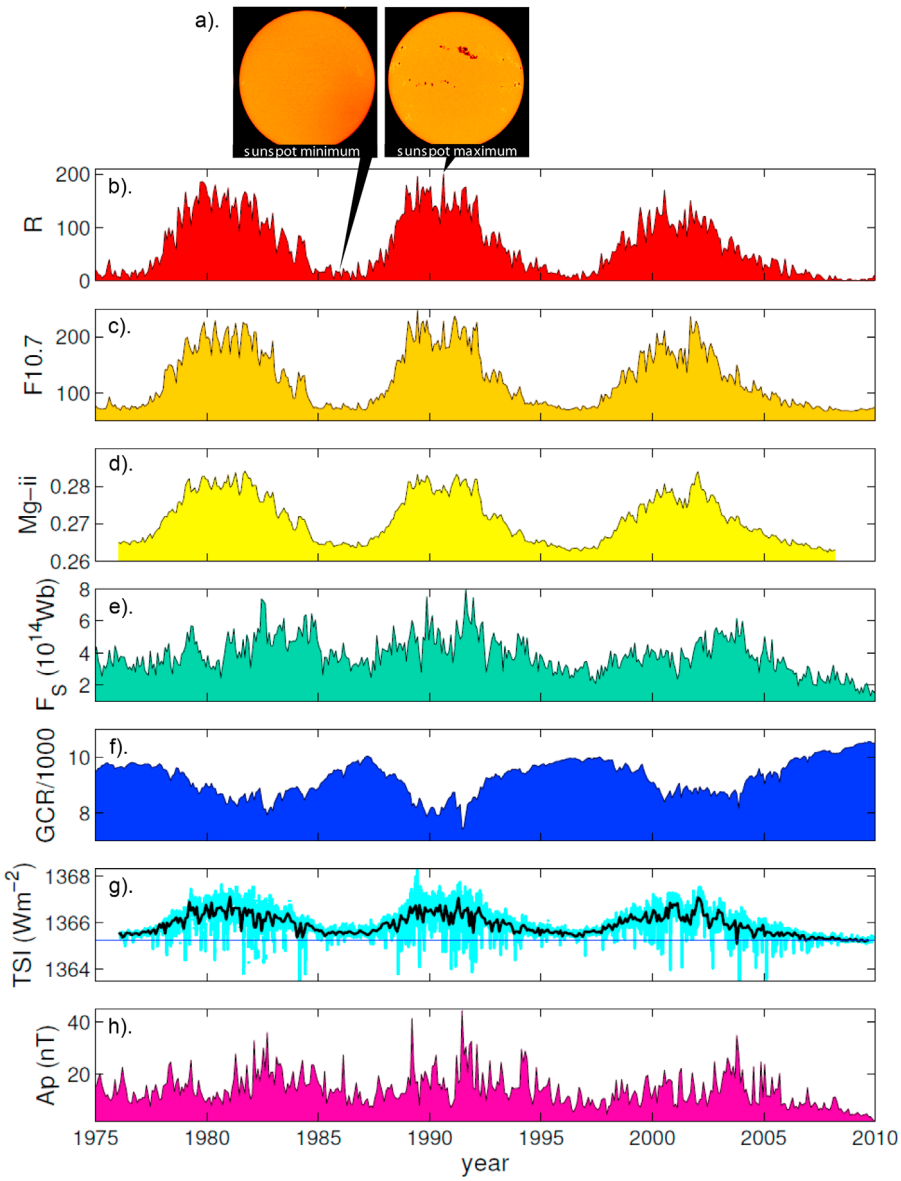

Figure 1. (a) Images of the Sun at sunspot minimum and sunspot maximum. Observed variations of (b) the sunspot number R (a dimensionless weighted mean from a global network of solar observatories, given by $R = 10N + n$, where N is the number of sunspot groups on the visible solar disk and n is the number of individual sunspots); (c) the 10.7 cm solar radio flux, $F_{10.7}$ (in W m^{-2} Hz^{-1}, measured at Ottawa, Canada); (d) the Mg ii line (280 nm) core-to-wing ratio (a measure of the amplitude of the chromospheric Mg II ion emission, which on time scales up to the solar cycle length has been found to be correlated with solar UV irradiance at 150–400 nm); (e) the open solar flux F_S derived from the observed radial component of interplanetary field near Earth; (f) the GCR counts per minute recorded by the neutron monitor at McMurdo, Antarctica; (g) the PMOD composite of TSI observations; and (h) the geomagnetic *Ap* index. All data are monthly means except the light blue line in Figure 1g, which shows daily TSI values. (Updated from *Lockwood and Fröhlich* [2007].)

times of few or no sunspots, e.g., during the Maunder Minimum (~1645–1715), the Sun's radiative output was reduced, leading to a colder climate. Although many of the early reported relationships between solar variability and climate have been questioned on statistical grounds, some correlations have been found to be more robust, and the addition of more years of data has confirmed their significance. In what was the start of a series of classic papers, *Labitzke* [1987] and *Labitzke and van Loon* [1988] suggested that while a direct influence of solar activity on temperatures in the stratosphere (~10–50 km) was hard to see, an influence became apparent when the winters were grouped according to the phase of the quasi-biennial oscillation (QBO). The QBO is an approximately 2 year oscillation of easterly and westerly zonal winds in the equatorial lower stratosphere [*Baldwin et al.*, 2001; *Gray*, 2010]. Labitzke's initial study used data for the period 1958–1986. It is very convincing that this relationship still continues to

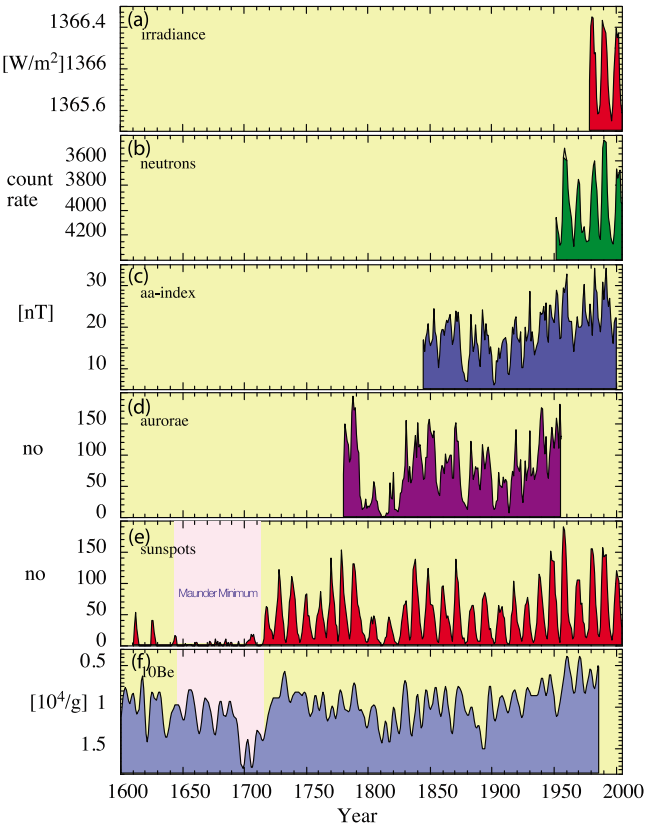

Figure 2. (a) Total solar irradiance (W m^{-2}); (b) galactic cosmic ray neutron count (counts per minute) as seen at Climax, Colorado; (c) *aa* index (nT); (d) incidence of low-latitude aurorae (number per year); (e) sunspot number; and (f) ^{10}Be concentrations (10^4 g^{-1}) as functions of time (reprinted from *Beer et al.* [2006] with kind permission of Springer Science and Business Media). Note that the scales for neutron flux and ^{10}Be have been inverted.

hold for the extended period 1942–2008 (i.e., with the addition of data from a further four solar cycles). Many other relationships between proxies for solar activity and climate have been noted, including variations in ozone, temperatures, winds, clouds, precipitation, and modes of variability such as the monsoons and the North Atlantic Oscillation (NAO). More details of these are provided in section 3.

[9] Mechanisms proposed to explain the climate response to very small solar variations can be grouped broadly into two categories. The first involves a response to variations in solar irradiance. Figure 3 (top) shows the spectral irradiance, *I*, which is the power arriving at the Earth per unit area, per unit wavelength. TSI is the integral of *I* over all wavelengths contributing significant power. Almost all of the incoming irradiance at the top of the Earth's atmosphere (black line) is in the ultraviolet, visible, and infrared regions, and approximately half of this radiation penetrates the atmosphere and is absorbed at the surface (blue line). Variations in the direct absorption of TSI by oceans are likely to be significant because of the large oceanic heat capacity, which can therefore "integrate" long-term, small variations in heat input. Additionally, some of the radiation is absorbed in the atmosphere, primarily by tropospheric water vapor in several wavelength bands and by stratospheric ozone in the UV region, which gives rise to the sharp drop in the blue curve near 300 nm.

[10] Although the UV absorption composes only a small proportion of the total incoming solar energy, it has a relatively large 11 year SC variation, as shown in Figure 3 (bottom). Variations of up to 6% are present near 200 nm where oxygen dissociation and ozone production occur and up to 4% in the region 240–320 nm where absorption by stratospheric ozone is prevalent. This compares with variations of only ~0.07% in TSI (see earlier discussion). Figure 3 also shows the approximate height in the atmosphere at which these wavelengths are absorbed. At very short wavelengths (~100 nm) the variations are ~100% and impact temperatures very high in the atmosphere. For

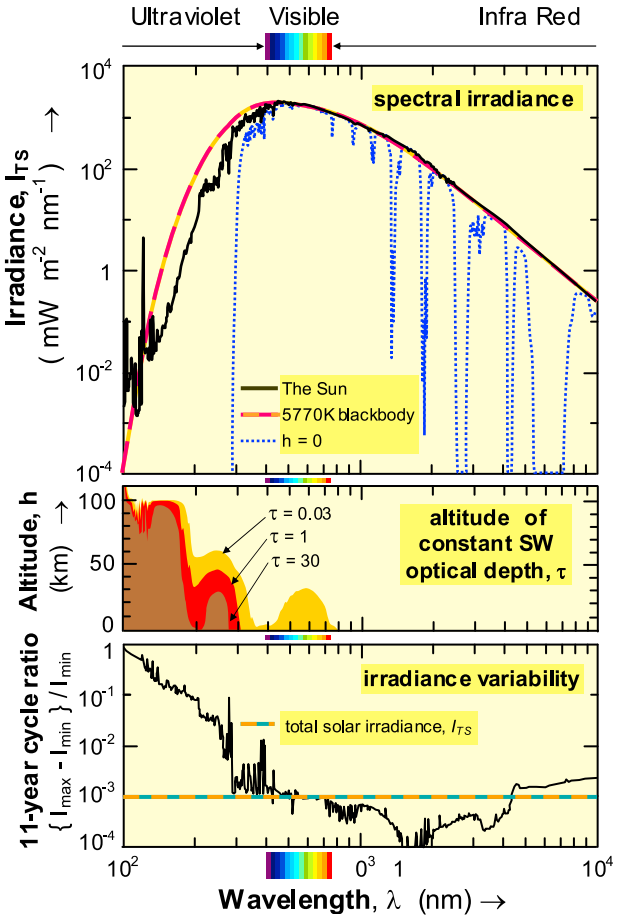

Figure 3. (top) Spectrum of solar irradiance, *I*, compared with that of a 5770 K blackbody radiator [after *Lean*, 1991]. The blue dotted line shows the spectrum of radiation reaching the surface of the Earth. (middle) Indicator of altitude of penetration of shortwave solar radiation for three different smoothed optical depths. (bottom) Spectral variability of the irradiance, defined as the difference between the S_{max} and S_{min} values, as a ratio of the S_{min} value, based on the last two solar cycles. The horizontal dashed line gives the corresponding value for the total solar irradiance, I_{TS}, i.e., the integral over all wavelengths.

example, the Earth's exosphere (~500–1000 km above the Earth's surface) has 11 year SC variations of ~1000 K. However, we concentrate in this review on describing observations and mechanisms that involve the atmosphere below 100 km because at present there is little evidence to suggest a downward influence on climate from regions above this. Transfer mechanisms from the overlying thermosphere have been proposed, such as through wave propagation feedbacks suggested by *Arnold and Robinson* [2000]. However, there is little observational evidence for any significant influence, although this cannot be ruled out.

[11] At stratospheric heights Figure 3 shows a variation of ~6% at UV wavelengths over the SC. This region of the atmosphere has the potential to affect the troposphere immediately below it and hence the surface climate. Estimated stratospheric temperature changes associated with the 11 year SC show a signal of ~2 K over the equatorial stratopause (~50 km) with a secondary maximum in the lower stratosphere (20–25 km [see, e.g., *Frame and Gray*, 2010]). The direct effect of irradiance variations is amplified by an important feedback mechanism involving ozone production, which is an additional source of heating [*Haigh*, 1994; see also *Gray et al.*, 2009]. The origins of the lower stratospheric maximum and the observed signal that penetrates deep into the troposphere at midlatitudes are less well understood and require feedback/transfer mechanisms both within the stratosphere and between the stratosphere and underlying troposphere, further details of which are provided in section 4.

[12] The second mechanism category involves energetic particles, including solar energetic particle (SEP) events and GCRs. Low-energy (thermal) solar wind particles modulate the thermosphere above 100 km via both particle precipitation and induced ionospheric currents. Whereas it is longer-wavelength (lower-energy) photons that deposit their energy in the upper atmospheric layers, it is the more energetic particle precipitations that penetrate to lower altitudes. SEPs are generated at the shock fronts ahead of major solar magnetic eruptions and penetrate the Earth's geomagnetic field over the poles where they enter the thermosphere, mesosphere, and, on rare occasions, the stratosphere. A large fraction of SEP ions are protons (so events are also referred to as "solar proton events" (SPEs)), but they are accompanied by a wide spectrum of heavier ions [e.g., *Reames*, 1999]. All cause ionization, dissociation, and the production of odd hydrogen and odd nitrogen species that can catalytically destroy ozone [e.g., *Solomon et al.*, 1982; *Jackman et al.*, 2008].

[13] The idea that cosmic ray changes could directly influence the weather originated with *Ney* [1959]. Although admitting to some skepticism, *Dickinson* [1975] considered that modulation of GCR fluxes into the atmosphere by solar activity might affect cloudiness and hence might be a viable Sun-climate mechanism. For instance, during S_{min}, the GCR flux is enhanced, increasing atmospheric ion production. Dickinson discussed ion-induced formation of sulphate aerosol (which can act as efficient cloud condensation nuclei (CCN)) as a possible route by which the atmospheric ion changes could influence cloudiness. A further GCR-cloud link has been proposed through the global atmospheric electric circuit [e.g., *Tinsley*, 2000]. The global circuit causes a vertical current density in fair (nonthunderstorm) weather, flowing between the ionosphere and the surface. This fair weather current density passes through stratiform clouds causing local droplet and aerosol charging at their upper and lower boundaries. Charging modifies the cloud microphysics, and hence, as the current density is modulated by cosmic ray ion production, the global circuit provides a possible link between solar variability and clouds.

[14] While the testing of solar influence on climate via changes in solar irradiance is relatively well advanced, the GCR cloud mechanisms have only just begun to be quantified. The connection between GCRs and CCN (the "ion-aerosol clear air" mechanism) has recently been tested in a climate model that calculates aerosol microphysics in response to GCR [*Pierce and Adams*, 2009]. They find that GCR-induced changes in CCN are 2 orders of magnitude too small to account for observed changes in cloud properties. Quite apart from the sign or amplitude of the GCR-cloud effects, the sign of the net effect on climate would also depend on the altitude of the cloud affected. For enhanced low-altitude cloud the dominant effect would be reflection of incoming shortwave solar radiation (a cooling effect). For enhanced high-altitude cloud, the dominant effect would be the trapping of reradiated, outgoing longwave radiation (a warming effect). Thus, if GCRs act to enhance low-altitude cloud, the enhanced fluxes would lead to cooler surface temperatures during S_{min} and enhanced surface temperatures during S_{max}. This temperature change therefore has the same sense as that which would arise from a direct modulation by TSI. Solar modulation of climate by any of the proposed mechanisms described above may result in associated changes in cloudiness, so that any observational evidence linking solar changes with cloud changes does not uniquely argue for a solar effect through cosmic rays [*Udelhofen and Cess*, 2001]. The current status of research into the various mechanisms is described in more detail in section 4.

[15] In the context of assessing the contribution of solar forcing to climate change, an important question is whether there has been a long-term drift in solar irradiance that might have contributed to the observed surface warming in the latter half of the last century. Reconstructions of past TSI variations have been employed in model studies and allow us to examine how the climate might respond to such imposed forcings. The direct effects of 11 year SC irradiance variations are relatively small at the surface and are damped by the long response time of the ocean-atmosphere system. However, model estimates of the response to centennial time scale irradiance variations are larger since the accumulated effect of small signals over long time periods would not be damped to the same extent as decadal-scale responses.

[16] There are also large uncertainties in estimates of long-term irradiance changes (see section 2). The proxy quantities are indicators of magnetic activity on the Sun, and there are problems relating these magnetic indicators to TSI.

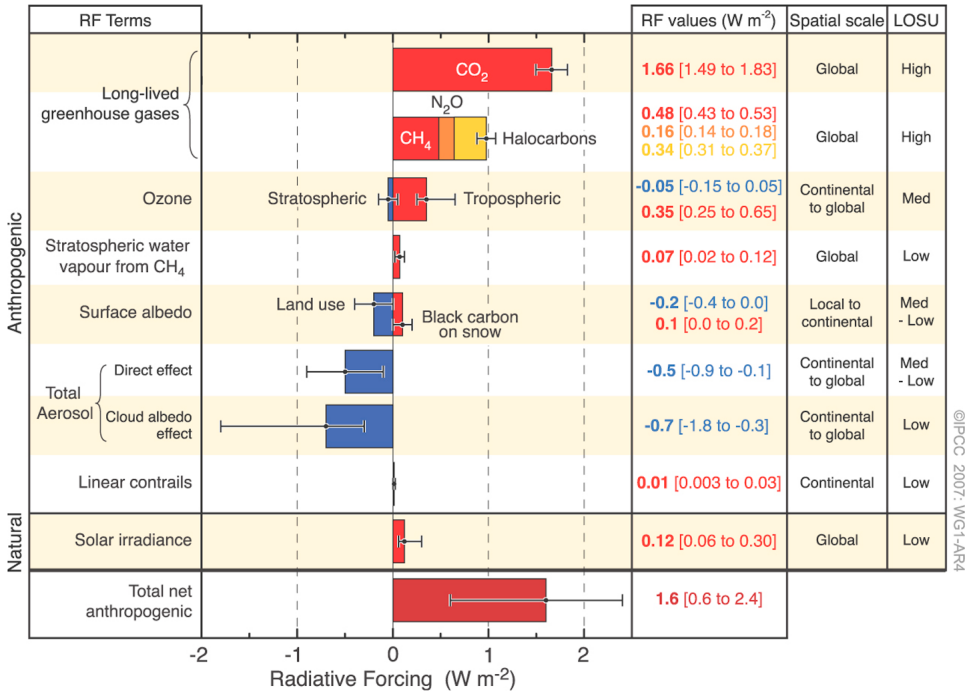

Figure 4. A comparison of the difference in radiative forcings from 1750 to 2005. LOSU, level of scientific understanding [from *IPCC*, 2007, Figure SPM.2].

For example, we know that TSI is greater at times of greater sunspot activity, but we do not know how much smaller the TSI was during extended periods when there were no sunspots, e.g., during the Maunder Minimum. However, the most recent minimum, between solar cycles 22 and 23, was unusually low and has provided a glimpse of what a grand minimum might look like.

[17] Recent estimates [*IPCC*, 2007] (see Figure 4) suggest that the most likely contribution from the Sun to the radiative forcing of climate change between 1750 (before the Industrial Revolution but at a time when solar activity was not much lower than today) and 2005 is 0.12 W m^{-2}, with an uncertainty between 0.06 and 0.30 W m^{-2}. This estimate is much smaller than the estimated total net anthropogenic contribution of 1.6 W m^{-2} (uncertainties of 0.6–2.4 W m^{-2}). However, the low level of scientific understanding of the solar influence is noted [*IPCC*, 2007]. The uncertainty is probably also underestimated because of the poorly resolved stratosphere in most of these models. Nevertheless, *IPCC* [2007] concludes that changes in the Sun have played a role in the observed warming of the Earth since 1750, but these changes are very small compared to the role played by increasing long-lived greenhouse gases in the atmosphere.

[18] The purpose of this review is to present up-to-date information on our knowledge of solar variability and its impact on climate and climate change, as an update to previous reviews such as that of *Hoyt and Schatten* [1997; see also *NRC*, 1994; *Calisesi et al.*, 2006]. Only solar processes on decadal or longer time scales are considered, although we acknowledge the possibility that short-term processes which occur repeatedly may lead to an integrated longer-term effect. For brevity, where authors have reported work in a series of publications, only the most recent is referenced, and the reader may access the earlier papers via these.

[19] In section 2, observations of solar variability are described, and the reconstruction of historical solar climate forcing is discussed. In section 3 we provide an overview of recent atmospheric observations that indicate a significant influence of the Sun's variations on the Earth's climate. Section 4 describes the mechanisms currently proposed that might account for these observed solar-related climate variations. Section 5 discusses solar variability in the context of understanding global climate change, and finally, concluding remarks and future directions are provided in section 6.

2. SOLAR VARIABILITY

[20] The Earth's heliographic latitude varies during the year, but by far the largest annual variation in TSI arises from the variation in the Earth-Sun distance. This varies by 3.3% (minimum-to-maximum) during the course of the year giving a 6.7% variation in TSI, i.e., 92 W m^{-2}. The observed TSI data in Figure 1g have been corrected by normalizing them to the mean heliocentric distance of Earth. The TSI observations show variations ranging from a few days up to the 11 year SC and also suggest a small drift on longer time scales, although instrument stability and intercalibration must be studied in detail before one can be confident that such drifts are real [*Lockwood and Fröhlich*, 2008]. The daily averages (in light blue in Figure 1g) show many large negative excursions lasting several days. These are caused by the passage of sunspot groups across the visible disc of the Sun and are more common, and of larger amplitude, at

S_{max}. The mean rotation period of the Sun as seen from Earth is 27 days, and so a sunspot group lasting several rotations can cause several of these negative excursions lasting almost 13 days each. On the other hand, the brightening effect of faculae is contributed by many small features that are more uniformly spread over the solar disc (but are brighter when seen closer to the limb). As a result, the faculae effects are less visible in solar rotations, and the main variation is the 11 year SC.

2.1. Causes of TSI Variability

[21] Recent research indicates that variability in total solar irradiance associated with the 11 year SC arises almost entirely from the distribution of sizes of the patches where magnetic field threads through the visible surface of the Sun (the photosphere). The advent of solar magnetographs, measuring the line-of-sight component of the photospheric field by exploiting the Zeeman effect, has revolutionized our understanding of how these vary over the SC [*Harvey*, 1992]. *Spruit* [2000], for example, has developed the theory of how these photospheric magnetic fields influence TSI. The dominant effect for large-diameter (greater than about 250 km) magnetic flux tubes is that they inhibit the convective upflow of energy to the surface and cause cool, dark sunspots with a typical temperature of $T_S \approx 5420$ K (averaged over umbral and penumbral areas) compared with the more typical value of the quiescent photospheric temperature of $T_{QS} \approx 6050$ K. The blocked energy is mainly returned to the convection zone which, because it has such a huge thermal capacity, is not perturbed. However, a small fraction of the blocked energy may move around the flux tube and enhance the surface intensity in a slightly brighter ring around the spot with effective photospheric temperature $T_{BR} \approx 6065$ K.

[22] The key difference between sunspots and the magnetic flux tubes called faculae is that the magnetic flux tube diameter is smaller for faculae. This allows the temperature inside smaller flux tubes to be maintained by radiation from the tube walls, and the enhanced magnetic pressure within the tube means that density is reduced in pressure equilibrium. This allows radiation to escape from lower, hotter layers in a facula, so that the effective temperature is in the region of $T_f \approx 6200$ K (see review by *Lockwood* [2004]). The additional brightness is greatest near the solar limb where more of the bright flux tube walls are visible [e.g., *Topka et al.*, 1997]. Because the ratio of the total areas of the Sun's surface covered by faculae and by sunspots has remained roughly constant over recent solar cycles [e.g., *Chapman et al.*, 2001] and because the net effect of faculae is approximately twice that of sunspots, the TSI is increased at S_{max} [*Foukal et al.*, 1991; *Lean*, 1991]. The facular contribution is made up of many smaller flux tubes, and hence, the net brightening they cause is a smoother variation in both time and space than the darkening effect of the less numerous but bigger sunspots.

[23] The variation of the effect of faculae is often quantified using emissions from the overlying bright regions in the chromosphere, the thin layer of the solar atmosphere immediately above the photosphere [e.g., *Fröhlich*, 2002]. These bright spots in the chromosphere are called plages, and they lie immediately above photospheric faculae. Their effect is thought to be quantified by the Mg ii line "core-to-wing" index (see Figure 1d). Faculae contribute to TSI increases whether they are around sunspots in active regions or in other regions of the Sun's surface [*Walton et al.*, 2003]. Sunspots and faculae are two extremes of a continuous distribution of flux tube sizes: at intermediate sizes, flux tubes form micropores which appear bright near the limb, like faculae, but dark near the center of the solar disk, like spots.

[24] An additional source of TSI and solar spectral irradiance (SSI) variability has been proposed. These are called "shadow" effects and are associated with magnetic fields below the photosphere in the convection zone (CZ) interrupting the upflow of energy [*Kuhn and Libbrecht*, 1991]. It is now thought that solar magnetic field is generated and stored just below the CZ in an "overshoot layer" which extends into the radiation zone beneath (see reviews by *Lockwood* [2004, 2010]). This blocks upward heat flux, but the huge time constant of the CZ above it means that variations on time scales shorter than about 10^6 years would not be seen. The stored field can bubble up through the CZ (breaking through the surface in sunspots and faculae) in an interval of only about 1 month. Thus, it is thought that the flux below (but not threading) the photosphere, yet close enough to it to give shadow effects on decadal and centennial time scales, would be small. An interesting test of this may well be provided by the exceptionally low TSI values being observed at the time of writing (late 2009). If these are not fully explained by the loss of solar minimum faculae, we would need to invoke shadow and associated solar radius effects as well as the known effects of surface emissivity in sunspots and faculae.

2.2. Decadal-Scale Solar Variability

2.2.1. Total Solar Irradiance

[25] TSI has been monitored continuously from space since 1977. The individual TSI monitors have operated for only limited intervals so a combination of data from several different instruments is required to compile a continuous data set. This means that intercalibration of those instruments, and how they change with time as the instruments degrade, is a key issue in the compilation of a composite data set. There are many corrections that are needed [e.g., *Fröhlich*, 2006].

[26] Figures 5a–5c show a comparison of the three main TSI composites: Institut Royal Meteorologique Belgique (IRMB) [*Dewitte et al.*, 2004], Active Cavity Radiometer Irradiance Monitor (ACRIM) [*Willson and Mordvinov*, 2003], and Physikalisch-Meteorologisches Observatorium Davos (PMOD) [*Fröhlich*, 2006]. All three use time series of the early data from the Hickey-Frieden (HF) Radiometer instrument on the Nimbus 7 satellite and the ACRIM I and II instruments (on UARS and ACRIMsat, respectively) until early 1996. The IRMB composite is constructed by first referring all data sets to the Space Absolute Radiometric

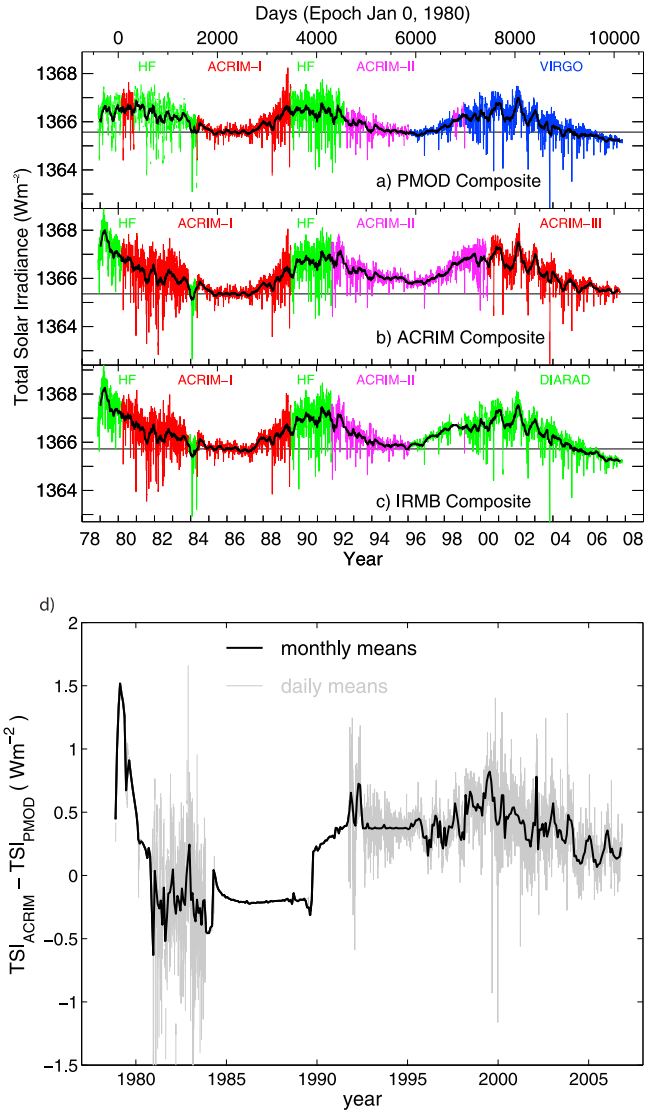

Figure 5. Composites of total solar irradiance 1978–2007: (a) PMOD (TSI_{PMOD}), (b) ACRIM (TSI_{ACRIM}), and (c) IRMB (TSI_{IRMB}). Colored lines show daily values, with color indicating the instrumental source. Thick black lines indicate 81 day running means. Horizontal black lines drawn through the minimum around 1985 (between solar cycles 21 and 22) to highlight the trends in minimum values of the composites. For each plot the bottom horizontal scale gives the year, and the top scale gives the day number, where day 1 is 1 January 1980. (d) Difference between the PMOD and ACRIM composites, $TSI_{PMOD} - TSI_{ACRIM}$. Grey line indicates daily values; black line indicates 81 day running means. During several intervals, the gray line is hidden behind the black line because the two composites employ data from the same instruments (but the difference is not zero as they apply different calibrations).

Reference [*Crommelynck et al.*, 1995], although this absolute calibration has recently been called into question because the Total Irradiance Monitor instrument on the SORCE satellite has obtained values about 5 W m^{-2} lower [*Kopp et al.*, 2005]. After 1996 the ACRIM composite continues to use ACRIM II supplemented by ACRIM III, whereas the PMOD composite uses data from the Variability of Solar Irradiance and Gravity Oscillations (VIRGO) instrument on the SoHO spacecraft (specifically the Differential Absolute Radiometer (DIARAD) and PM06 cavity radiometer data), and IRMB uses just the DIARAD VIRGO data. Besides the different time series used after 1996 (during solar cycle 23), the main difference is the way the data have been combined and corrected.

[27] The most significant difference between the PMOD, IRMB, and ACRIM composites is in their long-term trends. Figure 5d shows the largest and most significant disagreement, which is that between the PMOD and ACRIM composites [*Lean*, 2006; *Lockwood and Fröhlich*, 2008]. The rapid relative drift between the two before 1981 arises because although both employ the Nimbus HF data, ACRIM (like IRMB) has not used the reevaluation of the early degradation of the HF instrument. The second major difference is a step function change within what is termed the "ACRIM gap" between the loss of the ACRIM I instrument in mid-1989 and the start of the ACRIM II data late in 1991. Both the ACRIM and the PMOD composites use the Nimbus HF data for this interval as these are the best available data for this interval. The HF data series shows several sudden jumps attributable to changes in the orientation of the spacecraft and associated with switch-off and switch-on. PMOD makes allowance for such a jump in the ACRIM gap, but the ACRIM composite does not, which gives rise to the step change in late 1989 and accounts for virtually all of the difference between the long-term drifts of the two composites over the first two solar cycles [see *Fröhlich*, 2006; *Lockwood*, 2010, and references therein].

[28] Additional support for the inclusion of the glitch effect in the PMOD composite has recently come from an analysis of solar magnetogram data [*Wenzler et al.*, 2006]. In recent years, modeling has developed to the point where >93% of the TSI variation observed by the SoHO satellite has been reproduced by sorting pixels of the corresponding magnetograms into five photospheric surface classifications (sunspot umbra; sunspot penumbra; active region faculae; network faculae; and the quiet, field-free Sun). Each pixel is then assigned a time-independent spectrum for that classification on the basis of a model of the surface in question, as developed by *Unruh et al.* [1999]. From this and the disc location, the intensity can be estimated, and the TSI is computed by summation over the whole disc [*Krivova et al.*, 2003]. This work has further developed into the so-called four-component Spectral and Total Irradiance Reconstructions (SATIRE) model [*Solanki*, 2002; *Krivova et al.*, 2003]. Figure 6 shows a scatterplot of the daily TSI values for 1996–2002 derived by this method using magnetograms from the Michelson Doppler Interferometer (MDI) instrument on board the SoHO spacecraft, as a function of the simultaneous TSI value observed by the VIRGO instrument, also on SoHO. The agreement is exceptional: the correlation coefficient is 0.96, and the best fit linear regression (dashed mauve and orange line) is very close to ideal agreement (light blue). Recently, *Wenzler et al.* [2006] have extended this analysis to ground-based magnetograms. This is not

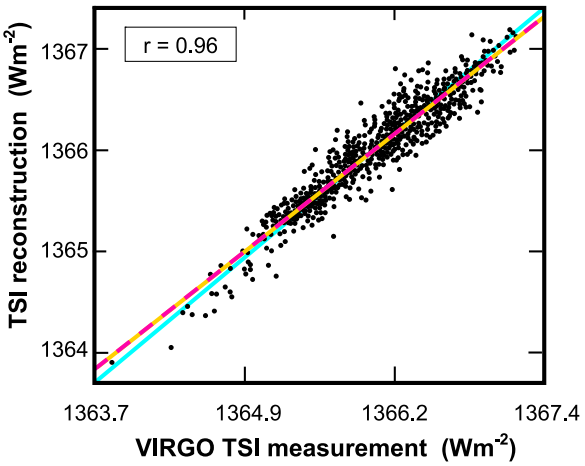

Figure 6. Scatterplot of daily values of TSI, as simulated from SoHO MDI magnetograms using the SATIRE procedure, as a function of the simultaneous value observed by the VIRGO instrument on SoHO. Data are for 1996–2002; correlation coefficient is 0.96. Dashed mauve and orange line indicates the best least squares linear regression fit; light blue line indicates the ideal line of perfect agreement.

trivial because additional factors such as (partial) cloud cover must be corrected for. The use of ground-based data is significant as it extends the interval which can be studied back to 1979 so that it covers the same interval as the ACRIM and PMOD composites (including the ACRIM gap).

[29] These TSI model reconstructions are so accurate that they provide a definitive test of the solar surface contribution to the various TSI composites. They confirm that unless shadow effects are significant, the PMOD composite is more accurate and that the ACRIM composite is in error because it fails to account for the Nimbus HF pointing anomaly during the ACRIM gap [*Lockwood and Fröhlich*, 2008]. Note that this conclusion does not depend on tuning the SATIRE model to the PMOD composite: the model has only one free fit parameter, and the glitch in the ACRIM gap cannot be matched even if the ACRIM composite is used to tune the model.

[30] To understand the implications of this correction, note that in Figures 5a and 5b the PMOD composite gives a decline in TSI since 1985 [*Lockwood and Fröhlich*, 2007], whereas the ACRIM composite gives a rise up until 1996 and a fall since then [*Lockwood*, 2010]. The difference arises entirely from the pointing direction glitch during the ACRIM gap. The PMOD composite trend matches that in the sunspot number, whereas the ACRIM composite trend matches that in the galactic cosmic ray counts. Hence, the long-term trend in the PMOD composite is in the same direction as the solar cycle variation, whereas the ACRIM composite trend is in the opposite direction (remember that TSI peaks at sunspot maximum when the GCR flux is a minimum). To explain this inconsistency of the ACRIM composite would require two competing effects in the relationship between TSI and GCR fluxes that work in opposite directions, such that the TSI and GCR fluxes are anticorrelated on time scales of the 11 year SC and shorter, yet are correlated on time scales longer than the 11 year SC. The PMOD TSI data have fallen to unprecedentedly low levels during the current solar minimum, although estimates vary on the magnitude of this decline [*Lockwood*, 2010]. The mean of the PMOD TSI composite for September 2008 is 1365.1 W m^{-2}, which is lower than that for the previous minimum by more than 0.5 W m^{-2}.

2.2.2. Spectral Irradiance

[31] Measurements of SSI were made by the Solar Stellar Irradiance Comparison Experiment and Solar UV Spectral Irradiance instruments on the UARS satellite in the 1980s and 1990s. They revealed variations of the order of a few percent in the near UV over an 11 year SC. The launch of the SORCE satellite in 2003 carrying the Spectral Irradiance Monitor (SIM) has provided the first measurements of SSI across the whole spectrum from X-ray to near IR. The measurements suggest that over the declining phase of the solar cycle between 2004 and 2007 there was a much larger (factor of 4–6) decline in UV than indicated in Figure 3, and this is partially compensated in the TSI variation by an increase in radiation at visible wavelengths [*Harder et al.*, 2009]. These observed changes to the shape of the solar spectrum variations were completely unexpected, and if correct they will require the associated temperature and ozone responses to be reassessed (see also sections 4.2.1 and 5).

[32] For longer time periods, reconstructions of SSI can be made using multicomponent models. For example, the SATIRE modeling concept can be applied independently to different spectral wavelengths, and so the variability within the irradiance spectrum can be estimated. The main requirement is that the contrasts of the different types of solar surface be known at each wavelength [*Unruh et al.*, 2008]. Work at present is aimed at improving our knowledge of the short UV wavelengths, which is required for accurate modeling of irradiance absorption in the stratosphere and upper atmosphere (see Figure 3). Improvements made to date suggest that UV irradiance during the Maunder Minimum was lower by as much as a factor of 2 at and around the Ly-α wavelength (121.6 nm) compared to recent S_{min} periods and up to 5%–30% lower in the 150–300 nm region [*Krivova and Solanki*, 2005]. However, this work is still in its infancy. The model estimates match observed spectra between 400 and 1300 nm very well but begin to fail below 220 nm and also for some of the strong spectral lines.

[33] Interestingly, the large change observed by the SORCE SIM instrument was not reflected in TSI, the Mg ii index, $F_{10.7}$, nor existing models of the UV variation. The implications are not yet clear, but these recent data open up the possibility that long-term variability of the part of the UV spectrum relevant to ozone production is considerably larger in amplitude and has a different temporal variation compared with the commonly used proxy solar indices (Mg ii index, $F_{10.7}$, sunspot number, etc.) and reconstructions.

2.3. Century-Scale Solar Variability

[34] Apart from a few isolated naked eye observations by ancient Chinese and Korean astronomers, sunspot data

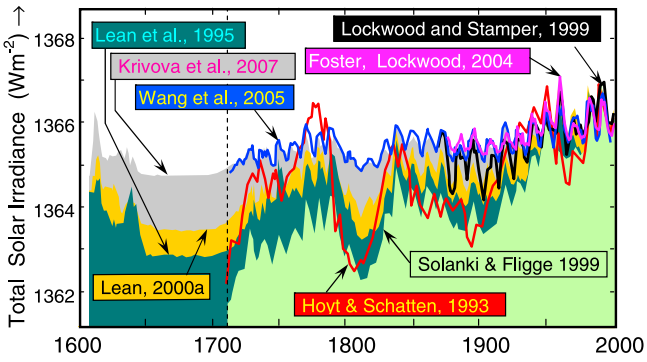

Figure 7. Reconstructions of past variations in TSI using different solar proxies. *Hoyt and Schatten* [1993] estimates are based on solar cycle length, *L*. *Solanki and Fligge* [1999, 2000] used the annual sunspot number, *R* (available back to 1713, dashed line). *Lean et al.* [1995] and *Lean* [2000a] used a combination of the group sunspot number R_G (available back to 1611) and its 11 year running mean. In these early reconstructions, the amplitude of the slowly varying component was derived by comparison of the modern-day Sun and Maunder Minimum Sun with distributions of cyclic and noncyclic Sun-like stars. *Lockwood and Stamper* [1999] used the observed, but unexplained, correlation between the variations of TSI and the open coronal source flux on decadal time scales [*Lockwood*, 2002]. *Wang et al.* [2005] used a solar magnetic flux transport model constrained to fit the observed open solar flux variation [*Lockwood et al.*, 1999]: the prediction presented here allows for a secular variation of ephemeral magnetic flux. *Foster* [2004] and *Lockwood* [2004] used Greenwich sunspot observations (available back to 1874). *Krivova et al.* [2007] used R_G.

series only extend back to the invention of the telescope (around 1610), and well-calibrated systematic measurements only began about 100 years later. However, solar variability on time scales of centuries to millennia can be reconstructed using cosmogenic radionuclides such as ^{10}Be and ^{14}C whose production rate in the atmosphere is modulated by solar activity. In this way, at least the past 10,000 years can be reconstructed [*Vonmoos et al.*, 2006], although the temporal resolution is poorer, signal-to-noise ratio is lower, and the record must be corrected for variations in the geomagnetic field. Recently, *Steinhilber et al.* [2009] derived from ^{10}Be the first TSI record covering almost 10,000 years. First, they calculated the interplanetary magnetic field (IMF) necessary to explain the observed production changes corrected for the geomagnetic dipole effects. They then used the relationship between instrumental IMF and TSI data during sunspot cycle minima to derive an estimate of the TSI record.

[35] Sunspot numbers clearly reveal trends in solar magnetic phenomena, e.g., during the first half of the twentieth century. There are also clear indications of cycles longer than the 11 year SC, e.g., the Gleissberg cycle (80–90 years) with variable amplitudes. The cosmogenic radionuclides confirm the existence of these and other longer periodicities (e.g., 208 year DeVries or Suess cycle, 2300 year Hallstatt cycle, and others) and also the present relatively high level of solar activity, although there is some controversy as to how unusually high it really is [*Muscheler et al.*, 2007; *Usoskin et al.*, 2004; *Steinhilber et al.*, 2008].

[36] Periodicities, trends, and grand minima are features of solar activity which, if detectable in climate records, can be used to attribute climate changes to solar forcing [*Beer et al.*, 2000; *Beer and van Geel*, 2008]. However, one must be aware that this may not always work well because there are other forcings as well and the climate is a nonlinear system which can react in a variety of ways. There are two common methods employed to estimate TSI variations. One is based on sunspot numbers and chromospheric indices to quantify sunspot darkening and facular brightening, respectively [*Fröhlich*, 2006]. The second uses solar magnetograms and the SATIRE irradiance modeling [*Wenzler et al.*, 2006]. While both are very successful in explaining short-term TSI changes over the past 3 decades [*Solanki et al.*, 2005], it is not yet clear to what extent TSI has changed on multidecadal to centennial time scales [*Krivova et al.*, 2007], for example, to what extent TSI and SSI are reduced during the Maunder Minimum, although estimates have converged somewhat in recent years.

[37] Through the sunspot record we have good information about the effect of sunspot darkening on TSI on these time scales. Unfortunately, we have no direct measurements, nor even a proxy indicator, of the corresponding variation of facular brightening on these time scales, nor of the corresponding effect in the overlying chromosphere that modulates UV emission. As mentioned in section 2.1, there could be effects of magnetic fields deeper in the convection zone, the so-called shadow effects, and there may be small solar radius changes [*Lockwood*, 2010]. The SATIRE modeling has shown that surface emissivity effects explain recent solar cycles in TSI rather well, and these shadow (and solar radius) effects are not significant effects over the past 30 years or so. However, this does not eliminate them as factors on longer time scales.

[38] Several reconstructions of TSI variations on century time scales have been made (see Figure 7) on the basis of a variety of proxies including the envelope of the sunspot number cycle *R* [*Reid*, 1997]; the length of the sunspot cycle, *L* [*Hoyt and Schatten*, 1993]; the structure and decay rate of individual sunspots [*Hoyt and Schatten*, 1993]; the average sunspot number *R* and/or the group sunspot number R_G [*Hoyt and Schatten*, 1993; *Zhang et al.*, 1994; *Reid*, 1997; *Krivova et al.*, 2007]; the solar rotation and diameter [*Nesme-Ribes et al.*, 1993; *Mendoza*, 1997]; a combination of *R* and its 11 year running mean, R_{11} [e.g., *Lean*, 2000a, 2000b], or a combination of *R* and *L* [e.g., *Solanki and Fligge*, 2000]; sunspot group areas [*Fligge and Solanki*, 1998]; Greenwich sunspot maps [*Lockwood*, 2004]; *p* mode amplitudes (estimated from *R*) [*Bhatnagar et al.*, 2002]; cosmogenic isotopes deposited in terrestrial reservoirs [*Bard et al.*, 2000; *Steinhilber et al.*, 2009]; and the open magnetic flux of the Sun derived from geomagnetic activity data [*Lockwood*, 2002].

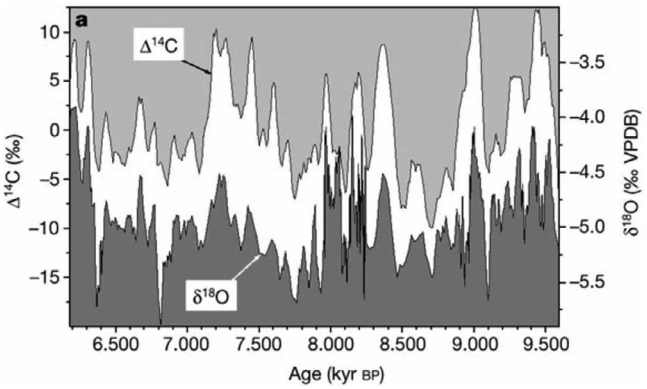

Figure 8. The $\delta^{18}O$ time series from the Hoti cave in northern Oman compared with $\Delta^{14}C$ [from *Neff et al.*, 2001].

[39] For most of the early reconstructions (specifically those by *Lean et al.* [1995], *Lean* [2000a, 2000b], *Solanki and Fligge* [1999, 2000], and *Hoyt and Schatten* [1993]) the change in mean TSI between the Maunder Minimum and recent decades was estimated using the observed distribution of the brightness of Sun-like stars in their chromospheric emissions. This scaling assumed that brighter Sun-like stars (of similar age and chemical abundance to the Sun) show a decadal-scale activity cycle and are analogous to the present-day Sun, whereas the less bright stars were found to be noncyclic and are analogous to the Sun during its Maunder Minimum state. The use of such stellar analogs for estimating the long-term changes in TSI was based on the work of *Baliunas and Jastrow* [1990], who surveyed observations of Sun-like stars. However, recent surveys have not reproduced their results and suggest that the selection of the original set may have been flawed [*Hall and Lockwood*, 2004; *Giampapa*, 2004]. Thus, the extent of the positive drift in TSI between the Maunder Minimum and the present day is uncertain.

[40] Some authors suggest there may be no actual change [*Foukal et al.*, 2004], while others suggest a long-term positive drift which is smaller than previously estimated [*Lean et al.*, 2002] (see, e.g., the *Krivova et al.* [2007] estimate in Figure 7). There are, however, two reasons to believe that the latter is the most likely. First, there is a correlation of TSI with open solar flux [see, e.g., *Lockwood*, 2002]. The numerical modeling of emerged flux transport and evolution [e.g., *Wang et al.*, 2005] suggests that the long-term drift in open flux is matched by a similar drift in the TSI [see also *Krivova et al.*, 2007]. Second, *Lockwood and Fröhlich* [2007] have recently demonstrated that there is a coherent variation between the minimum TSI and the mean sunspot number R_{11}, as employed by *Lean et al.* [1995, 2002] (although the TSI data sequence is short and covers only three solar minima, so that extrapolating back to the Maunder Minimum is full of uncertainty). Between 1985 and 2007, R_{11} fell from 83 to 63, and the S_{min} value in 2007 is 0.39 W m^{-2} lower than that in the 1985 minimum. Linear extrapolation gives a value of TSI in the Maunder Minimum ($R_{11} = 0$) that is 1.6 W m^{-2} lower than the 1985 S_{min} value. This agrees well with the field-free irradiance estimated by *Foster* [2004] and *Lockwood* [2004] and with the reconstructions by *Lean* [2000a] and *Lockwood and Stamper* [1999] (also shown in Figure 7). *Krivova et al.* [2007] used sunspot data and the open flux modeling of *Solanki et al.* [2002] and found a value of 1.3 W m^{-2} with an uncertainty range of 0.9–1.5 W m^{-2}, which is similar to but slightly lower than the above estimate. These estimates for century-scale TSI changes of ~0.9–1.6 W m^{-2} correspond to a change in mean global radiative forcing of only 0.16–0.28 W m^{-2}.

2.4. TSI and Galactic Cosmic Rays

[41] Paleoclimate studies have revealed links between cosmogenic isotopes and climate indicators. For example, one very striking result, shown in Figure 8, is due to *Neff et al.* [2001], who correlated the $\delta^{18}O$ from a stalagmite in a cave in northern Oman with the $\Delta^{14}C$ from tree rings. They argue that $\delta^{18}O$ is a good proxy for monsoonal rainfall in that region, while $\Delta^{14}C$ is a proxy for solar activity derived from the abundance of ^{14}C found in ancient tree trunks around the world. The remarkable similarity between the $\delta^{18}O$ and $\Delta^{14}C$ time series has been interpreted to indicate a northward shift in the Intertropical Convergence Zone (ITCZ), which is believed to have been a controlling influence on the strength of the monsoon at the stalagmite location, which plays a key role in its formation. It is usually assumed that the link between cosmogenic isotopes and climate indicators arises because the cosmogenic isotopes are inversely correlated with TSI [e.g., *Bond et al.*, 2001; *Neff et al.*, 2001]. Indeed, *Bard et al.* [2000] and *Steinhilber et al.* [2010] have used cosmogenic nuclides to reconstruct TSI over the past 1200 years. Figure 9 demonstrates that such an anticorrelation exists over recent solar cycles in both monthly and annual mean data. Comparison of Figures 7 and 2 shows that this anticorrelation is also predicted on century time scales by most TSI reconstructions [*Lean et al.*, 1995].

[42] The processes by which the Sun's magnetic field modulates GCR fluxes are complex. However, simple anticorrelations [e.g., *Rouillard and Lockwood*, 2004] suggest that much of the variation (~75%) of the GCR flux at Earth is explained by the open solar flux, F_S. The production rate of ^{10}Be and other cosmogenic radionuclides in the atmosphere is directly proportional to the flux of cosmic ray protons with energy from 1 to 3 GeV. On decadal to centennial time scales it is dominated by solar activity; on longer time scales it is dominated by the geomagnetic dipole field [*Masarik and Beer*, 2009]. After production, on the way from the atmosphere to the polar ice caps, ^{10}Be is influenced by changes in climate. However, comparison between Greenland and Antarctic records, as well as modeling, shows that these effects are relatively small for production changes on decadal and longer time scales [*Heikkilä et al.*, 2009] but become increasingly more serious for annual resolution. Another issue is the accuracy of ice cores covering thousands of years. Hence, there are several complications in interpreting these indirect measures of solar irradiance.

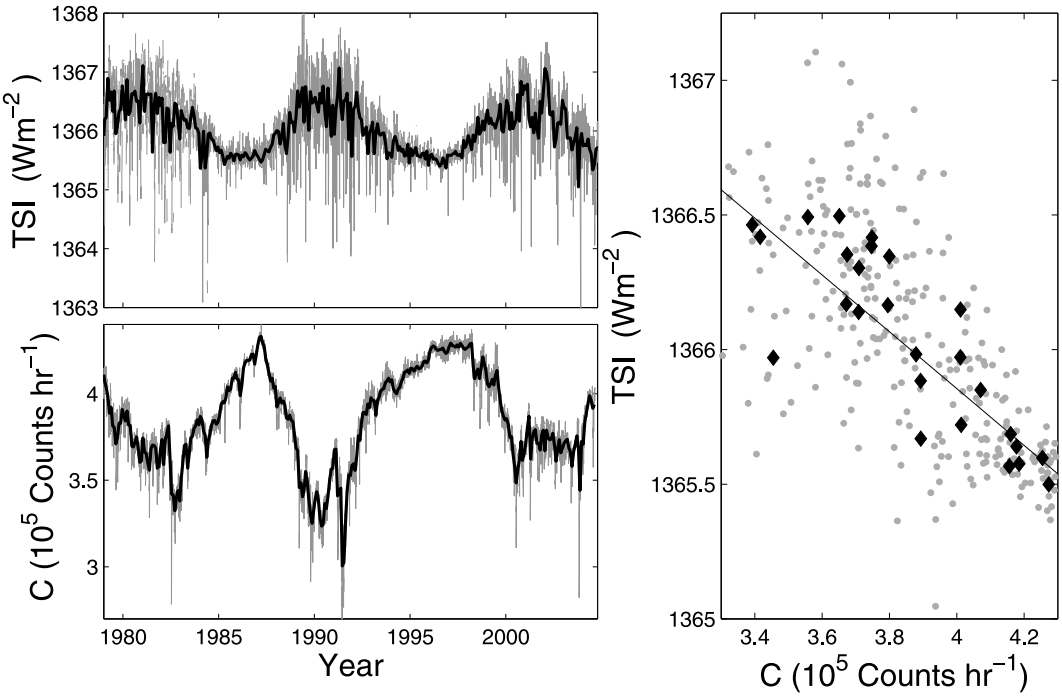

Figure 9. The anticorrelation of GCR fluxes with the TSI since 1978. Variations of (top left) PMOD TSI composite and (bottom left) counts, *C*, detected by the neutron monitor at Climax. The grey line indicates daily values, and the black line indicates the monthly means. (right) Scatterplot of TSI as a function of *C*. Grey points are monthly means; black diamonds are annual means. The best fit linear regression to the annual data is also plotted. The correlation coefficients (and significance levels) are −0.68 (99.99%) and −0.85 (91.5%) for monthly and annual data, respectively (reprinted from *Lockwood* [2006] with kind permission of Springer Science and Business Media).

[43] The connection between GCR and TSI is another method for reconstructing TSI, with the potential to encompass recent millennia using cosmogenic isotope measurements [*Usoskin et al.*, 2003; *Solanki et al.*, 2004]. However, there is a key unknown parameter: the average quiet Sun photospheric field $[B]_{QS}$ at sunspot minimum during the Maunder Minimum [see *Lockwood*, 2004].

[44] In summary, a number of studies have demonstrated that cosmogenic isotopes may indeed provide a proxy indicator of long-term TSI variations. The TSI does not vary linearly with cosmogenic isotopes, but it does vary monotonically with the isotope production rate [*Lockwood*, 2006]. We note, however, that the available observational data set is of the polar deposition of ^{10}Be and not of the actual production rate $P[^{10}\text{Be}]$. The production is influenced by additional factors such as geomagnetic activity and geomagnetic field strength, for which the data can be adjusted, and the abundance in any one terrestrial reservoir is also modified by climate-induced changes in deposition rate, which is more difficult to estimate and account for. However, these are usually checked for using a combination of the ^{10}Be and ^{14}C (and other) cosmogenic isotopes because their deposition and history is so different they cannot be influenced in the same way by climate changes. Because ^{14}C is exchanged with the biomass and oceans in the carbon cycle it does not show the SC variation seen in ^{10}Be abundances; however, centennial-scale changes in the two generally match very closely.

3. CLIMATE OBSERVATIONS

[45] Perhaps the first place to look for solar impact on the Earth's climate is in the upper atmosphere because it interacts most directly with the radiation, particles, and magnetic fields emitted by the Sun. Solar signals in the stratosphere are relatively large and well documented during the past few 11 year SCs since satellite observations became widespread and are described in section 3.1. We then move down in the atmosphere and describe the 11 year SC signals in the troposphere (section 3.2) and the surface (section 3.3). Finally, because of its inertia and slow feedback mechanisms, the climate system is also sensitive to long-term solar changes, and an overview of these observations is provided in section 3.4.

3.1. Decadal Variations in the Stratosphere

3.1.1. Stratospheric Ozone

[46] Ozone is the main gas involved in radiative heating of the stratosphere. Solar-induced variations in ozone can therefore directly affect the radiative balance of the stratosphere with indirect effects on circulation. Solar-induced ozone variations are possible through (1) changes in solar UV spectral solar irradiance, which modifies the ozone

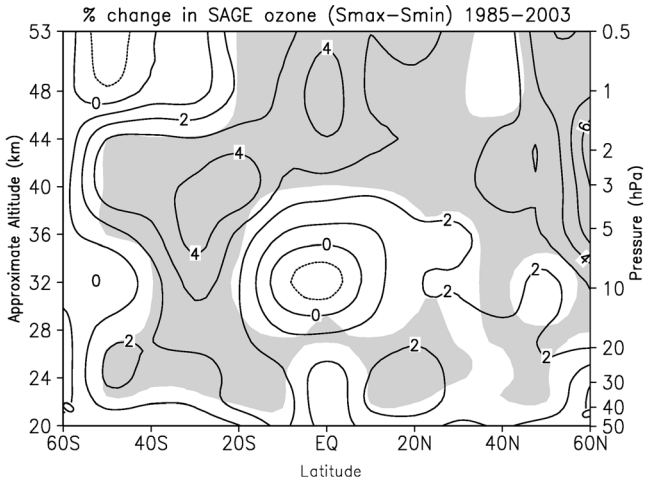

Figure 10. Annual averaged estimate of S_{max} minus S_{min} ozone differences (%) from a multiple regression analysis of SAGE II ozone data for the 1985–2003 period. Shaded areas are significant at the 5% level [from *Soukharev and Hood*, 2006].

production rate through photolysis of molecular oxygen, primarily in the middle to upper stratosphere at low latitudes [*Haigh*, 1994], and (2) changes in the precipitation rate of energetic charged particles, which can indirectly modify ozone concentrations through changes in the abundance of trace species that catalytically destroy ozone, primarily at polar latitudes [e.g., *Randall et al.*, 2007]. In addition, transport-induced changes in ozone can occur [e.g., *Hood and Soukharev*, 2003; *Rind et al.*, 2004; *Shindell et al.*, 2006; *Gray et al.*, 2009] as a consequence of indirect effects on circulation caused by the above two processes.

[47] On the 11 year time scale, the mean irradiance near 200 nm has varied by ~6%, over the past two solar cycles (see Figure 3). Figure 10 shows the mean solar cycle ozone variation as a function of latitude and altitude obtained from a multiple regression statistical analysis of SAGE satellite data for 1985–2003, excluding several years following the Mt. Pinatubo volcanic eruption [see also *Chandra and McPeters*, 1994; *McCormack and Hood*, 1996; *Soukharev and Hood*, 2006; *Randel and Wu*, 2007]. In the upper stratosphere where solar UV variations directly affect ozone production rates, a statistically significant response of 2%–4% is evident. Positive responses are also present at middle and higher latitudes in the middle stratosphere and in the tropics below the 20 hPa level. A statistically insignificant response is obtained in the tropical middle stratosphere. The lower stratospheric ozone response occurs at altitudes where ozone is not in photochemical equilibrium and the ozone lifetime exceeds dynamical transport time scales, which implies that these ozone changes are induced by changes in transport arising from a secondary dynamical response (see also section 4).

[48] The density-weighted height integral of ozone at each latitude gives the "total column" ozone, and a clear decadal oscillation in phase with the 11 year solar cycle is evident in both satellite data [*Soukharev and Hood*, 2006] and ground-based (Dobson) data; the latter show a signal going back at least to the middle 1960s (four cycles) [*Chipperfield et al.*, 2007; see also *Zerefos et al.*, 1997]. The ozone response in the lower stratosphere is believed to be the main cause of the total column ozone signal because of the high number densities at those levels.

3.1.2. Stratospheric Temperatures and Winds

[49] There is also statistically significant evidence for 11 year SC variations in stratospheric temperature and zonal winds. Figure 11 shows the temperature signal estimated

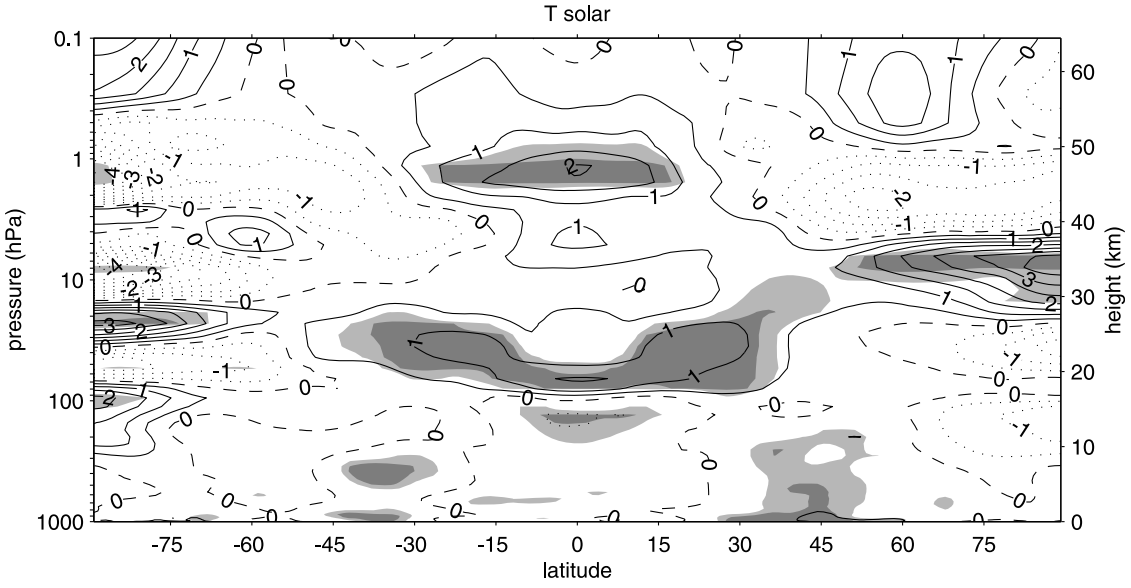

Figure 11. Annual averaged estimate of S_{max} minus S_{min} temperature difference (K) derived from a multiple regression analysis of the European Centre for Medium Range Weather Forecasts (ECMWF) Reanalysis (ERA-40) data set (adapted from *Frame and Gray* [2010]). Dark and light shaded areas denote statistical significance at the 1% and 5% levels, respectively.

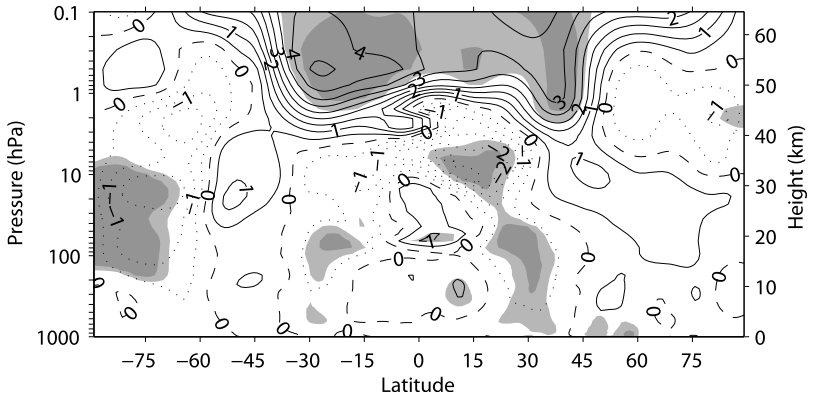

Figure 12. Annual averaged S_{max} minus S_{min} differences in zonally averaged zonal wind (m s^{-1}) from the ground to 0.1 hPa (~65 km) derived from a multiple regression analysis of the ERA-40 data set (adapted from *Frame and Gray* [2010]). Dark and light shaded areas denote statistical significance at the 1% and 5% levels, respectively. Contour values are 0, ±0.5, ±1, ±2, and ±3 m s^{-1} and a contour interval of 2 m s^{-1} thereafter. Solid (dotted) contours denote positive (negative) values, and the dashed line is zero.

from a multiple regression analysis of European Centre for Medium Range Weather Forecasts (ECMWF) reanalysis (ERA-40) data, in which observations have been assimilated into model data [*Frame and Gray*, 2010; see also *Crooks and Gray*, 2005; *Shibata and Deushi*, 2008]. A maximum response of ~2 K is found in the tropical upper stratosphere, at around the level of the maximum percentage ozone response in Figure 10. Estimates suggest that approximately half of this signal is the direct result of solar irradiance changes and half is due to the additional ozone feedback mechanism [e.g., *Gray et al.*, 2009]. A second statistically significant response is seen in the tropical and subtropical lower stratosphere, similar to the ozone regression result of Figure 10. As in the ozone analysis, the lower stratospheric temperature response is indicative of a large-scale dynamical response, e.g., changes in net equatorial upwelling rates [*Shibata and Kodera*, 2005; *Gray et al.*, 2009].

[50] An alternative approach to estimating the 11 year SC temperature signal has been to directly analyze the satellite observations, which are recalibrated data from the TIROS Operational Vertical Sounder (TOVS) infrared radiometers [*Scaife et al.*, 2000; *Randel et al.*, 2009]. This approach has the advantage of avoiding model influences and minimizing instrument intercalibration errors that were not taken into account by the ERA-40 (or National Centers for Environmental Prediction (NCEP)) reanalysis data sets. On the other hand, the TOVS data have a somewhat lower vertical resolution of ~10 km. The TOVS data analysis yields a reduced response in the upper stratosphere of ~1.1 K, and the response is much broader in height, decreasing monotonically to ~0.5 K in the lower stratosphere, without the twofold maximum in the tropical middle stratosphere that is evident in Figure 11. This difference may be due to the low vertical resolution of the TOVS observations [*Gray et al.*, 2009], or it may be a spurious feature of the regression technique [*Lee and Smith*, 2003; *Smith and Matthes*, 2008].

[51] There is also an 11 year SC signal in zonal wind fields. Figure 12 shows a strong positive zonal wind response in the ERA-40 regression analysis in the subtropical lower mesosphere and upper stratosphere, which has been shown to come predominantly from the winter signal in each hemisphere [*Crooks and Gray*, 2005; *Frame and Gray*, 2010]. This lower mesospheric subtropical jet response near winter solstice had also been noted in previous analyses of rocketsonde and NCEP data [*Kodera and Yamazaki*, 1990; *Hood et al.*, 1993]. The zonal wind anomaly is observed to propagate downward with time over the course of the winter [*Kodera and Kuroda*, 2002], and wave-mean-flow interactions are likely involved in producing this response [*Kodera et al.*, 2003].

[52] As already noted in section 1 there is an added complication from the QBO [*Labitzke*, 1987; *Labitzke and van Loon*, 1988; *Labitzke et al.*, 2006]. Figure 13 shows an updated version of Labitzke's original results, which show a clear dependence of North Pole (NP) 30 hPa geopotential heights on the 11 year SC, provided the observations are first grouped into QBO phase. In QBO easterly years (QBO-E), the 30 hPa (~24 km) NP geopotential height decreases with increasing solar activity, whereas in QBO westerly years (QBO-W) it increases with increasing solar activity. Increased geopotential height at 30 hPa implies an increase in the mean temperature below that pressure level and vice versa. There is a well-known "Holton-Tan" relationship between the equatorial QBO and the NP geopotential height and temperatures [*Holton and Tan*, 1980, 1982]. In general, the QBO-E years (i.e., when the lower stratospheric winds are from the east) tend to favor a warmer, more disturbed Northern Hemisphere (NH) polar vortex than the QBO-W phase, with frequent large-scale wave disturbances to the vortex, known as stratospheric sudden warmings (SSWs). However, SSWs are by no means exclusive to the QBO-E phase. When they do occur in the QBO-W phase, they occur almost exclusively during an S_{max} period, so that SSWs tend to be favored in S_{min}–QBO-E and S_{max}–QBO-W years. *Labitzke and van Loon* [1988] have suggested that the Holton-Tan relationship actually reverses

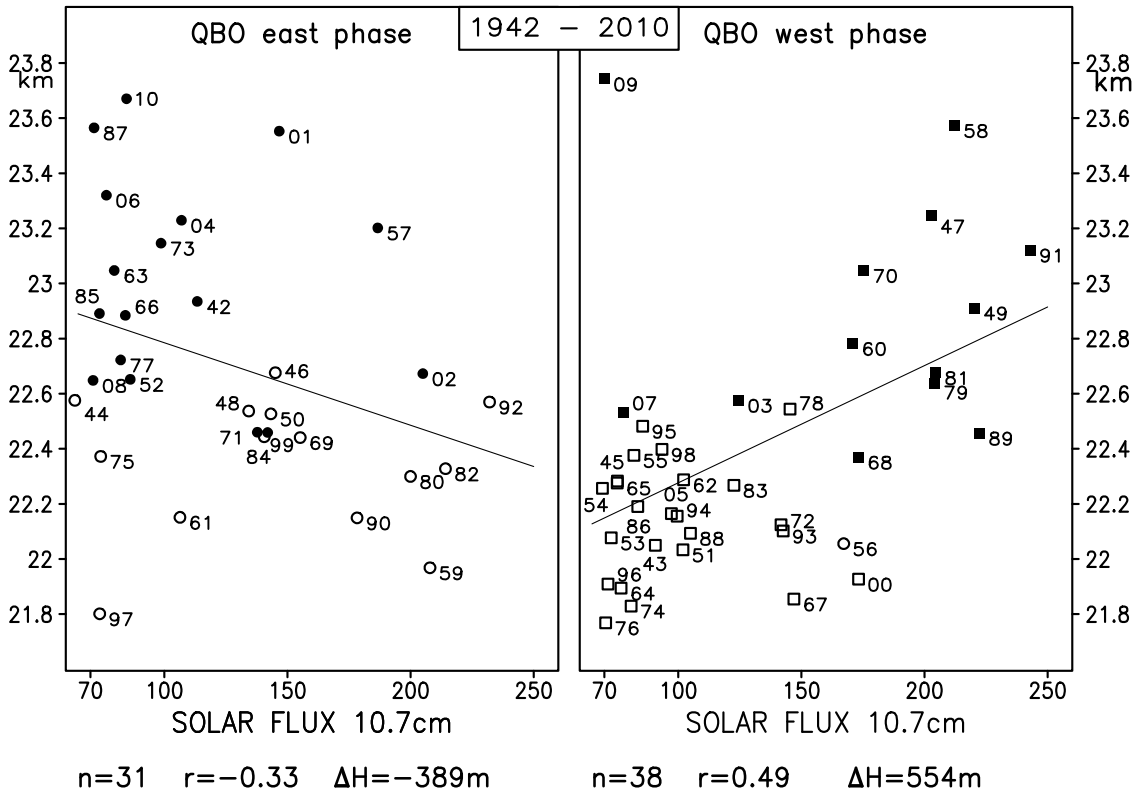

Figure 13. Scatter diagrams of the monthly mean 30 hPa geopotential heights (geopotential kilometers) in February at the North Pole (1942–2010), plotted against the 10.7 cm solar flux in solar flux units (1 sfu = 10^{-22} W m $^{-2}$ Hz^{-1}). (left) Years in the east phase of the quasi-biennial oscillation (QBO) (n = 31). (right) Years in the west phase (n = 38). The numbers indicate the respective years, solid symbols indicate major midwinter warmings, r is the correlation coefficient, and ΔH gives the mean difference of the heights (geopotential meters) between solar maxima and minima (minima are defined by solar flux values below 100). Updated from *Labitzke et al.* [2006], http://www.borntraeger-cramer.de.

during S_{max} periods, although *Gray et al.* [2001] find only that it is disrupted [see also *Naito and Hirota*, 1997; *Camp and Tung*, 2007]. There is also a suggestion that the period of the QBO in the equatorial lower stratosphere is modulated by the 11 year solar cycle, with a longer QBO-W phase during S_{max} than during S_{min} years [*Salby and Callaghan*, 2000, 2006; see also *Pascoe et al.*, 2005], although this has been questioned by *Hamilton* [2002] and more recently by *Fischer and Tung* [2008].

[53] Although most observational studies have focused on the NH winter period, the 11 year SC is evident in both hemispheres and all seasons. Figure 14 shows high correlations in the NH summer between 10.7 cm solar flux and detrended 30 hPa temperatures. Although the correlations are relatively high (0.7) when all years are included (Figure 14, top), when the years are divided according to the phase of the QBO they are even higher (0.9) in QBO-E phase (Figure 14, middle), showing once again a dependence on the QBO. The seasonal evolution of the SC signal (not shown) also confirms that a temperature signal is present throughout the year in both hemispheres but the zonal wind signal is primarily present in the respective winter hemisphere [*Crooks and Gray*, 2005].

3.2. Decadal Variations in the Troposphere

3.2.1. Tropospheric Temperature and Winds

[54] Pioneering work of *Labitzke and van Loon* [1995] demonstrated an 11 year SC variation in the annual mean 30 hPa geopotential height Z_{30} at a location near Hawaii with an amplitude suggesting that the mean temperature of the atmosphere below about 24 km is 0.5–1.0 K warmer at S_{max} than at S_{min}. This is a large response, but from such results it was not clear whether the signal was confined locally or how the temperature anomaly was distributed in the vertical. Later work [*van Loon and Shea*, 2000] confirmed an 11 year signal in the mean summertime zonally averaged temperature of the NH upper troposphere with amplitude of 0.2–0.4 K. More recently, analysis of the NCEP/National Center for Atmospheric Research reanalysis data set shows a response in both tropospheric zonally averaged temperature and winds in which the midlatitude jets are weaker and farther poleward in S_{max} years [*Haigh*, 2003; *Haigh et al.*, 2005; *Haigh and Blackburn*, 2006, see Figures 4.5c and 4.5d], and these signals are also evident in Figures 11 and 12.

3.2.2. Tropical Circulations

[55] Estimates of the 11 year solar signal in tropical circulations are difficult to obtain because of the small-

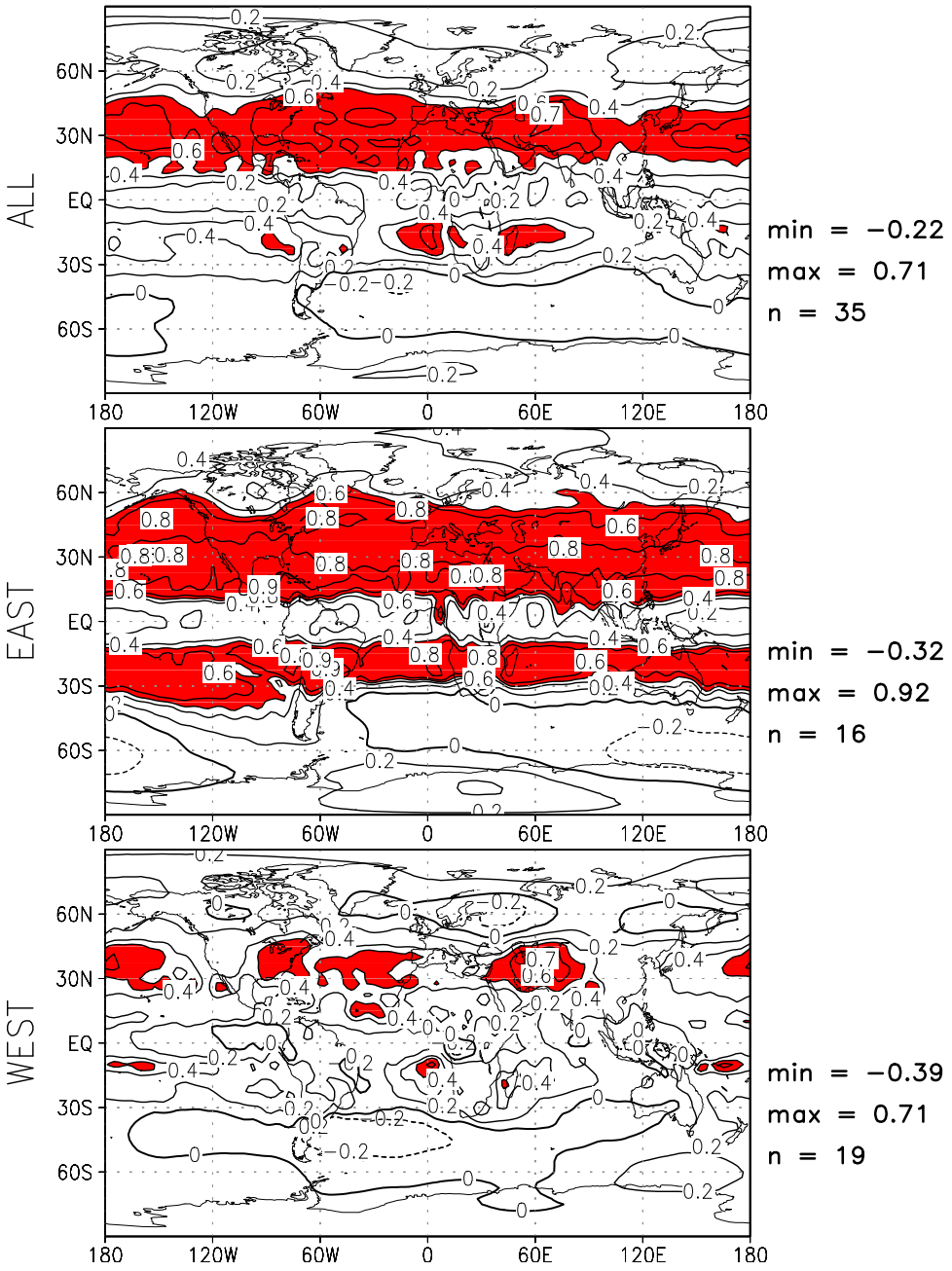

Figure 14. Correlation between the 10.7 cm solar flux and the detrended 30 hPa temperatures in July, shaded for emphasis where correlations are above 0.5. (top) All years (1968–2002). (middle) QBO-E years only. (bottom) QBO-W years only. (Adapted from *Labitzke* [2003], http://www.borntraeger-cramer.de).

amplitude signal, the short period of available data, and, particularly, the large errors associated with estimates of vertical velocities. However, in their analysis of station radiosonde data from the tropics and subtropics, *Labitzke and van Loon* [1995] suggested that the Hadley cell (in which there is generalized upwelling at equatorial latitudes and descent in the subtropics) was stronger at S_{max}. In an analysis of NCEP vertical velocities, *van Loon et al.* [2004, 2007] found a similar dependence of the Hadley cell strength, and *Kodera* [2004], using the same data, noted a suppression of near equatorial convective activity at S_{max} and enhanced off-equatorial convection in the Indian monsoon. *Haigh* [2003] and *Haigh et al.* [2005] analyzed NCEP zonal mean temperature and zonal wind data and found a weakened and broadened Hadley cell under S_{max}, together with a poleward shift of the subtropical jet and Ferrel cell. *Gleisner and Thejll* [2003], again using NCEP vertical velocities, found a similar poleward expansion of the Hadley circulation at S_{max} with stronger ascending motions at the edge of the rising branch. *Brönnimann et al.* [2007] used a new extended upper air temperature and geopotential height data set based on radiosonde and aircraft observations

and concurred with the poleward displacement of the subtropical jet and Ferrel cell but could find no clear solar signal in the strength of the Hadley circulation.

[56] Other studies have sought to identify solar influences on the strength and extent of the Walker circulation (i.e., the east–west tropical circulation pattern, which is intimately connected with the north–south tropical "Hadley" circulation). *van Loon et al.* [2007] and *Meehl et al.* [2008] found a strengthened Walker circulation at S_{max} which was distinct from the El Niño–Southern Oscillation (ENSO) signal [*van Loon and Meehl*, 2008]. *Lee et al.* [2009] also found a strengthening of the Walker circulation. The associated sea surface temperature (SST) response at S_{max} was a cool anomaly in the equatorial eastern Pacific and poleward shifted ITCZ and South Pacific Convergence Zone (SPCZ) [*van Loon et al.*, 2007; *Meehl et al.*, 2008]. This was followed by a warm anomaly with a lag of a couple of years [*Meehl et al.*, 2008; *White and Liu*, 2008a, 2008b]. *Gleisner and Thejll* [2003] also found a stronger Walker circulation at S_{max} with enhanced upward motion in the tropical western Pacific connected to stronger descending motions in the tropical eastern Pacific during S_{max}. *Kodera et al.* [2007] have also suggested a solar modulation of the ENSO cycle which is manifest mainly in the western extent of the Walker cell and links to the behavior of the Indian Ocean monsoon.

[57] Unequivocal identification of a solar signal in tropospheric mean circulation (if one is indeed present) might help to disentangle the various proposed mechanisms for solar influence on climate (see section 4). The "top-down" influence based on solar heating of the stratosphere [*Haigh*, 1996, 1999; *Kodera and Kuroda*, 2002; *Kodera*, 2004; *Shindell et al.*, 1999, 2006] (see section 4.2) tends to suggest strengthened tropical convection with poleward shifted ITCZ and SPCZ at S_{max}, as do the "bottom-up" mechanisms (based on solar heating of the sea surface and dynamically coupled air-sea interaction [*Meehl et al.*, 2003, 2008]). Recent studies suggest that these two mechanisms work in the same direction and add together to produce an amplified SST, precipitation, and cloud response in the tropical Pacific to a relatively small solar forcing [*Rind et al.*, 2008; *Meehl et al.*, 2009]. Results of observational analyses suffer from the short data periods available, though the model simulations do not have this limitation. There are also indications from both observations and model studies that the responses depend on complex nonlinear interactions between the various influencing processes, which makes the task of identifying and understanding the detailed tropical response much more difficult.

3.2.3. Extratropical Modes of Variability

[58] Annular modes are hemispheric-scale patterns of climate variability and owe their existence to internal atmospheric dynamics in the middle to high latitudes. They describe variability in deviations from the seasonal cycle. In the pressure field, the annular modes are characterized by north–south shifts in atmospheric mass between the polar regions and the middle latitudes. In the wind field, the annular modes describe north–south vacillations in the extratropical zonal wind with centers of action located at ~55°–60° and ~30°–35° latitude. By convention, a positive annular mode index is defined as lower than normal pressures over the polar regions and stronger westerly winds along ~55°–60° latitude. While the terms northern annular mode (NAM) and southern annular mode (SAM) are used to describe hemispheric behavior at any level in the atmosphere, the Arctic Oscillation (AO) and NAO are the corresponding surface measures of variability in the middle- to high-latitude NH and the North Atlantic–European region, respectively.

[59] Several authors [e.g., *Kuroda and Kodera*, 1999; *Castanheira and Graf*, 2003] have found evidence for modulation of the NAO by the state of the stratosphere, and some [e.g., *Kodera*, 2002; *Boberg and Lundstedt*, 2002; *Thejll et al.*, 2003; *Kuroda and Kodera*, 2004, 2005; *Kuroda et al.*, 2007; *Lee and Hameed*, 2007; *Barriopedro et al.*, 2008; *Lee et al.*, 2008] have found a solar cycle signal in the NAM and SAM, though others such as *Moore et al.* [2006] have not. Most of these studies, however, have used simple linear regression or confined their discussions to correlation coefficients and so have not considered the impact of other potential forcing factors nor found the magnitude of the implied solar signals.

[60] In an attempt to refine this, *Haigh and Roscoe* [2009] carried out a multiple regression analysis of time series of the NAM and SAM indices throughout the depth of the atmosphere. A significant response to the 11 year SC was not evident if the solar and QBO terms were included separately, but when they were combined into a single term (solar multiplied by QBO) to represent their interaction, then a statistically significant response was found, particularly near the surface: the polar vortices were weaker and warmer in S_{max}–QBO-W and S_{min}–QBO-E years and stronger and colder in S_{max}–QBO-E and S_{min}–QBO-W years. This is consistent with the results shown in Figure 13. Nevertheless, volcanic aerosols also have a large impact on the annular modes. Given the timing of large eruptions during the late twentieth century (1982 and 1991), great care is required to avoid confusing the solar and volcanic signals during recent decades. Recent analysis using a data set extended to include the most recent S_{max} period during which there was no coincident volcanic eruption has enabled an improved separation of the two signals [*Frame and Gray*, 2010] and showed that the solar signal is statistically significant.

3.2.4. Clouds and Precipitation

[61] *Marsh and Svensmark* [2003] reported a strong positive correlation of the monthly time series of low cloud amount (LCA) and GCRs over the period 1983–2005. The GCRs are represented by neutron monitor data measured at Climax in Colorado (see section 2.4), and cloud amounts were taken from the International Satellite Cloud Climatology Project (ISCCP) D2 data set. However, their study included an adjustment to the cloud data which they proposed was required to take account of an intercalibration problem with the ISCCP cloud data between September 1994 and January 1995, in the absence of a polar satellite. In fact, the various satellites used in the ISCCP composite are not intercalibrated across the 1994–1995 gap, but each sat-

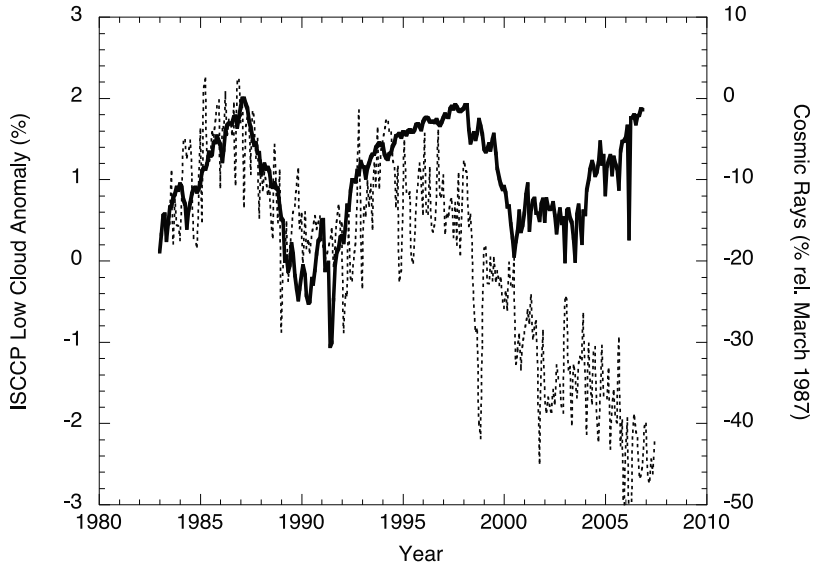

Figure 15. Monthly averages of ISCCP D2 IR global low cloud amount derived from a combination of polar orbiting and geostationary satellites (thin dashed line) and cosmic rays (thick solid line). The low cloud amount has not been adjusted to allow for a possible intercalibration problem after 1994 suggested by *Marsh and Svensmark* [2003].

ellite is calibrated individually against the record considered to be most reliable, that of the earlier NOAA 9 satellite. Hence, while intercalibration differences between satellites could lead to a one-time jump as a new satellite enters the data set, they cannot produce spurious trends. The controversial adjustment applied by *Marsh and Svensmark* [2003] dramatically alters the entire time series after 1994. If one examines the ISCCP data and GCR records directly (see Figure 15), it becomes clear that without the doubtful alterations made to the post-1994 satellite record, there is no evidence for correlation after the early 1990s. As there is no compelling evidence that the time-varying adjustment of *Marsh and Svensmark* [2003] is required, we conclude that the current data do not provide substantial support to the hypothesized cloud cover linkage to cosmic rays.

[62] Alternative analyses of correlations between GCR and low cloud cover, using ISCCP and ship-based cloud data, also find that the observations do not support the hypothesized cloud cover–cosmic ray linkage. *Sun and Bradley* [2002] found that the effect was only present in the North Atlantic within specific data sets [see also *Marsh and Svensmark*, 2004; *Sun and Bradley*, 2004]. More recently, *Sloan and Wolfendale* [2008] found that less than 23% of the 11 year cycle in cloud could be attributed to the solar modulation of cosmic rays.

[63] A number of studies have indicated that the ISCCP data set is not suitable for long-term trend or variation studies [*Klein and Hartmann*, 1993; *Kernthaler et al.*, 1999; *Evan et al.*, 2007]. We note also that the overall (one sigma) accuracy of ISCCP cloud amount at the global mean level is of the order of 2%, and thus, none of the long-term trends or apparent cyclic behavior, which are at about the 1% level, are significant (G. Tselioudis, personal communication, 2008). It is therefore unclear whether current data can resolve this issue, though it is clear that it cannot offer the strong support for long-term impacts of GCR fluxes on cloud cover that have been claimed by some. Nevertheless, using short-term (3-hourly) ISSCP data, high-pass filtered to remove long-term trends, a positive correlation between low cloud and GCR is still evident, indicating a 3% cloud variation [*Brown*, 2008].

[64] An analysis which does not suffer from these problems of long-term data stability is to search for the effect of sudden reductions in GCR fluxes called Forbush decreases. These are caused by the transient effect of coronal mass ejections that pass over or close to the Earth. Using a superposed epoch (compositing) analysis of the largest of these events, *Svensmark et al.* [2009] have recently reported large (up to 7%) global cloud cover decreases, as detected by a number of satellites, following these Forbush decreases in GCR fluxes. The difficulty with this kind of study is that there are very few large Forbush decreases when satellite cloud data are available, so results tend to be dominated by a single event. This possibility is increased because the authors reduce the set of events to those common to all the available satellite cloud data sets used. The cloud response in this study peaked 7 days after the GCR decrease, which is not an expected delay. With the greater spatial and spectral resolution available in the Moderate Resolution Imaging Spectroradiometer (MODIS) satellite data, *Kristjánsson et al.* [2008] found only weak negative correlations between GCR and cloud properties during Forbush events, except for the eastern Atlantic Ocean region in which both the negative correlations between GCR and cloud and between GCR and cloud thickness were statistically significant. In a very detailed correlation analysis of the effective calculated spatial ionization changes using six Forbush decreases and allowing for different lags between cosmic ray flux and

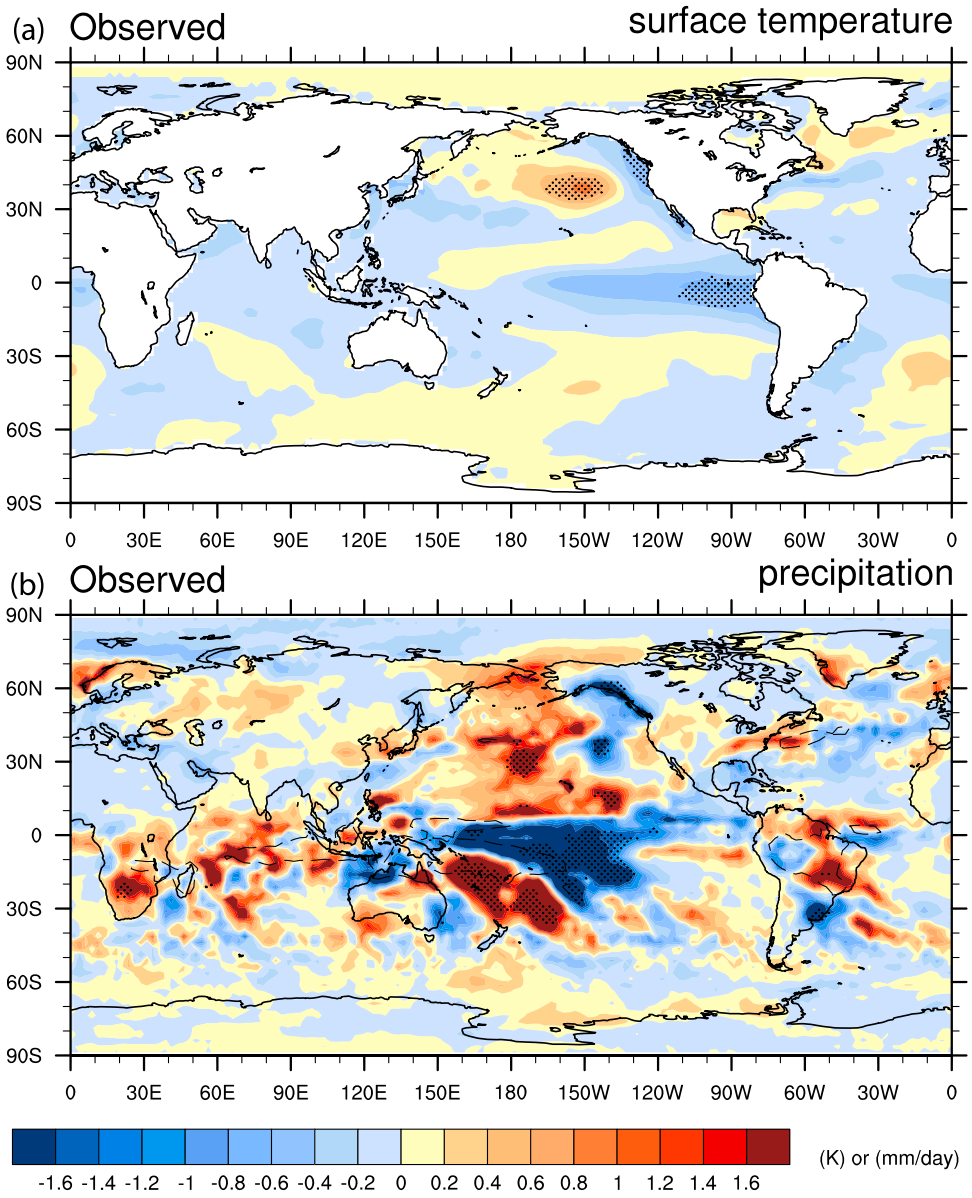

Figure 16. (a) Composite average sea surface temperature anomaly in the Pacific sector for December, January, and February (DJF) for 11 peak solar years (°C). (b) Same as Figure 16a but for composite average surface precipitation anomaly from three available peak solar years (mm s^{-1}). Adapted from *Meehl et al.* [2009]. Reprinted with permission from AAAS.

cloud cover, no significant effect of cosmic rays on low cloud cover could be found [*Calogovic et al.*, 2010]. Discussion of the significance of these studies has been reviewed by *Lockwood* [2010].

[65] An entirely different approach to cloud measurements, which is also unaffected by the long-term calibration issues of satellite instruments, employs surface-based cloud determinations, using solar radiation measurements [*Duchon and O'Malley*, 1999; *Long and Ackerman*, 2000; *Calbó et al.*, 2001; *Harrison et al.*, 2008]. *Harrison and Stephenson* [2005] employed 50 years of UK data and found that days with high cosmic rays had greater odds of being overcast and, on average, coincided with days having a 2% increased diffuse fraction, which implied slightly increased cloud cover. Since linear correlation explained less than 0.2% of the variance in cloud cover, a nonlinear relationship was concluded. A response in UK tree ring data to cosmic rays has also been suggested to be related to diffuse radiation changes [*Dengel et al.*, 2009].

[66] Solar effects on clouds can also be inferred from changes in precipitation. Figure 16b shows precipitation anomalies during peak solar activity years from an analysis of observed data. The pattern shows a decrease of precipitation around the equator which coincides with a "cold tongue" of anomalous SSTs (Figure 16a) analogous to the pattern that occurs during ENSO cold event (La Niña) years. The increase in precipitation both north and southwest coincides with a shift away from the equator of the ITCZ and SPCZ [*Meehl et al.*, 2008, 2009]. Besides direct records of precipitation rates, there is documentary information on

lake and river levels (e.g., the Nile [*Fraedrich and Bantzer*, 1991; *de Putter et al.*, 1998; *Eltahir and Wang*, 1999; *Kondrashov et al.*, 2005]) and catastrophic floods and droughts [*Verschuren et al.*, 2000; *Hong et al.*, 2001; *Ruzmaikin et al.*, 2006]. These changes do not, however, distinguish direct GCR effects on clouds from other mechanisms.

3.3. Decadal Variations at the Earth's Surface

[67] Many studies have investigated whether 11 year SC variations can be detected in recent, more accurate observations of temperatures at the Earth's surface. This poses considerable challenges as many other factors were also influencing climate during this period, including increasing greenhouse gases, volcanic eruptions, and aerosol changes. Some of these are themselves poorly quantified, such as aerosols, and some may have similar impacts on surface climate to solar irradiance changes. Additional complications arise when different forcings have similar temporal changes, as has been the case with the solar cycle and volcanic forcing over parts of the twentieth century. Hence, isolation of any solar signal is not straightforward.

[68] Nonetheless, some signals of solar forcing appear to be present at decadal time scales in particular regions. *White et al.* [1997] examined basin average ocean temperatures with two independent SST data sets: surface marine weather observations (1900–1991) and upper ocean bathythermograph temperature profiles (1955–1994). They found variations in phase with solar activity across the Indian, Pacific, and Atlantic oceans. Global averages yielded maximum changes of 0.08 ± 0.02 K on decadal (~11 year period) scales and 0.14±0.02 K on interdecadal (~22 year period) scales. The highest correlations were obtained with ocean temperatures lagging solar activity by 1–2 years, which is roughly the time scale expected for the upper layers of the ocean (<100 m) to reach equilibrium.

[69] A number of studies have also noted a strong regional response to the 11 year SC. For example, *White et al.* [1997, 1998] found that the 11 year SC associated with SST variability during the twentieth century was remarkably similar to the spatial pattern of the ENSO, which has a 3–5 year period (see section 3.2.2 and Figure 16). *Allan* [2000] and *White and Tourre* [2003] detected this 11 year signal, which they referred to as a quasi-decadal oscillation, in global SST and sea level pressure patterns rising significantly above the background noise, along with ENSO and QBO periods. *White and Liu* [2008a, 2008b] have subsequently noted an El Niño–like warm event in the tropical eastern Pacific SSTs that is coincident with peaks in solar forcing, preceded and succeeded by cold events, which they proposed were associated with nonlinear phase locking of odd harmonics and could explain a significant fraction of equatorial eastern Pacific SST variability (see also section 4.1). *Meehl et al.* [2008], on the other hand, noted a cold (La Niña–like) event which coincided with the peak in sunspot numbers, followed a few years later by a warm El Niño–like event. Thus, there is an apparent disagreement between these two analyses. However, *Roy and Haigh* [2010] have noted that the peak in sunspot number occurs a year or so in advance of the peak in the observed decadal solar irradiance variability, so that the *Meehl et al.* [2008] cold event coincident with sunspot year maximum is not inconsistent with the White and Liu results.

[70] Land temperatures also show SC relationships in some regions. Recent analyses indicate significant correlations between 11 year SC forcing and surface climate that appear to be robust both to the data set used and the methodology employed [*Camp and Tung*, 2007; *Tung and Camp*, 2008].

3.4. Century-Scale Variations

[71] Going back in time, it is inevitable that instrumental and documentary records of climate become increasingly sparse and unequally distributed around the globe. On longer time scales, evidence for a Sun-climate linkage must rely entirely on indirect information stored in natural archives, such as ice cores, marine and lacustrine (lake bed) sediments, peat deposits, speleothems (stalactites and stalagmites), and tree rings. These archival reservoirs provide only indirect measures of temperature and precipitation by using climate proxies such as isotopic ratios, elemental concentrations, layer thicknesses, and biological indicators. Nevertheless, there are many advantages of using climate proxy records: they cover very long time periods of up to several 10^3–10^4 years with relatively high temporal resolution, providing information on past climate for many parts of the globe. They also allow investigation of solar forcing of climate change prior to large-scale human influences on the atmosphere.

3.4.1. Solar Proxies

[72] As described in section 2, it has been known for about 50 years that GCR intensity reflects solar activity because of modulation by solar magnetic fields carried away from the Sun by the solar wind. The larger the solar activity, the stronger the shielding, and the lower the cosmic ray intensity penetrating into the atmosphere. In the atmosphere cosmic rays interact with nitrogen and oxygen, producing cosmogenic radionuclides such as ^{10}Be and ^{14}C, so that measuring ^{10}Be and ^{14}C stored in terrestrial reservoirs provides a means to reconstruct the history of solar activity over millennia. Precise calibration remains challenging, however, and is based on the comparatively short period of overlap with modern observations. Hence, these solar proxies provide a much more precise estimate of the temporal variations of solar irradiance than its magnitude. In addition, the ^{10}Be and ^{14}C signals stored in ice and tree rings do not solely reflect changes in solar activity. For example, the geomagnetic field also shields Earth from cosmic rays and varies on long time scales. In the case of ^{14}C, the newly produced ^{14}C is mixed with ^{14}C already present in the carbon reservoirs (atmosphere, biosphere, and ocean), causing an attenuation and a delay of the production signal. In the case of ^{10}Be the production signal can be altered to some extent by the transport processes from the point in the atmosphere where it is produced to the site where it becomes stored in an ice core. While the effect of the geomagnetic dipole moment

can be removed relatively easily using paleomagnetic data, the transport effects are more difficult to deal with. One approach makes use of the fact that the ^{10}Be and ^{14}C records are produced by a common signal but are transported in different ways [*Heikkilä et al.*, 2008; *Field et al.*, 2006].

3.4.2. Climate Proxies

[73] Care is also required in proxy climate data quality and chronological control. Although they can be calibrated against more recent instrumental records, there is a risk that calibration using relatively short periods may not be fully valid for preinstrumental times because climate proxies may depend in a complex way on multiple climatic and environmental parameters that are likely to change over longer time scales [*Jones and Mann*, 2004; *Jones et al.*, 2009]. A good example of a climate proxy is peat, for example, the Holocene peat deposits in the rainwater-fed raised bogs in northwest Europe. Plant remains in peat deposits can be identified, and by using ecological information of peat-forming species, changes in species composition of sequences of peat samples can be interpreted as evidence for climate change in the past. The degree of decomposition of the peat-forming plants is also related to former climatic conditions (e.g., more decomposed peat when formed under drier conditions and better preserved plant remains during periods of wetter climatic conditions).

[74] Calibration of single radiocarbon dates usually yields irregular probability distributions in calendar age, quite often over long time intervals. This is problematic in paleoclimatological studies, especially when a precise temporal comparison between different climate proxies is required. However, closely spaced sequences of (uncalibrated) ^{14}C dates of peat deposits display wiggles, which can be fitted to the wiggles in the radiocarbon calibration curve. The practice of dating peat samples using ^{14}C "wiggle-match dating" has greatly improved the precision of radiocarbon chronologies since its application by *van Geel and Mook* [1989]. By ^{14}C wiggle-matching peat sequences, high-precision calendar age chronologies can be generated [*Blaauw et al.*, 2003] which show that increased mire surface wetness occurred together with suddenly increasing atmospheric production of ^{14}C during the early Holocene, the subboreal-subatlantic transition, and the Little Ice Age (Wolf, Spörer, Maunder, and Dalton minima of solar activity). Peat records showing this phenomenon are available from the Netherlands [*van der Plicht et al.*, 2004; *Kilian et al.*, 1995; *van Geel et al.*, 1998], the Czech Republic [*Speranza et al.*, 2002], the UK, and Denmark [*Mauquoy et al.*, 2002].

[75] Precise chronologies are crucial to determine leads and lags and rates of climate change and to help establish causal relationships. Chronological uncertainties of paleoclimate time series are typically 1%–2% of the absolute age, for example, between 100 and 200 years for a 10,000 year old sample. This age error corresponds to a full Gleissberg (~90 years) and de Vries (208 years) solar cycle. However, recent progress has considerably improved the accuracy, e.g., in the case of stalagmites to a few years throughout the Holocene. In some cases, there is a well-established data record, e.g., ice core layers containing ash from a well-documented historical volcanic eruption. Also, some archives such as ice cores provide information on climate forcing (solar activity as derived from ^{10}Be) and at the same time on climate response (e.g., δ^{18}O), which is independent of the dating accuracy. Finally, we note that some archives, such as ice cores, are restricted for obvious natural reasons to certain geographical areas.

3.4.3. Twentieth Century Changes

[76] In climate models, the pattern of surface response (i.e., land plus sea) to solar irradiance variations is fairly similar to the response to greenhouse gases [*Wetherald and Manabe*, 1975; *Nesme-Ribes et al.*, 1993; *Cubasch et al.*, 1997, 2006; *Santer et al.*, 2003], with amplification at high latitudes, where strong positive snow and ice albedo feedbacks operate, and amplification of continental interiors relative to oceans. Hence, while century-scale data show global or hemispheric mean surface air temperatures that are correlated with solar indices, e.g., using solar cycle length as a proxy for irradiance [*Thejll and Lassen*, 2000], this simple correlation is no guarantee of a causal relationship. In fact, a comparison of solar cycle length over the past several centuries shows that if the apparent relationship between solar variability and mean surface air temperature in twentieth century data were indeed real, then solar variations should have driven much larger global or hemispheric temperature variations in the longer-term past than are seen in proxy reconstructions [*Laut*, 2003]. Similarly, global mean SSTs and sunspot numbers are correlated during the twentieth century [*Reid*, 2000], but attributing this relationship to solar forcing of SSTs implies a climate sensitivity that is inconsistent with evidence from earlier centuries. More likely, the apparent relationship results from coincidental similarity in the temporal evolution of sunspots and global or hemispheric mean temperatures, with the latter responding to gradually increasing greenhouse gases and highly variable temporal trends in aerosols.

[77] Advanced statistical detection and attribution methodologies have been developed to take account of uncertainties in the magnitude of various forcings, including solar irradiance forcing [see, e.g., *Stott et al.*, 2003]. These analyses scale the response patterns to each forcing to determine the best match to observations. Also, to distinguish between the various possible forcings, additional observations are incorporated. For example, although the surface response to solar and greenhouse gas (GHG) forcings is similar, as noted above, the GHG response in the stratosphere is opposite to that in the troposphere [*Ramaswamy et al.*, 2006], giving a so-called GHG "fingerprint" that has a very different vertical structure from the solar one.

[78] Model simulations of twentieth century climate that include all the major, known forcings (solar, volcanoes, GHGs, aerosols, and ozone), together with the detection-attribution techniques based on observed patterns, have shown that most of the global warming in the first half of the twentieth century was natural in origin, and much of this can be attributed to an increase in solar forcing [*Tett et al.*, 2002; *Stott et al.*, 2000, 2003; *Shiogama et al.*, 2006; *Meehl et al.*, 2004; *Knutson et al.*, 2006; *Hegerl et al.*, 2003; *IPCC*,

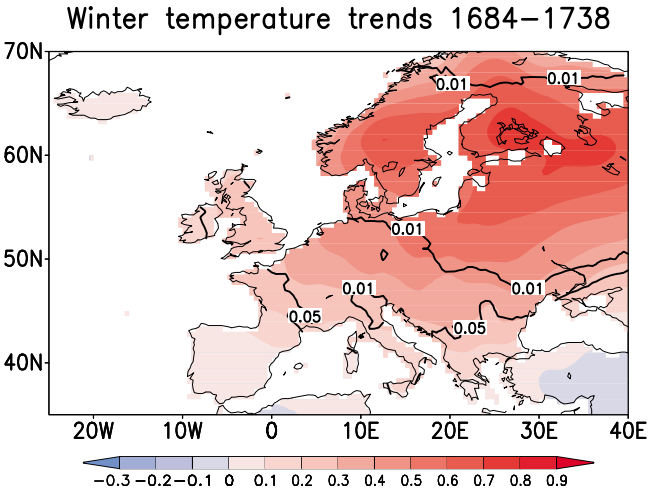

Figure 17. Winter temperature trends (°K decade^{-1}) from 1684 to 1738. The thick solid lines represent the 95% and 99% confidence levels (error probabilities of 0.05 and 0.01, respectively) using a Mann-Kendall trend test. Except for the Mediterranean area, the warming trends are statistically significant over the whole of Europe. From *Luterbacher et al.* [2004]. Reprinted with permission from AAAS.

2007]. These same studies and others [e.g., *North and Stevens*, 1998] also concluded that most of the warming in the latter twentieth and early 21st centuries was due to increasing GHGs that have overwhelmed any natural changes in solar forcing. Results for the past 20 years continue to indicate that solar forcing is playing at most a weak role in current global temperature trends [*Lockwood and Fröhlich*, 2007]. There have been controversial suggestions of much larger solar control of global temperatures [*Friis-Christensen and Lassen*, 1991; *Svensmark and Friis-Christensen*, 1997], but these have been severely criticized on the basis of their statistical approach [*Laut*, 2003; *Damon and Laut*, 2004].

3.4.4. Maunder Minimum

[79] Since the pioneering work of *Eddy* [1976] on the Maunder Minimum period, much more detailed work has been done on the climate change in Europe during this pronounced solar minimum. In historical temperature reconstructions, enhanced solar irradiance is correlated with a shift toward a positive NAO index (see section 3.2.3) and vice versa for reduced solar irradiance periods such as the Maunder Minimum [*Waple et al.*, 2002; *Mann et al.*, 2009]. There is also a distinct shift to the positive NAO index in the 1–2 years immediately following large tropical volcanic eruptions [*Shindell et al.*, 2004]. Enhanced solar irradiance and large volcanic eruptions both lead to continental Europe warming through enhanced westerlies associated with the positive shift of the NAO. However, long-term solar forcing appears to dominate over volcanic eruptions, which induce a more homogeneous hemisphere-wide cooling.

[80] Analysis of early surface pressure data from Europe is also consistent with enhanced northeasterly winds associated with a negative NAO index during the Maunder Minimum [*Wanner et al.*, 1995; *Slonosky et al.*, 2001; *Luterbacher et al.*, 2001; *Xoplaki et al.*, 2001]. Ocean sediment cores also support a shift toward a negative NAO during the Maunder Minimum [*Keigwin and Pickart*, 1999]. Increased solar irradiance through the first half of the eighteenth century might also have induced a shift toward a positive NAO/AO index, suggested by independent proxy NAO reconstructions [*Luterbacher et al.*, 1999, 2002; *Cook et al.*, 2002]. Unforced variability in the NAO/AO is large, however, which is one reason why solar irradiance accounts for only a modest portion of the total variability in this pattern. For example, solar irradiance estimates stayed at relatively high values until the turn of the nineteenth century, whereas NAO/AO index reconstructions and European winter and spring temperatures indicate lower values [*Luterbacher et al.*, 2004; *Xoplaki et al.*, 2005].

[81] *Luterbacher et al.* [2004] report a cooling trend in Europe during the early Maunder Minimum, followed by a strong warming trend in winter over Europe between 1684 and the late 1730s (see Figure 17). Such an intense increase in European winter temperature over a comparable time period has not been observed at any other time in the 500 year record. The spatial trend map indicates particularly strong trends over Scandinavia and the Baltic region of up to 0.8 K decade^{-1}. Climate reconstructions for Europe in springtime back to 1500 A.D. using multiproxy climate data [*Xoplaki et al.*, 2005] also show a strong increase in wintertime temperature at around the same time as that shown in Figure 17. This also agrees with seasonally resolved NH temperature reconstructions based on borehole data [*Harris and Chapman*, 2005]. In addition, *Pauling et al.* [2006] found a European-wide increase in winter precipitation for the same period. These large changes in temperature and precipitation also had implications for glaciers in Scandinavia. *Nesje and Dahl* [2003] suggest that the rapid glacial advance in the early eighteenth century in southern Norway was mainly due to increased winter precipitation and mild winters related to the strong positive NAO trend. A comparison of recent mass balance records and glacier fluctuations in southern Norway and the European Alps suggests that the asynchronous "Little Ice Age" maxima in the two regions may be attributed to multidecadal trends in the north–south dipole NAO pattern. Hence, there is ample evidence that reduced solar irradiance during the Maunder Minimum modulated the NAO variability pattern, creating distinct shifts in European temperatures, winds, and precipitation. Similar, but oppositely signed, changes are likely to have taken place during the medieval period of comparatively enhanced irradiance [*Mann et al.*, 2009; *Trouet et al.*, 2009].

3.4.5. Past Millennium and the Holocene

[82] Glaciers advance during periods of low solar activity [*Wiles et al.*, 2004], indicating increased winter precipitation and/or reduced summer temperatures. Similar results have been obtained from tropical Andean glaciers [*Polissar et al.*, 2006]. Studies of Mg/Ca ratios of lacustrine ostracodes (types of crustaceans) in sediments in the northern Great

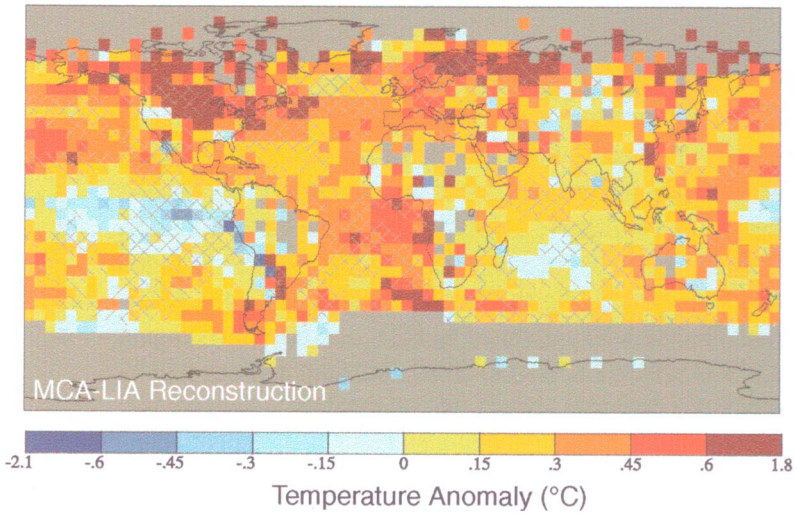

Figure 18. Spatial pattern of surface temperature difference between the Medieval Climate Anomaly and the Little Ice Age derived from proxy-based temperature reconstructions. Reproduced from *Mann et al.* [2009]. Reprinted with permission from AAAS.

Plains [*Yu and Ito*, 1999] provide an indication of water temperature and evaporation/precipitation balance and suggest that dry periods coincided with lower solar activity. The abundance of the planktonic foraminifer *Globigerinoides sacculifer* in marine sediments from the western and northern Gulf of Mexico has been used as a proxy for the mean latitudinal position of the ITCZ and suggests that migration of the ITCZ is, in part, linked to solar activity, with a more southerly position of the ITCZ during centennial-scale intervals of low solar activity [*Poore et al.*, 2004]. This result is consistent with that inferred from the Ti content of sediment cores in the Cariaco basin off Venezuela [*Haug et al.*, 2001] and from the northward shift of the ITCZ during 11 year peaks in solar forcing noted in section 3.2.2. A comprehensive review of climate variability and forcings during the past 6000 years is given by *Wanner et al.* [2008].

[83] These proxies and many others from different areas provide consistent evidence that solar grand minima affect climate. At the same time, however, clear differences indicate that solar forcing is only one factor among others and cannot explain the full variance of climate change evident in these proxy records. Furthermore, for example, analyses of lake records from West Africa show opposite results to those from East African lakes, suggesting complex changes in the hydrologic cycle that resulted in a shift in precipitation from the western to the eastern part of the continent during periods of decreased irradiance [*Russell and Johnson*, 2007]. Such changes may result from solar modulation of coupled variability patterns at high and tropical latitudes, such as the NAO and ENSO, in addition to the position of the ITCZ.

[84] Analyses of NH mean temperatures during the last millennium reconstructed from a network of proxies, including ice cores, tree rings, corals, and documentary evidence, as well as reconstructions based on tree rings alone, show substantial correlations with solar forcing at multidecadal time scales [*Weber*, 2005]. Regression of these time series yields a response of 0.2–0.3 K $(\mathrm{W\ m^{-2}})^{-1}$ at multidecadal time scales. The spatial pattern of the centennial-scale response shows a distinct regional surface temperature response [*Waple et al.*, 2002; *Mann et al.*, 2009], as illustrated in Figure 18. The response maximizes at time scales of more than 4 decades and is less for the 11 and 22 year periodicities. The spatial structure resembles that of the AO/NAO, a result also seen in the analyses of *Trouet et al.* [2009] and *Mann et al.* [2009], and also shows an enhanced response in the western Pacific warm pool region.

[85] Studies over the whole Holocene period (past approximately 11,000 years) have also indicated clear links to solar activity [see *Wanner et al.*, 2008, and references therein]. Figure 19 shows three comparisons of climate proxies with solar variability on centennial to millennial time scales, using the ^{14}C production rate as the solar proxy. The ice-rafted debris (Figure 19, top) found in sediment cores of the North Atlantic [*Bond et al.*, 2001] originates from well-defined areas in Greenland, Iceland, and Svalbard where particles are picked up by glaciers moving toward the coast. When the ice melts in the North Atlantic the particles are released and preserved in the sediment. Their amount is therefore a measure of the transport of cooler, ice-bearing surface waters eastward from the Labrador Sea and southward from the Nordic seas, probably accompanied by shifts to strong northerly winds north of Iceland.

[86] The biogenic silica content in Lake Arolik in southwestern Alaska (Figure 19, middle) reflects the sedimentary abundance of diatoms that are single-celled algae. Detailed comparisons with other parameters show that these diatoms play a central role in the primary productivity and are clearly linked to climate parameters such as moisture (precipitation minus evaporation) and atmospheric temperature. The $\delta^{18}O$ from a stalagmite in Oman (Figure 19, bottom) is mainly a proxy for the amount of monsoon precipitation [*Fleitmann et al.*, 2003]. Advances in dating techniques for this type

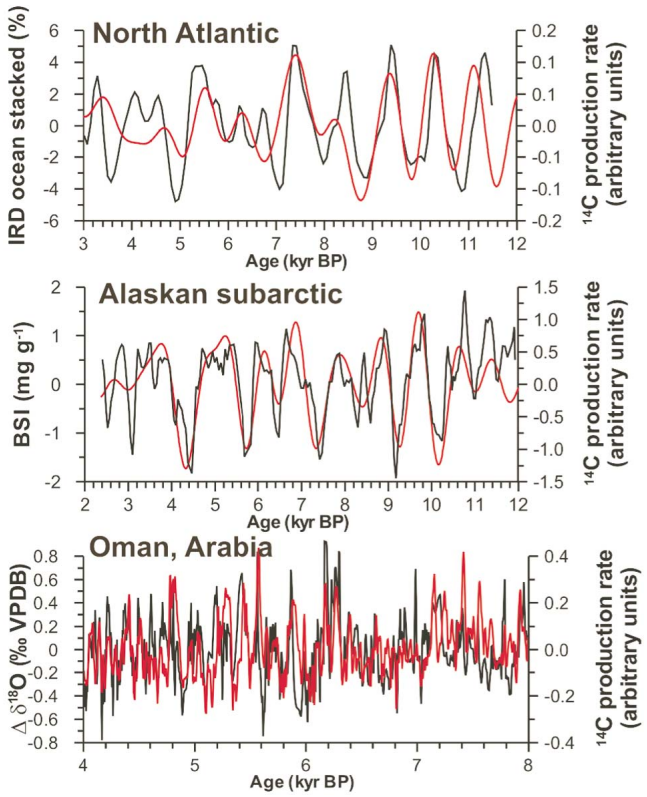

Figure 19. Comparison between the ^{14}C production rate (red curve in each plot) and (top) North Atlantic ice-rafted debris (IRD) [*Bond et al.*, 2001], (middle) biogenic silica (BSi) from Arolik Lake in the Alaskan subarctic [*Hu et al.*, 2003], and (bottom) detrended stalagmite δ^{18}O record from southern Oman [*Fleitmann et al.*, 2003]. Minima in solar activity (higher ^{14}C production rates) coincide with greater extent in sea ice in the North Atlantic (positive IRD values), wetter and colder conditions in the Alaskan subarctic (more negative BSi values), and reduced monsoon precipitation in southern Oman (more positive δ^{18}O values).

of record allow extremely good temporal resolution and accuracy of dating.

[87] All three paleorecords provide clear evidence for a centennial to millennial solar signal in various climate proxies, provided that the proxy is suitable and comes from a sensitive site. It is important to note that some of the climate records are based on rather weak age models consisting of only a couple of ^{14}C dates, which can lead to some shifts between the well-dated forcing function (^{14}C production rate) and the climate proxy.

[88] In summary, a suite of high- and low-latitude paleoclimatic records suggests a drop in air temperatures associated with reduced solar activity [e.g., *van Geel et al.*, 1996; *Björck et al.*, 2001; *Hannon et al.*, 2003; *Hu et al.*, 2003; *Mangini et al.*, 2005; *Wiles et al.*, 2004]. The spatial reconstructions based on proxy networks [cf. *IPCC*, 2007], however, show that while some regions cooled, others warmed [*Waple et al.*, 2002], confirming that proxy records from different locations do not show similar changes. In the case of precipitation the observed pattern is less consistent, especially at middle and high latitudes, although a shift in monsoon precipitation is suggested by numerous paleoclimate records [*van Geel et al.*, 1998; *Black et al.*, 2004; *Dykoski et al.*, 2005; *Fleitmann et al.*, 2003; *Hong et al.*, 2001; *Wang et al.*, 2005; *Zhang et al.*, 2008], possibly associated with an increase in tropical precipitation maxima [*Meehl et al.*, 2008]. There is also the possibility that a modulation of ENSO may be important [*White and Liu*, 2008b], as well as shifts in large-scale temperature and precipitation associated with the overall global forcing [e.g., *Graham et al.*, 2007].

4. MECHANISMS

[89] As described in section 1, there are two broad categories of solar forcing mechanisms, involving solar irradiance variations and the modulation of corpuscular radiation. In both of these cases the forcing is likely to be very small. However, even a very weak forcing can cause a significant climate effect if it is present over a long time or if there are nonlinear responses giving amplifying feedbacks. Figure 20 shows an overview of the various solar processes that give rise to these irradiance and corpuscular radiation variations (see also section 2). In Figure 21, an overview is given of the proposed mechanisms for transfer of these solar-induced variations to the Earth's surface where they can influence our weather and climate. Each of the processes is described in more detail in sections 4.1–4.4.

[90] Much of the evidence for solar influence on climate presented in section 3 relies on simple statistical associations, such as correlation coefficients, which suggest a link but are not sufficient to indicate any causal mechanism. In addition, there is substantial internal variability in the climate system, and the observed record is only one realization of the possible responses. This presents a substantial challenge when trying to test mechanism hypotheses.

[91] The detection of a solar signal in climate depends strongly on how the climate system responds to a particular forcing. Since the climate system may react in a nonlinear way the response function can be quite different from the forcing function. The only way to overcome this problem is to employ appropriate climate models. In spite of the fact that present climate models are far from perfect they have the potential to simulate the spatial and temporal variability of the climate system as a result of a particular forcing mechanism, and many simulations (multiple ensembles) can be carried out to assess internal variability. Evaluation of climate models' ability to match the observed pattern of regional sensitivity to solar forcing is an essential step in improving our understanding of solar forcing of climate change.

[92] An important question is how to distinguish between the different mechanisms. The TSI forcing encompasses the UV forcing since both arise from variations in solar irradiance, and it may not at first appear necessary to distinguish between them. However, as noted in section 1, energy from the different parts of the solar spectrum is absorbed at different heights above the Earth's atmosphere (see Figure 3).

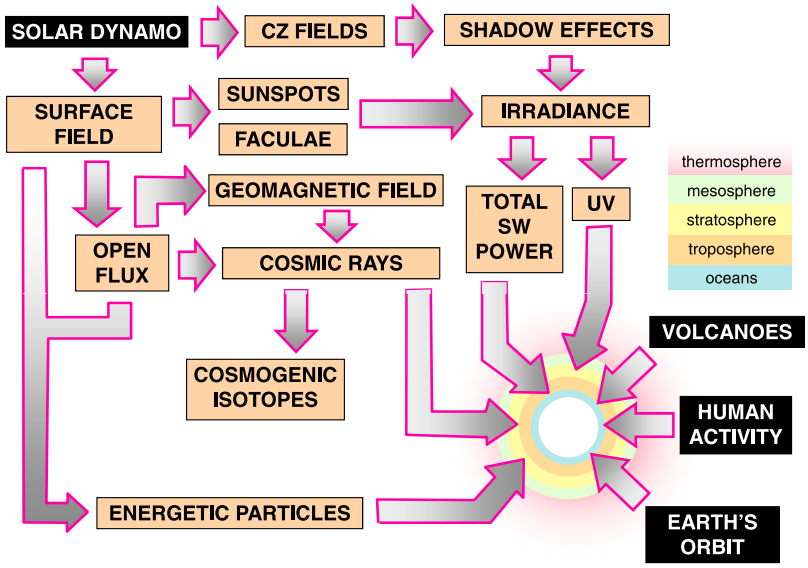

Figure 20. Schematic overview showing various climate forcings of the Earth's atmosphere, with factors that influence the forcing associated with solar variability (irradiance and corpuscular radiation) shown in more detail on the left-hand side, as discussed in section 2.

Changes in TSI can directly impact the surface (see Figure 21), while changes in UV directly impact the stratosphere, so that indirect stratosphere-troposphere coupling mechanisms are required for these stratospheric changes to impact the surface. It is therefore necessary to distinguish between these mechanisms, in order to determine which of them is required in climate models to accurately simulate the past, current, and future climate.

[93] Most current climate models include a representation of TSI variations, but their upper boundary does not extend sufficiently high to fully resolve the stratosphere, so most do not include the UV influence. Hence, the primary solar influence mechanisms in these models are ocean heat uptake and SST changes, which affect evaporation and low-level moisture in the atmosphere. This mechanism is often referred to as the bottom-up mechanism and is described in more detail in section 4.1.

[94] Atmospheric models that include a good representation of the stratosphere, including interactive ozone chemistry, are available, but they do not generally include a fully coupled ocean at present. The prime solar mechanism for influence in these models is therefore the change in stratospheric temperatures and winds due to changes in UV irradiance and ozone production, and the influence on the

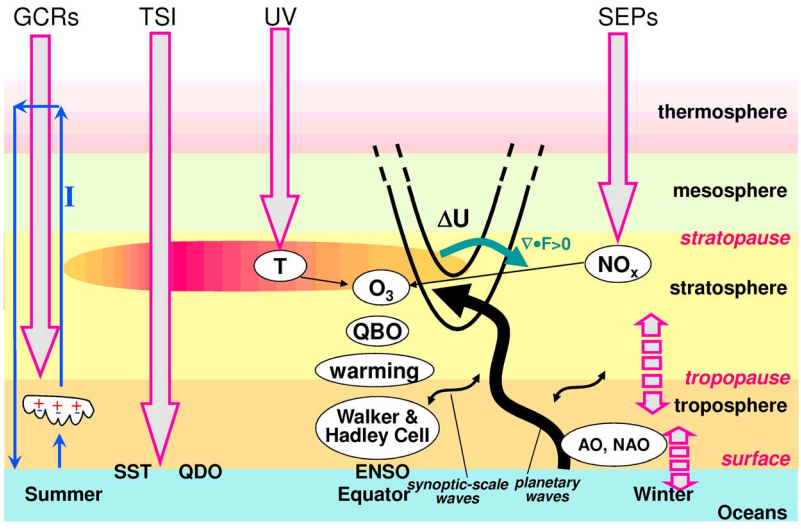

Figure 21. Schematic diagram of solar influence on climate based on *Kodera and Kuroda* [2002]. Shown are the direct and indirect effects through solar irradiance changes (TSI and UV) with respect to S_{max} as well as corpuscular radiation effects (energetic particles and GCRs). The two dashed arrows denote the coupling between the stratosphere and the troposphere and the coupling between the ocean and the atmosphere.

underlying troposphere and surface climate involves stratosphere-troposphere coupling processes. This mechanism is often referred to as the top-down mechanism (see section 4.2). Comparison of results from these two types of models can help assess the contribution from the two mechanisms.

[95] However, recent recognition of the influence of stratospheric processes on climate in general [*Baldwin and Dunkerton*, 2001] has prompted the vertical extension of coupled ocean-atmosphere climate models to include the stratosphere, so that fully coupled ocean-troposphere-stratosphere climate and Earth system models are now becoming available and the TSI (bottom-up) and UV (top-down) influences can be assessed in the same model [e.g., *Meehl et al.*, 2009].

[96] At present, assessment of the various proposed GCR mechanisms is very much in its infancy, and some of the theories are not sufficiently well developed to have been tested even in relatively simple mechanistic models. The horizontal resolution of global climate models is tightly constrained by computing capacity since they must be global in nature and run for hundreds of years. Therefore, they do not resolve clouds explicitly, and inclusion of GCR mechanisms for assessment of their impacts requires careful parameterization [e.g., *Pierce and Adams*, 2009]. Despite this very different level of maturity in the testing of the proposed GCR mechanisms compared with the irradiance mechanisms, as well as suggestions of questionable data analysis in some of the GCR-cloud papers, we nevertheless include a brief review of the various GCR theories for balance and completeness in section 4.4.

4.1. TSI Variations

[97] The most obvious direct effect of solar variability on climate is its influence on the Earth's mean energy balance through variations in TSI. The radiative forcing (RF) has an impact on global mean surface temperature that can be estimated for a given climate sensitivity parameter (see section 1). Because of the large uncertainty in centennial-scale variations in TSI, however, solar radiative forcing of climate *change* is not well established, as discussed further in section 5.

[98] For reasonable climate sensitivities, the ~1 W m^{-2} variation in TSI associated with the 11 year SC translates to an estimated change in temperature at the Earth's surface of a mere 0.07 K (see section 1) and is of the same order of magnitude as observed, e.g., in global mean SST (0.08 ± 0.02 K [*White et al.*, 1997]). Similarly, simple mean energy balance calculations using the long-term centennial-scale TSI change estimates of ~1.3 W m^{-2} (see section 2.3) can explain the order of magnitude changes in global mean temperatures estimated from the various climate proxies (section 3.4.2). However, much of the observational evidence for SC influence in the troposphere and at the surface appears to be regional rather than global in extent. These regional responses are much larger than the global mean values, which suggests that an amplifying mechanism is involved, such as changes in the Hadley and Walker circulations [*Haigh*, 1996; *van Loon et al.*, 2007; *Kodera et al.*, 2007; *Meehl et al.*, 2008, 2009] (see section 3.2.2) and possible associated cloud feedbacks that could decrease clouds and hence increase solar input to some regions of the tropics and subtropics [*Meehl et al.*, 2003, 2008, 2009].

[99] The principal bottom-up mechanism proposed for solar influence on tropical circulations through direct TSI effects at the surface involves solar absorption over relatively cloud-free subtropical oceans, which increases during solar maximum [*Cubasch et al.*, 1997, 2006]. This increases evaporation, and the increased moisture converges into the precipitation zones, which then intensifies the climatological precipitation maxima and associated upward vertical motions, resulting in stronger trade winds, greater equatorial Pacific ocean upwelling, and colder SSTs consistent with stronger Hadley and Walker circulations [*Meehl et al.*, 2003, 2008] (see Figure 22). This strengthened circulation also enhances the subtropical subsidence, resulting in a positive feedback that reduces clouds and thus further increases solar forcing at the surface [e.g., *Meehl et al.*, 2008, 2009].

[100] However, in a series of diagnostic thermal budget studies of SST and ocean heat storage, *White et al.* [2003] and *White* [2006] concluded that the observed 11 year SC signals in SSTs could not be explained solely by this bottom-up direct impact of radiative forcing at the surface (~0.15 W m^{-2}). They showed that the temperature anomalies in the tropical lower troposphere were warmer than the tropical upper ocean anomalies and that these anomalies increased upward, from ~0.2°C in the tropical lower troposphere to ~0.5°C in the tropical middle to upper troposphere and ~1°C in the tropical lower stratosphere. This anomalous lapse rate was matched by a corresponding downward sensible plus latent heat flux anomaly across the air-sea interface of ~0.5 W m^{-2}, which was larger than the direct solar radiative forcing by a factor of ~3 and also explained the correct phase of the response. This therefore represents a different kind of amplification of the 11 year solar cycle and is not associated with changes in trade wind strength or cloud cover since these did not have the correct magnitude or phase.

[101] This result implies a role for the top-down influence of UV irradiance via the stratosphere. *White et al.* [2003] also noted that time sequences of tropical tropospheric temperatures lead those in the lower stratosphere, which appears to argue against the top-down influence. They suggest, however, that this should not be interpreted as a tropospheric signal forcing a stratospheric response because the stratospheric temperature response appears to be in radiative balance and hence is in phase with the 11 year solar cycle, while the troposphere responds to anomalous heating and advection which peaks during the period leading up to solar maximum and not at the maximum itself. This is a good example of the difficulties and dangers of interpreting observed signals from different parts of the atmosphere and especially in using their time response to try to infer cause and effect.

[102] As noted in section 3.3 the observed SC signal in Pacific SST resembles the ENSO signal, which is the dominant mode of variability in this region. *White et al.*

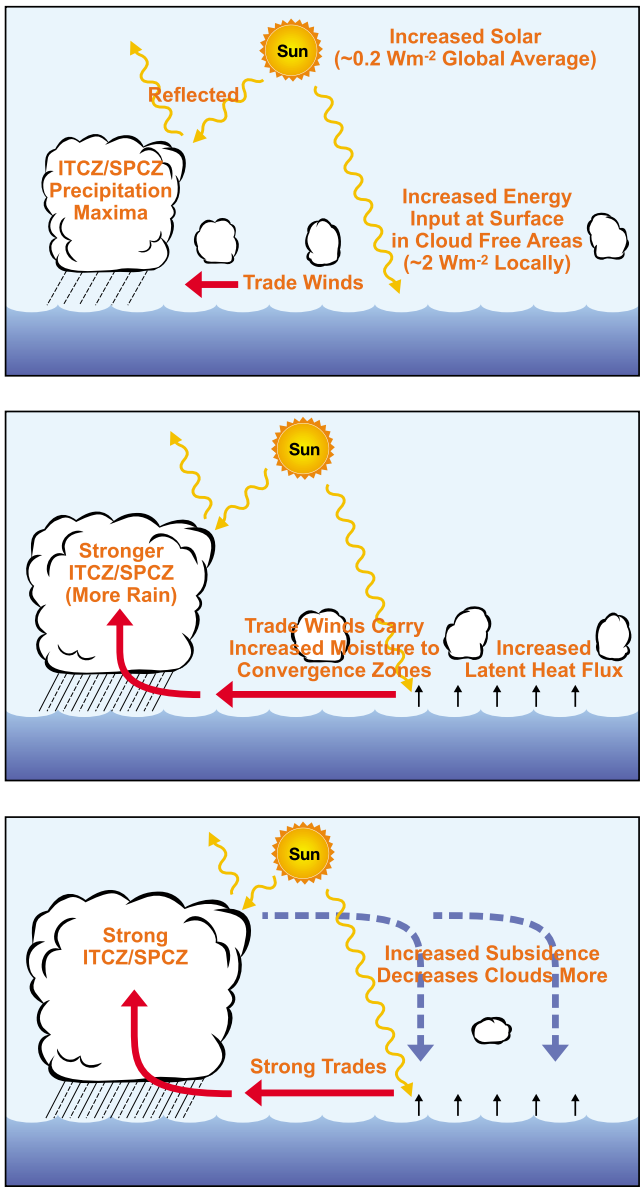

Figure 22. Schematic diagram showing processes involved with the Pacific coupled air-sea response coincident with peak years of solar forcing [after *Meehl et al.*, 2008].

[2003] examined the quasi 11 year oscillation and also the ENSO and QBO signals in global upper ocean temperature and surface wind evolution and proposed that they are governed by a "tropical Pacific delayed action oscillator" [see also *Zebiak and Cane*, 1987; *Graham and White*, 1988; *Schopf and Suarez*, 1988] associated with negative feedback by Rossby waves propagating at different equatorial latitudes. This hypothesis was tested in a fully coupled ocean-atmosphere model by *White and Liu* [2008a], who found that the eastern tropical Pacific warm phase of the 11 year cycle lagged the peak solar forcing by 1–3 years, similar to observations and consistent with a near-resonant excitation by the imposed 11 year SC forcing. In a follow-on study, *White and Liu* [2008b] noted nonlinear phase locking of odd harmonics of equatorial Pacific SSTs that produced La Niña–like conditions coincident with peak solar forcing, followed by El Niño–like conditions a couple of years later as also noted by *Meehl et al.* [2008]. In similar observational [e.g., *van Loon et al.*, 2007; *van Loon and Meehl*, 2008] and coupled general circulation model (GCM) studies [*Meehl and Arblaster*, 2009; *Meehl et al.*, 2008, 2009], La Niña–like conditions align with peaks in ~11 year SC forcing, with lagged El Niño–like conditions a year or two later (see also sections 3.2.2 and 3.3).

4.2. UV Irradiance Variations

4.2.1. Stratospheric Ozone Feedback

[103] Most early stratospheric model studies examined only the response to irradiance variations [e.g., *Wetherald and Manabe*, 1975; *Kodera et al.*, 1991; *Balachandran and Rind*, 1995; *Cubasch et al.*, 1997; *Balachandran et al.*, 1999]. *Haigh* [1994] first noted that the associated stratospheric ozone changes (see, e.g., Figure 10) also need to be included since these will result in further heating increases in the stratosphere and thus modulate radiative forcing of the atmosphere below. Studies that included this feedback mechanism by imposing idealized ozone changes taken from simple 2-D chemistry models [e.g., *Haigh*, 1999; *Shindell et al.*, 1999, 2001; *Larkin et al.*, 2000; *Rind et al.*, 2002; *Matthes et al.*, 2003; *Haigh*, 2003] reproduced the maximum warming around the equatorial stratopause in Figure 11. They also demonstrated that the SC signal extended down into the troposphere, primarily at subtropical latitudes (see section 4.2.3) [*Haigh*, 1996, 1999]. However, they did not reproduce other features, such as the observed poleward and downward propagation of the signal at polar latitudes [*Matthes et al.*, 2003] or the secondary maximum in the equatorial lower stratosphere (20–30 km). There is general consensus that this latter feature results from transport processes (see section 4.2.2).

[104] More recent improved models with fully interactive stratospheric chemistry have been employed [*Labitzke et al.*, 2002; *Tourpali et al.*, 2003; *Egorova et al.*, 2004; *Rozanov et al.*, 2004; *Shindell et al.*, 2006; *Schmidt and Brasseur*, 2006; *McCormack et al.*, 2007; *Marsh et al.*, 2007; *Austin et al.*, 2007, 2008; *Matthes et al.*, 2007], so that the imposed irradiance variations affect both the radiative heating and the ozone photolysis rates and, additionally, changes in ozone and its transport can feed back onto the diabatic heating. These models are now simulating an improved vertical structure of the annual mean ozone signal in the tropics, including the lower stratospheric maximum. Figure 23 shows the equatorial ozone distributions from an international comparison of simulations by 11 models [*Austin et al.*, 2008]. Although the peak in the upper stratosphere is slightly lower than observed, the simulations are generally within the observational error bars. However, it is still not clear to which factor (SSTs, time-varying solar cycle, or inclusion of a QBO) the improvements can be ascribed. *Marsh and Garcia* [2007] show an aliasing effect of ENSO events in their model that does not appear to be supported in observations [*Hood and Soukharev*, 2010], while *Matthes et al.* [2010] highlight the importance of the QBO for the vertical structure of the solar signal in ozone.

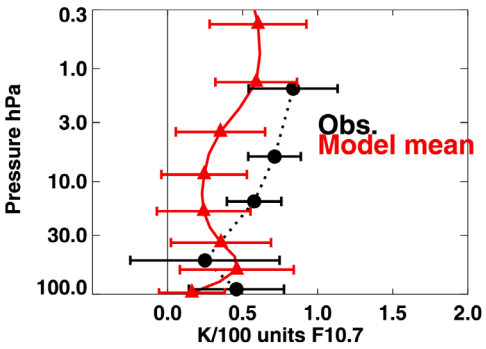

Figure 23. Ozone solar response averaged over 25°S–25°N from a range of different coupled chemistry climate models that included the effect of 11 year SC irradiance variations on radiative heating and photolysis rates (% per 100 units of $F_{10.7}$ flux; multiply by ~1.3 to obtain average estimate over the past three solar cycles). The red line indicates the average of all the modeled estimates. The black line indicates the average of estimates from three independent satellite instruments taken from *Soukharev and Hood* [2006]. All uncertainty ranges are 95% confidence intervals [from *Austin et al.*, 2008].

In addition, Figure 23 is an average from 25°S–25°S and masks the fact that many of the models do not reproduce the latitudinal structure seen in the observations (Figure 10). Hence, despite these general improvements, there are many details that are not reproduced by models. Further studies, including fully coupled ocean-troposphere-stratosphere models with interactive chemistry, will be required to improve the simulated ozone signal and distinguish between the various influences.

[105] Recent measurements of SSI by the SORCE SIM satellite instrument suggest that variations in the UV may be much larger, by a factor of 4–6, than previously assumed [*Harder et al.*, 2009]. If correct, this would imply a very different response in both stratospheric ozone and temperature [*Haigh et al.*, 2010] (see also section 5).

4.2.2. Planetary Wave Feedback

[106] The 11 year SC temperature anomalies of ~1–2 K near the equatorial stratopause (Figure 11), resulting from UV irradiance changes and the ozone feedback mechanism, alter the meridional temperature gradient and hence the wind field through thermal wind balance. *Hines* [1974] suggested a mechanism whereby these wind anomalies could influence the propagation of planetary waves in the winter hemisphere. This suggestion was developed by *Kodera* [1995] [see also *Geller and Alpert*, 1980; *Bates*, 1981; *Geller*, 1988; *Balachandran and Rind*, 1995]. During S_{max} years, a westerly wind anomaly develops in the subtropical upper stratosphere of the winter hemisphere and vice versa in S_{min} years. Planetary wave propagation is sensitive to the background winds, and a positive feedback is suggested through which the wind anomaly moves poleward and downward with time and grows significantly in amplitude [*Kodera and Kuroda*, 2002]. Figure 24 illustrates the time evolution of this poleward-downward propagation of the 11 year SC wind anomaly from a model simulation [*Matthes et al.*, 2006] that compares well with observations.

[107] Through this mechanism the associated changes in planetary wave forcing (as indicated by the Eliassen-Palm

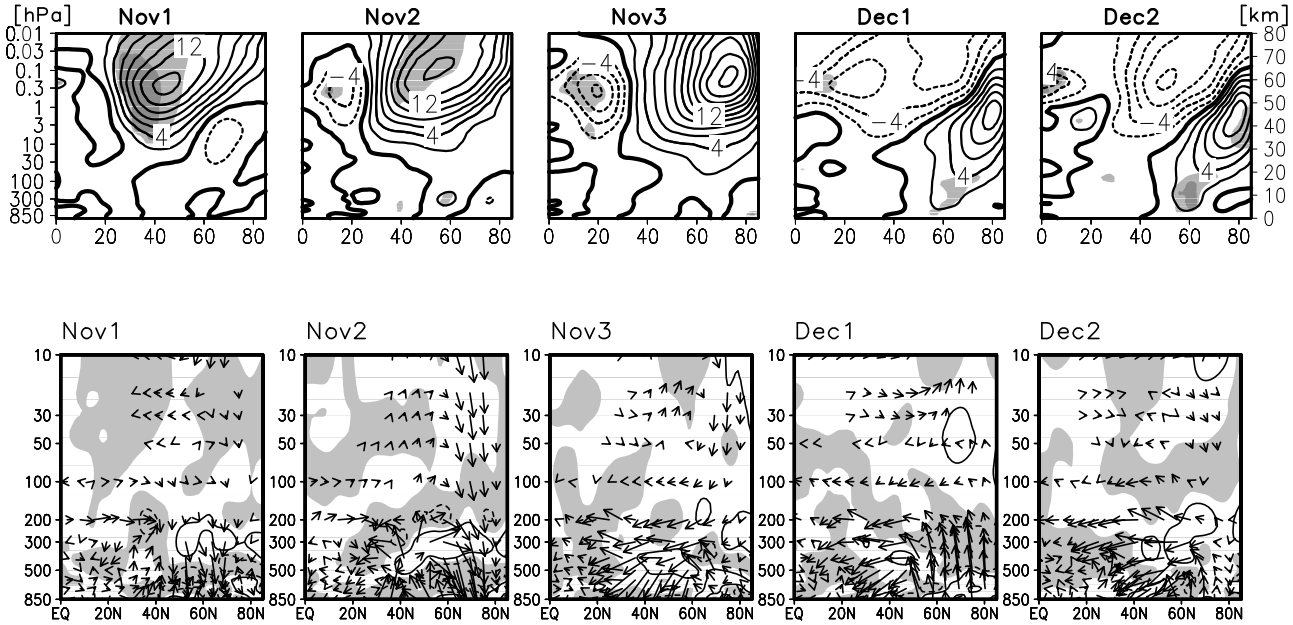

Figure 24. (top) Long-term 10 day mean differences of NH zonally averaged zonal wind between S_{max} and S_{min} from GCM experiments for 1–10 November (Nov1) and 11–20 November (Nov2) through to 11–20 December (Dec2). Contour interval is 2 m s^{-1}. Light (heavy) shading indicates the 5% (1%) significance level calculated with a Student's *t* test. (bottom) Corresponding plots for Eliassen-Palm flux vectors (arrows, scaled by the inverse of pressure) and its divergence. Only the 1 m^{-1} s^{-1} d^{-1} contour is shown; negative values are shaded [from *Matthes et al.*, 2006].

flux divergence $\nabla \cdot F$ in Figure 24) also influence the strength of the large-scale Brewer-Dobson (B-D) circulation. Thus, in S_{max} years the polar winter vortex is less disturbed, the B-D circulation is weaker, and the polar lower stratosphere is colder than average because of the weaker adiabatic heating in the descending arm of the B-D circulation. The converse would be true in S_{min} years. In this way, it has been proposed that a very small temperature anomaly of 1–2 K at the equatorial stratopause can be transferred to the lower polar stratosphere and significantly amplified.

[108] Through the same mechanism, the return upwelling arm of the B-D circulation at the equator would be similarly weakened in S_{max} years, which results in less adiabatic cooling and hence a warmer equatorial lower stratosphere, as seen in Figure 11, with the converse in S_{min} years. This dynamical feedback mechanism also modulates the transport of ozone [*Hood and Soukharev*, 2003; *Hood*, 2004; *Gray et al.*, 2009] as mentioned in section 4.2.1. The weaker B-D circulation in S_{max} years, with reduced upwelling in the equatorial lower stratosphere, would result in positive ozone anomalies in that region and hence produce a positive temperature anomaly through diabatic heating. This feedback mechanism is consistent with the observed lower stratospheric ozone maximum in Figure 10 and would also reinforce the adiabatic temperature mechanism described above. *Matthes et al.* [2004, 2006] included these effects in a model with climatological SSTs so that there could be no solar signal from the oceans and achieved lower stratosphere and troposphere responses that were similar to the observations. However, they did not reproduce the full magnitude, persistence, or latitudinal structures, suggesting that an ocean feedback may also be operating (see sections 4.1 and 4.2.3). Further studies using fully coupled ocean-troposphere-stratosphere models will be required to explore the relative contributions and interactions of the top-down and bottom-up mechanisms.

[109] As already noted in section 3.1.2, observations of 11 year SC variations of the polar lower stratospheric vortex in NH winter are complicated by the QBO (Figure 13), so that anomalously warm polar regions tend to occur in S_{min}–QBO-E and S_{max}–QBO-W. In a series of model and data analysis papers, *Gray et al.* [2001] and *Gray* [2003] suggested that the observed 11 year SC–QBO interaction could be due to the interaction of their respective wind anomalies in the upper equatorial–subtropical stratosphere influencing the development and timing of SSW [*Gray et al.*, 2004, 2006; see also *Hardiman and Haynes*, 2008]. This work was subsequently supported by the modeling study of *Matthes et al.* [2004], which also confirmed the Kodera and Kuroda mechanism of the solar modulation of the polar vortex and the B-D circulation.

[110] The transfer of this SC-QBO interaction in the upper stratosphere to the tropical low latitudes via modulation of the B-D circulation is only one possible explanation for the observed SC-QBO interactions there (see section 3.1.2). Another possible mechanism is a solar modulation of the descent rates of the QBO [*McCormack*, 2003; *Pascoe et al.*, 2005; *Salby and Callaghan*, 2006; *McCormack et al.*, 2007], which occurs entirely within the equatorial region and does not rely on the polar route via SSWs and the B-D circulation. A direct modulation of the descent rate of the QBO may also help to explain the summer hemisphere signal (see Figure 14) since the strength of the subtropical QBO temperature and ozone anomaly depends on the locally induced meridional circulation caused by the descending QBO zonal wind anomaly. The two mechanisms of polar and equatorial solar influence transfer are not mutually exclusive, and both may be operating.

[111] *Cordero and Nathan* [2005] and *Nathan and Cordero* [2007] have also proposed a wave-induced ozone heating mechanism linking the solar signal to the QBO, although *Mayr et al.* [2006] found a solar modulation of the QBO without wave-ozone feedback in their model. This pathway requires testing in future coupled chemistry climate model (CCM) studies. Finally, although wave activity plays a lesser role in the summertime stratosphere, modeling studies suggest that the ozone response to solar UV plays an important role in solar modulation of summer stratospheric circulation as well as in winter [*Lee et al.*, 2008].

4.2.3. Stratosphere Troposphere Coupling

[112] It is clear that variations in solar UV radiation directly influence stratospheric temperatures, and the dynamical response to this heating extends the solar influence both poleward and downward to the lower stratosphere and tropopause region. Evidence that this influence can also penetrate into the underlying troposphere is accruing from a number of different sources. Observational analyses [e.g., *Baldwin and Dunkerton*, 2001; *Kuroda and Kodera*, 2004; *Thompson et al.*, 2005] suggest a downward propagation of NAM anomalies (see section 3.2.3), although *Plumb and Semeniuk* [2003] note that this does not necessarily imply propagation of information in the same direction. Similarly, at equatorial latitudes *Salby and Callaghan* [2005] identified an interaction between the stratospheric B-D circulation and the tropospheric Hadley circulation; Figure 25 shows coherent variation between observed temperatures in the region of the tropical tropopause and tropospheric and polar stratospheric temperatures that are consistent with possible changes in the Hadley circulation, tropical convection, and latent heat release, but again, this does not provide a chain of causality.

[113] Early model studies of UV variations in the stratosphere [*Haigh*, 1996, 1999; *Shindell et al.*, 1999; *Balachandran et al.*, 1999; *Larkin et al.*, 2000] obtained a response in the troposphere even though the near surface in these model runs was constrained by imposed SSTs. The pattern of the zonal wind anomalies was similar to the tropospheric SC response seen in Figure 12. *Shindell et al.* [2006] have confirmed this response using a fully coupled ocean-atmosphere model with interactive stratospheric chemistry. A more detailed analysis showed that while the general response is a strengthening of the Walker circulation and broadening of the Hadley cell, there were substantial seasonal variations in the response and also dependencies on the background greenhouse gas abundance of the atmo-

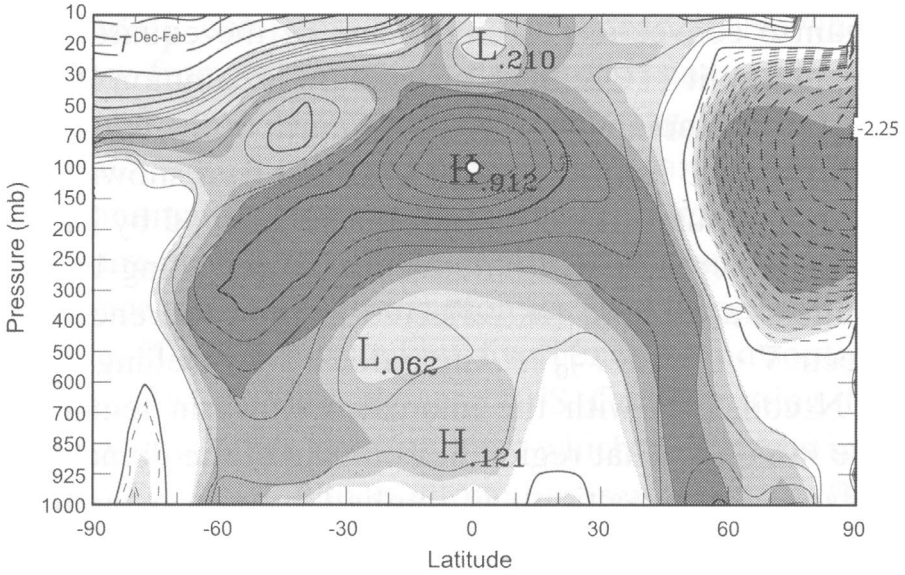

Figure 25. Correlation between observed DJF averaged zonal mean temperature at 100 hPa over the equator with temperatures throughout the troposphere and lower stratosphere [from *Salby and Callaghan*, 2005].

sphere [*Lee et al.*, 2009]. A relatively robust result appeared to be an enhancement of the ascending branch of the Hadley cell and a northward shift of the ITCZ during the boreal winter during increased solar forcing, and this was qualitatively consistent with the observed signal in NCEP reanalysis data.

[114] There are many proposed mechanisms for a downward influence from the lower stratosphere into the troposphere (see reviews by *Shepherd* [2002] and *Haynes* [2005]). These include quasi-instantaneous geostrophic adjustment within the troposphere to changes in the potential vorticity structure of the tropopause region [e.g., *Hartley et al.*, 1998; *Black*, 2002], modification of the refraction [*Hartmann et al.*, 2000] or reflection [*Perlwitz and Harnik*, 2003] of upward propagating planetary-scale waves, and feedbacks between changes in the mean flow and tropospheric baroclinic eddies [*Kushner and Polvani*, 2004; *Song and Robinson*, 2004].

[115] The response to external forcing often has the same spatial structure as, and involves similar eddy mean flow feedbacks to, the dominant pattern of variability, e.g., the annular mode (NAO/AO) signal at middle to high latitudes and the ENSO signal at tropical latitudes. The high-latitude anomaly patterns represent a shift in position and strength of the tropospheric jets. Feedback of these tropospheric zonal wind changes on the tropospheric eddy momentum fluxes appears to be important [e.g., *Polvani and Kushner*, 2002; *Kushner and Polvani*, 2006; *Song and Robinson*, 2004]. Coupling between the Hadley circulation and midlatitude eddies may also play a key part: in a mechanistic study, *Haigh et al.* [2005] obtained a zonal mean tropospheric response, qualitatively similar to the observed 11 year SC response, by imposing anomalous diabatic heating in the low-latitude lower stratosphere (see Figure 26). Consistent with this, the enhanced Hadley circulation response in the coupled chemistry simulations of *Shindell et al.* [2006] was linked to the additional heating in the upper tropical troposphere and lower stratosphere relative to simulations with fixed ozone. *Simpson et al.* [2009] have shown that it is the response of the eddy momentum fluxes to changes in structure of the tropopause region that drives this tropospheric response.

[116] In the GCM studies by *Matthes et al.* [2006] and *Meehl et al.* [2009], the response in tropical vertical velocity was not uniformly distributed in longitude but was largest over the Indian and West Pacific oceans, indicating an influence on the Walker circulation similar to that found in observations [*Kodera*, 2004; *Kodera et al.*, 2007]. The model reproduced these signals despite having imposed SSTs, suggesting that their tropospheric signal was a response to changes in the stratosphere and not to the bottom-up mechanism of TSI heating of the ocean surface (see section 4.1). The weakened ascent during S_{max} in the zonally averaged equatorial troposphere may result from the increased static stability in the tropopause region suppressing equatorial convection but allowing enhanced off-equatorial convection in the climatological precipitation maxima [*Kodera and Shibata*, 2006; *Matthes et al.*, 2006]. This would be consistent with the results of *Salby and Callaghan* [2005] (see Figure 25), whose analysis suggested that the stratosphere and troposphere are linked by a large-scale transfer of mass across the tropopause resulting in a coupling of the B-D circulation in the stratosphere and the tropical Hadley circulation in the troposphere. However, as discussed in section 4.2.2, this does not preclude the possibility that there is an additional positive feedback from the oceans so that both top-down and bottom-up mechanisms are acting in the real world.

[117] In addition to the observed ENSO-like SC response in SSTs in the Pacific Ocean, *Kodera* [2004] found a SC modulation of Indian monsoon circulations and suggested

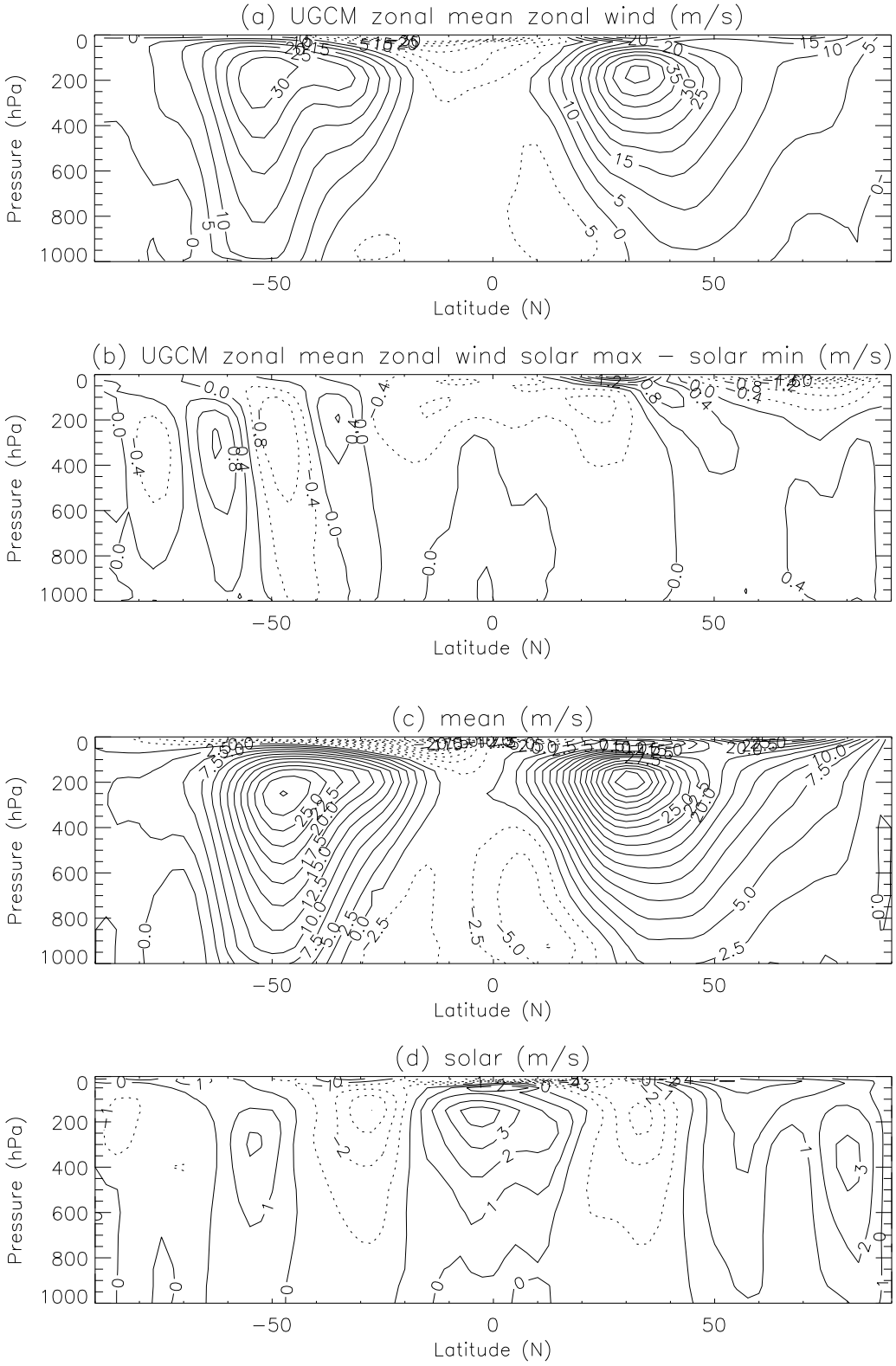

Figure 26. Zonally averaged zonal wind fields from (a) January climatology from the GCM experiment of *Haigh and Blackburn* [2006], (b) solar signal from the GCM experiment, (c) NCEP reanalysis annual mean for 1979–2002, and (d) solar signal from multiple regression analysis of the NCEP data (reprinted from *Haigh and Blackburn* [2006] with kind permission of Springer Science and Business Media).

that stratospheric circulations may suppress equatorial convection in S_{max} years with an enhancement of the off-equatorial monsoon precipitation over India. *Kodera et al.* [2007] further suggest a coupling between the Pacific ENSO and Indian Ocean Dipole, with a SC modulation of the extension of ENSO into the Indian Ocean associated with a shift in location of the descending branch of the Walker circulation. Much work is still required to fully characterize the nature of these complicated interactions and hence to verify these mechanisms. Finally, *Meehl et al.* [2009] note that the top-down and bottom-up mechanisms both act together in the same sense to intensify the climatological precipitation regimes in the tropics, thus adding together and reinforcing each other to produce a larger response in the troposphere than either one alone.

[118] Although details of the mechanisms involved are still not fully established, it is becoming increasingly clear that the top-down mechanism whereby UV heating of the stratosphere indirectly influences the troposphere through dynamical coupling is viable and may help to explain observed regional signals in the troposphere.

4.3. Centennial-Scale Irradiance Variations

[119] The majority of model studies of multidecadal effect of TSI on climate employ "low-top" models that do not include a representation of the stratosphere and hence primarily capture only the bottom-up mechanism described in section 4.1. Early studies [*Cubasch et al.*, 1997; *Rind et al.*, 1999; *Cubasch and Voss*, 2000] found that the 11 year SC, even though present in the forcing, was rarely seen in the modeled response, but a response to the 70–80 year Gleissberg cycle was seen in the near-surface temperature. Because of this, the earlier coupled ocean-atmosphere model studies of solar impact have concentrated on long-term climate, e.g., over the last 100–1000 years, and addressed the question of whether historically documented climate events like the Medieval Warm Period or the Little Ice Age could be simulated. The model simulations are then compared to the climate variations experienced today, and predictions are made for the future [*Ammann et al.*, 2003; *Ammann*, 2005; *Zorita et al.*, 2004; *Stott et al.*, 2000, 2003; *Stendel et al.*, 2006; *Goosse et al.*, 2006].

[120] In an extension to these low-top model studies, *Shindell et al.* [2001, 2003] employed a high-top stratosphere-resolving atmospheric model coupled to a mixed layer ocean. They found a tropical-subtropical warming during increased solar activity which induces a warmer tropical upper troposphere via moist convective processes. The sunlit portion of the stratosphere also warms because of the increased UV irradiance and the ozone feedback mechanism. These processes led to an increased latitudinal temperature gradient in the vicinity of the tropopause during the extended cold season, resulting in enhanced lower stratosphere westerly winds, causing increased angular momentum transport to high latitudes and enhanced tropospheric westerlies. This dynamical response in the lower stratosphere was enhanced by roughly a factor of 2 by the interaction between UV radiation and ozone in the upper stratosphere, indicating a downward propagation of stratospheric influence, as described in section 4.2.

[121] According to this model, prolonged periods of reduced solar activity (e.g., the Maunder Minimum) are associated with pronounced cooling over middle- to high-latitude continental interiors, also confirmed by *Langematz et al.* [2005]. Enhanced solar irradiance increases mid-latitude sea level pressure, generating enhanced westerly advection of relatively warm oceanic air over the continents and of cooler air from continental interiors to their eastern coasts [*Shindell et al.*, 2003]. This effect is most pronounced in the cold season. Most recently, a set of ensemble simulations using a fully coupled ocean-troposphere-stratosphere model including parameterized chemical responses to solar forcing (derived from a full chemistry model) was performed for the past 1000 years and compared with multi-proxy reconstructions [*Mann et al.*, 2009]. This comparison showed that the model was able to capture many features of the northern extratropical surface temperature change between the medieval period and the Little Ice Age seen in the proxy data but could not capture the equatorial responses. Interestingly, a low-top version (i.e., with a poorly resolved stratosphere) of another GCM without chemistry was unable to capture the responses in either area. Variations between ensemble members were large, suggesting that patterns in a single period of time (e.g., the Little Ice Age) may contain a substantial contribution from internal, unforced variability. However, both the model and the proxy reconstructions showed pronounced warming in the medieval period relative to the Little Ice Age over much of North America and northern Eurasia.

[122] Other multiproxy climate reconstructions (see section 3.4) show similar spatial structures in correlations of NH extratropical surface temperatures and solar output reconstructions [*Waple et al.*, 2002; *Luterbacher et al.*, 2004; *Xoplaki et al.*, 2005]. As the modeled response to solar forcing shows areas of both regional cooling and warming, the hemispheric or globally averaged changes are comparatively small. This result is also consistent with the small amplitude of surface temperature variations during the last millennium in most reconstructions for these spatial scales [*Briffa et al.*, 1998; *Mann et al.*, 1999; *Jones et al.*, 2003; *Mann et al.*, 2009].

[123] It appears, therefore, that observational climate evidence from Europe supports the modeled connection between solar forcing and modulation of extratropical variability via the NAO/AO/NAM pattern [*Shindell et al.*, 2001, 2003; *Ruzmaikin and Feynman*, 2002; *Tourpali et al.*, 2003; *Egorova et al.*, 2004; *Stendel et al.*, 2006], though *Palmer et al.* [2004] did not find such a link in their model. Solar irradiance changes at multidecadal time scales might therefore have been a major trigger to explain regional temperature anomalies over Europe and central and eastern North America such as the Medieval Warm Period and the Maunder Minimum cold period and might have contributed substantially to the more recent increases in European winter and spring temperatures and precipita-

tion and the connected exceptional growth of western Scandinavian glaciers.

[124] A somewhat different analysis of the influence of longer-term solar variations is presented by *Clement et al.* [1996]. They suggest that heating over the entire tropical region will result in the Pacific warming more in the west than the east because the strong ocean upwelling and surface divergence in the east moves some of the heat poleward, strengthening the east–west equatorial SST gradient, though this mechanism does not take into account effects of clouds that produce nonspatially uniform solar forcing at the surface in the tropics. *Emile-Geay et al.* [2007] find a similar response to variations in solar irradiance over the Holocene. Modulation of ENSO by solar forcing appears to be consistent with at least some paleoclimate evidence, especially for the Americas, where multiple proxies such as fire scars, lake varves (stratified deposits of glacial clay), tree rings, etc., indicate correlations between precipitation and solar irradiance that are similar to ENSO-related precipitation anomalies [*Graham et al.*, 2007]. As discussed in section 3.2.2, a mechanism of coupled atmosphere-ocean response to solar forcing in the tropical Pacific has been proposed [e.g., *Meehl et al.*, 2003, 2008]. Additionally, the UV-ozone feedback mechanism appears to cause enough heating near the tropical tropopause to significantly affect the tropical hydrologic cycle, with regional impacts on precipitation that are also broadly similar to those related to ENSO changes [*Shindell et al.*, 2006]. Thus, the two mechanisms may operate together to create the tropical-subtropical response to solar forcing with associated amplifying cloud feedbacks [*Meehl et al.*, 2009].

4.4. Charged Particle Effects

[125] Changes in energetic particle fluxes (EPP) (including electrons as well as ions of all species and covering particles of both solar/heliospheric and galactic origin) are prominent in the upper atmosphere. In particular, SEP events, often referred to as SPEs (see section 1), occur infrequently and generally last a few days. They produce high-energy particles precipitating into the thermosphere, mesosphere, and upper stratosphere at high geomagnetic latitudes. The resulting ionization and dissociation substantially influence chemical constituents (HO_x, NO_x, and ozone) in the polar middle atmosphere on time scales of days to months [*Jackman et al.*, 2006]. As well as this direct effect of SEPs, there is also an indirect effect on the stratosphere from less energetic SEPs and energetic magnetospheric electrons whose energy is deposited mainly in the thermosphere and upper mesosphere. The resulting EPP-NO_x can be transported by polar downwelling into the winter polar stratosphere, where it can influence ozone abundances [*Solomon et al.*, 1982; *Callis et al.*, 1996; *Siskind and Russell*, 1996; *Randall et al.*, 1998, 2005, 2006; *Siskind et al.*, 2000]. At high latitudes, at least in the Southern Hemisphere (SH) polar vortex, which is relatively strong and stable, observations have established that interannual variability of NO_x in spring correlates well with the geomagnetic *Ap* index (see Figure 1), which can be interpreted as a proxy measure of EPP [*Randall et al.*, 1998, 2007; *Siskind et al.*, 2000], and up to 10% of the total SH NO_x has been attributed to EPP-NO_x [*Funke et al.*, 2005; *Randall et al.*, 2007]. However, this external NO_x influence appears to be confined to the polar vortex region so that its overall contribution to the stratospheric ozone 11 year signal is likely to be relatively small.

[126] While it is relatively well established that the indirect EPP-NO_x mechanism can significantly perturb ozone abundances in the SH polar vortex at levels above ~10 hPa, it is much less clear that these ozone perturbations produce detectable changes in temperature and circulation. A recent study of ERA-40 reanalysis data by *Lu et al.* [2008], for example, finds some evidence for polar temperature and zonal wind variations that correlate with the *Ap* index. However, the inferred temperature and wind variations have a sign that is opposite to that expected from the EPP-NO_x mechanism; in addition, the detected signals are at least as strong in the NH as in the SH, which is unexpected in view of the observed, stronger NO_x responses in the SH.

[127] Similarly, there is currently little clear evidence that EPP-NO_x can significantly perturb the stratosphere outside of the polar vortices, except perhaps during the very largest events [*Thomas et al.*, 2007; *Damiani et al.*, 2006; *Ganguly*, 2010]. Some sensitivity studies using CCMs suggest that EPP-NO_x effects on ozone at low latitudes may be comparable to the effects of solar UV radiation [*Callis et al.*, 2000, 2001; *Langematz et al.*, 2005; *Rozanov et al.*, 2005]. However, analysis of UARS Halogen Occultation Experiment (HALOE) NO_x data over a 12 year period indicates no decadal NO_x variations at low latitudes that could significantly affect the solar cycle variation of global ozone, and this conclusion is consistent with a more recent CCM simulation by *Marsh et al.* [2007]. In summary, there is currently little evidence that the EPP-NO_x mechanism has a sufficient influence on stratospheric ozone and circulation that could significantly perturb tropospheric climate.

[128] GCRs generate ions throughout the troposphere down to the surface. GCRs are modulated by the solar wind, so that atmospheric processes influenced by, or dependent on, cosmic ray ion production might also show solar modulation [*Ney*, 1959]. These processes include current flow in the global atmospheric electrical circuit, charging of atmospheric aerosol particles and cloud edge water droplets, and the nucleation of ultrafine condensation nuclei (UCN) from trace vapors. For these processes to affect climate they must exert an appreciable influence on the atmosphere's radiative properties. There is a small direct infrared absorption by cluster ions in the atmosphere [e.g., *Aplin*, 2008], but as aerosol and cloud droplets are known to have large radiative influences, effects of cosmogenic ions on clouds and aerosols have so far received the most attention. In particular, the growth of UCN to sufficient sizes to permit cloud droplet formation (as CCN) has been suggested as a mechanism for a possible cosmic ray–cloud dependence (see also section 3.2.4), though this effect has been shown in a climate model study to be much smaller than observed changes in clouds would suggest [*Pierce and Adams*, 2009].

[129] It is important to emphasize that direct condensation of water on ions, as occurs in the Wilson cloud chamber at very high water supersaturations, will not occur in the atmosphere because natural supersaturations are too small [*Mason*, 1971]. Ion-induced particle formation is usually taken to mean the formation of UCN from the gas phase, in which ions take a direct (e.g., by enhancing molecular clustering) or indirect (e.g., by charge stabilizing a molecular cluster) part, usually in the initial stages. UCN are typically a few nanometers in diameter, which is too small to influence cloud droplet condensation at atmospheric supersaturation. Growth of UCN to ~100 nm diameter is required for them to become effective cloud condensation nuclei, which occurs on time scales of many hours. Direct observations have been made of the growth of ions in surface air [*Hõrrak et al.*, 1998] and the growth of cosmogenic ions in the upper troposphere [*Eichkorn et al.*, 2002]. A related mechanism under active investigation is the formation of particles via the clustering of a condensable vapor (generally sulphuric acid) with water [*Yu*, 2002; *Kazil and Lovejoy*, 2004], including through a substantial international laboratory study [*Duplissy et al.*, 2009].

[130] Simple model estimates of ion-induced particle production have been made under ambient conditions appropriate to the troposphere over the oceans [*Kazil et al.*, 2006]. In the tropical lower troposphere these simulations predicted negligible charged and neutral nucleation of H_2SO_4 and H_2O, even in the absence of preexisting aerosol. At midlatitudes the charged nucleation exceeded neutral nucleation as long as the preexisting aerosol concentration was depleted, e.g., following precipitation. An upper limit of 0.24 W m^{-2} was estimated for the change in daily mean shortwave radiative forcing between S_{max} and S_{min} from charged nucleation cloud cover changes. This upper limit is much smaller than the value of 1.2 W m^{-2} proposed by *Marsh and Svensmark* [2000] for the period 1983–1994 but closer to the value of *Kristjánsson and Kristiansen* [2000], who found radiative forcing reduced by 0.29 W m^{-2} in the 1986 S_{min} period compared with the 1990 S_{max} period, using the same satellite cloud data as Marsh and Svensmark.

[131] An alternative mechanism has been suggested via currents flowing in the global atmospheric electrical circuit [*Chalmers*, 1967; *Rycroft et al.*, 2000]. The combination of finite air conductivity, charge separation in disturbed weather regions, a conducting planetary surface, and a conductive lower ionosphere permits current flow between "disturbed" and "fair weather" regions [*Rycroft et al.*, 2008]. In fair weather regions, where there is no appreciable local charge separation, the vertical global circuit current density is about 2 pA m^{-2}. This "conduction current" occurs globally in the fair weather atmosphere and has been directly observed for over a century [*Wilson*, 1906; *Burke and Few*, 1978; *Harrison and Ingram*, 2005; *Bennett and Harrison*, 2008]. Modulation of the global circuit by solar-induced changes in GCR ionization [*Markson*, 1981] provides a conceivable route by which solar changes can be communicated to the lower atmosphere [*Tinsley et al.*, 1989; *Tinsley*, 2000]. Evidence for modulation of the conduction current by solar activity exists in balloon measurements obtained between 1966 and 1977 [*Markson and Muir*, 1980], continuing in surface measurements between 1978 and 1985 [*Harrison and Usoskin*, 2010].

[132] Studies of the effect of the conduction current density on clouds have concentrated on the edges of horizontal layer clouds, where sharp gradients in air conductivity can occur, causing space charge to be accumulated [*Chalmers*, 1967; *Gunn*, 1965; *Zhou and Tinsley*, 2007]. A necessary requirement is that the current density passes through such layer clouds, which has been demonstrated in recent work [*Nicoll and Harrison*, 2009; *Bennett and Harrison*, 2009]. Charge inhibits evaporation and influences particle-particle and droplet-particle collisions. Importantly, particle and droplet collection processes are not polarity dependent at small separations because of induced electrostatic image forces [*Tinsley et al.*, 2000; *Khain et al.*, 2004]. Two different mechanisms have been proposed which employ the attractive forces of image effects. In "electroscavenging" the collision efficiency of charged particles with liquid droplets is thought to be electrically enhanced [e.g., *Tinsley et al.*, 2001; *Tripathi et al.*, 2006], and for supercooled water clouds, electroscavenging could increase freezing by enhancing the rate of contact nucleation [*Harrison*, 2000; *Tinsley et al.*, 2000; *Tripathi and Harrison*, 2002]. Second, the increased charge could influence droplet size (or number), either through facilitating droplet formation and diffusive growth or through an increase in droplet-droplet coalescence, neither of which is restricted to supercooled clouds [*Harrison and Ambaum*, 2008, 2009; *Khain et al.*, 2004; *Kniveton et al.*, 2008].

[133] The development of approaches to discriminate between irradiance and cosmic ray effects is important. GCRs are so closely correlated with solar activity (see section 3.2.4) that observed variability in LCA correlates equally well with GCRs, TSI, or solar UV irradiances, and therefore, observed variations cannot be uniquely ascribed to a single mechanism [*Kristjánsson et al.*, 2002]. On time scales of days, sudden reductions can occur in GCRs (Forbush decreases), but as described in section 3.2.4, there is little evidence that these events are apparent in cloud data sets.

[134] A property which in principle can distinguish between TSI and GCR effects is geomagnetism as cosmic rays arriving at Earth are modulated by the geomagnetic field but solar irradiance is not. Variations in the local geomagnetic field therefore provide a basis on which the cosmic ray ionization effects on clouds can be investigated. Interestingly, no such effect could be found in a study of the Laschamp Event (41,000 years ago) when the geomagnetic field almost reversed its polarity and reduced its intensity to 10%–20% of the present value [*Wagner et al.*, 2001; see also *Usoskin et al.*, 2005; *de Jager and Usoskin*, 2006; *Sloan and Wolfendale*, 2008]. On interannual time scales, *Voiculescu et al.* [2006] studied the relationship between satellite cloud data, cosmic rays, and solar UV radiation using partial correlation analysis. Only in limited geographical regions was the cosmic ray effect robust. These

TABLE 1. Mechanisms of Cloud Changes Through Charge-Related Processes

Process	Solar Climate Modulation	Requirements	Probable Circumstances	Effect	Time Scale	Number of Elementary Charges Required	Upper Limit of Radiative Effect (W m^{-2})
Ion-induced particle formation	through cosmic ray production of cluster ions, aerosol physics, and clouds	condensable vapor and cluster ions	clean air, marine air, and upper troposphere	increase in ultrafine particles and, potentially, cloud condensation nuclei	~5–10 h		~0.2[a]
Electroscavenging	through fair weather global circuit current in supercooled clouds	charged aerosol particles and water droplets	boundaries of supercooled layer clouds	local latent heat release from freezing, change in cloud properties, and radiative changes	~minutes	~10–100 el on particles[b]	
Electroactivation	through fair weather global circuit current in liquid water clouds	charged aerosol particles, insoluble condensation nuclei, and supersaturation	boundaries of liquid layer clouds	change in cloud droplet properties and radiative changes	~minutes	~100–1000 el on pure droplets	~0.1[c]
Electrocoalescence[d]	through fair weather global circuit current in liquid water clouds	charged droplets	boundaries of liquid layer clouds	size distribution change, rain enhancement and fog formation, and radiative changes	~500 s	~10–100 el on ~1–10 μm droplets	

[a] *Kazil et al.* [2006].
[b] *Tinsley et al.* [2000].
[c] *Harrison and Ambaum* [2008].
[d] *Khain et al.* [2004].

regional findings have been supported by independent analysis of surface cloud data, in which signatures characteristic of cosmic rays (but not solar UV) have been identified [*Harrison*, 2008].

[135] Table 1 summarizes the different proposed mechanisms linking atmospheric charge modulation by solar activity to changes in cloud properties. For the ion-induced ("clean air") mechanism, work is needed in determining the relative importance of this route to produce cloud condensation nuclei compared with other routes. This requires detailed microphysical modeling, with appropriate rate constants for the successive processes active to form droplets. For the global circuit ("near-cloud") mechanisms, measurements of droplet and particle charges on layer cloud boundaries are lacking. Modeling of the magnitudes of the effects requires detailed representation of cloud microphysics, with which the relative contribution of the charged processes to cloud droplet formation, evolution, and lifetime can be assessed. A further difficulty in producing parameterizations is that measurements and monitoring of the global circuit have been neglected in recent decades, which prevents testing of the basic hypotheses except for some limited regions or by using historical data.

5. SOLAR VARIABILITY AND GLOBAL CLIMATE CHANGE

[136] The role of solar variability in climate has received much public attention because reliable estimates of the solar influence on the global mean surface temperature over the past 150 years are needed to limit uncertainty in the relative importance of human activity as a potential explanation for climate change. The most obvious impact of the Sun is its influence on the Earth's radiation budget through variations in TSI. A large body of research has focused on the extent to which global temperature records over the past millennium can be simulated using simple "energy balance models" with prescribed forcings. Thus, for example, *Crowley* [2000] included estimates of forcing by solar activity, greenhouse gas concentrations, volcanic dust, and tropospheric aerosol and was able to reproduce the gross variations of a global temperature reconstruction, including the cooler period of the seventeenth century and warming during the twentieth century. Similar studies using global climate models have been carried out, with similar general conclusions. However, comparisons of the model simulations with observational data for the seventeenth century are limited by the large uncertainties in the temperature reconstructions and estimated forcings, as well as internal noise/variability in the model and in the climate system itself.

[137] Long-term trends in solar irradiance have been discussed in section 2.3, and the choice of historical TSI record as input to the climate model will determine the simulated solar effect on temperature. To assess the importance of this uncertainty *Ammann et al.* [2007] carried out a set of 1000 year runs of a coupled atmosphere-ocean GCM using different estimates of historical solar irradiance. The TSI time series was based on ^{10}Be records from Antarctic ice

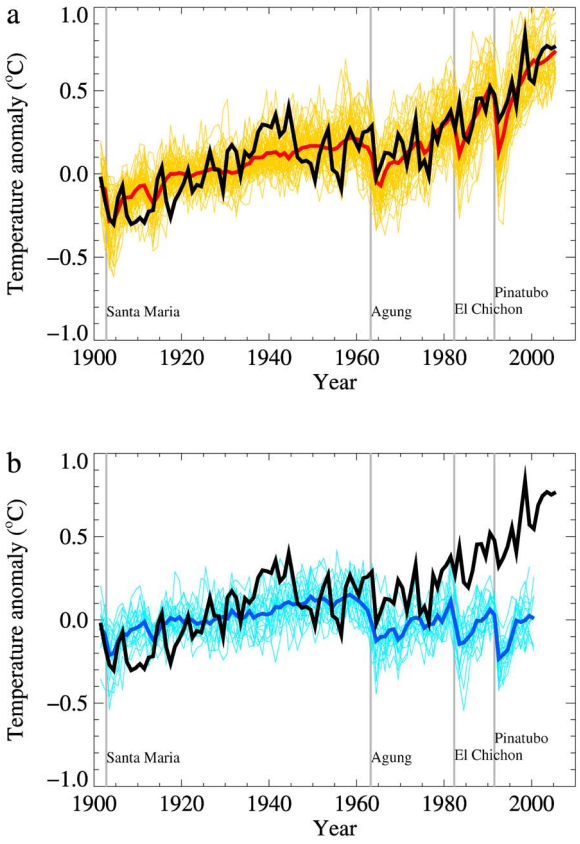

Figure 27. Global mean temperature anomalies, as observed (black line) and as modeled by (a) 58 simulations from 14 different models with both anthropogenic and natural forcings and (b) simulations from 5 models with natural forcings only. The individual simulations are shown in color, with bold curves of the same color indicating the ensemble mean. The observed and simulated time series in Figure 27a are expressed as anomalies relative to the 1901–1950 mean. The simulations in Figure 27b are expressed as anomalies relative to the corresponding model simulation that also includes anthropogenic forcing. Only models whose control simulations have a trend of less than 0.2°C century^{-1} are included [from *IPCC*, 2007, Figure 9.5; after *Stott et al.*, 2006].

cores, but then different scaling was applied, corresponding approximately to the range of published long-term TSI trends. They found that even low solar forcing could affect climate on multidecadal to centennial time scales, but the results using medium to low values (corresponding to the range of *Lean et al.* [2002]) fitted best within the range of temperature reconstructions. Note, however, that if the recent SORCE SIM measurements of spectrally resolved solar irradiance (discussed in section 2.2.2) are correct, then solar radiative forcing at the tropopause would vary out of phase with TSI. In this case, assessments of solar influence on climate, at least over the 11 year cycle and possibly on the longer term, would need to be entirely revisited [*Haigh et al.*, 2010].

[138] For comparisons over the past ~150 years, instrumental data can be used to provide records of global temperature instead of reconstructions based on proxy indicators. Figure 27 shows observed global mean temperature anomalies compared with simulations from climate models that included both natural (solar and volcanic) and anthropogenic (greenhouse gases, tropospheric sulphate and carbon aerosol, and stratospheric and tropospheric ozone) forcings. Note that the models are only able to reproduce the late twentieth century warming when the anthropogenic forcings are included, with the signals statistically separable after about 1980.

[139] In discussion of solar forcing and global change, it is important to note that the climate system has a chaotic element, so the climate response to solar (and other forcings) can be attributed partly to forced variability and partly to internal variability. For instance, Figure 28 shows comparisons between observed and modeled global temperatures for land only, ocean only, land and ocean, and for various regions for natural influences (solar variability and volcanic aerosols) as well as for natural plus anthropogenic influences. The shaded regions indicate the range of results from 19 simulations of 5 different climate models for the natural forcings simulations and from 58 simulations of 14 different climate models for the natural plus anthropogenic simulations. Multiple integrations are necessary because even with the same forcings and the same model, they give different responses because of the models' internal variability (their chaotic behavior). The natural climate system is similarly chaotic, but our observations of the climate system are taken from only a single realization of those that are possible. The natural plus anthropogenic simulations in Figure 28 show statistical agreement with observations, whereas the natural-only simulations do not, which suggests that anthropogenic forcings are needed to explain the observations after about 1975. It should be noted that this is true globally as well as in many, but not all, regions, indicating that internal variability is larger in some regions than in others and also is larger than in the global means. Evaluations of climate modeling for solar influences similarly need to consider internal model variability.

[140] Linear regression is an alternative approach to the attribution of temperature trends to different forcing factors. It requires knowledge of the spatial pattern of the surface temperature response to each individual forcing factor (e.g., solar, volcanic, and greenhouse gases). Linear regression techniques are then applied to find the combination of forcings which provides the best fit to the observed temperature series [*Hegerl et al.*, 1996; *Santer et al.*, 1996]. In this way the amplitude of each forcing does not need to be prescribed but can be found as a result of the fitting procedure to the spatial patterns. The derived amplitudes have large uncertainties, but *Stott et al.* [2003] found that the best fit for the TSI forcing had a larger amplitude than would be expected solely from direct radiative effects. Note, however, that the spatial patterns employed in these "detection-attribution" studies are for the most part from models driven via the bottom-up mechanism of TSI forcing (section 4.1) and do not include the top-down influence from spectrally varying irradiances and stratospheric ozone feedbacks.

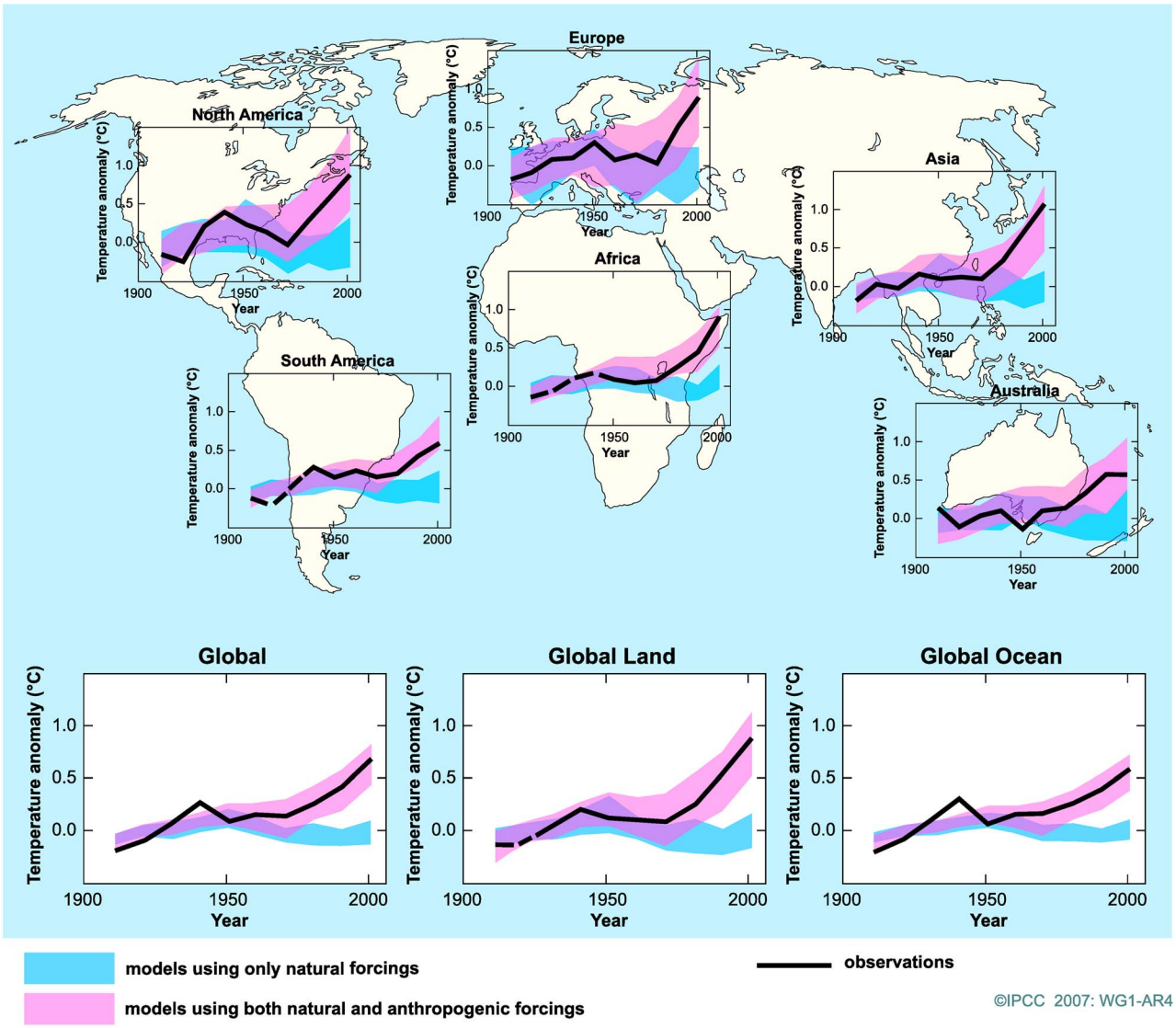

Figure 28. Comparison of observed continental-scale and global-scale changes in surface temperature with results simulated by climate models using natural and anthropogenic forcings. Decadal averages of observations are shown for the period 1906–2005 (black line) plotted against the center of the decade and relative to the corresponding average for 1901–1950. Lines are dashed where spatial coverage is less than 50%. Blue shaded bands show the 5%–95% range for 19 simulations from 5 climate models using only the natural forcings due to solar activity and volcanoes. Pink shaded bands show the 5%–95% range for 58 simulations from 14 climate models using both natural and anthropogenic forcings [from *IPCC*, 2007, FAQ 9.2, Figure 1].

[141] First-order estimates of the global response to different forcings can be assessed using the concepts of radiative forcing and climate sensitivity (section 1). Because of the large uncertainty in centennial-scale variations in TSI (section 2.3), solar radiative forcing of climate change is not well established. The *IPCC* [2007] report estimates a value of 0.12 W m^{-2} for solar radiative forcing change since 1750 (see Figure 4), which represents a change in TSI of 0.69 W m^{-2}, after taking into account the factor $(1 - A)/4$, where A is albedo (see section 1). Many of the present climate model simulations, including several in the latest *IPCC* [2007] report, use TSI reconstructions with a larger drift in TSI since 1750 than currently thought to be realistic. On the other hand, the period around the middle of the eighteenth century was a time of relatively high solar activity (see Figure 2) compared to the beginning and end of that century, so the IPCC's use of the 1750 radiative forcing value to represent the preindustrial atmosphere means that the change from 1750 to the present is very small. A choice of 1700 or 1800 instead of 1750 would approximately double the solar forcing while leaving anthropogenic forcings essentially unchanged. A value of 0.24 W m^{-2} solar radiative forcing difference from Maunder Minimum to the present is currently considered to be more appropriate than the 0.12 W m^{-2} estimated by IPCC (compare with the range of 0.16–0.28 W m^{-2} described in section 2.3). Despite these

uncertainties, even this approximate doubling of the solar forcing change is still much smaller than the 1.6 W m^{-2} estimated to be due to anthropogenic influences.

[142] The majority of climate models employed to date (including those in Figures 27 and 28) represent primarily the bottom-up TSI mechanism and have a very poor, or no, representation of the top-down mechanism that requires spectral variations in solar radiative input and ozone feedback effects. Only a few have an adequate representation of the stratosphere, and even those do not generate a complete representation of stratospheric effects such as an internally consistent quasi-biennial oscillation. Some of the models employed for future IPCC assessments are planned to incorporate these processes and thus should be better placed to assess the importance of these effects.

[143] There are additional uncertainties in estimates of solar radiative forcing which also require further consideration. In the usual definition of RF [*IPCC*, 2007] it is the instantaneous change in radiative flux *at the tropopause* which is used, and this assumes that the stratosphere has already adjusted to the forcing. This is justified on the basis of the faster equilibration time of the stratosphere and also because it has been shown that this "adjusted" forcing is a better indicator of global average surface temperature response [*Hansen et al.*, 1997]. For solar radiative forcing the first impact of this adjustment is to reduce the radiative forcing because the existence of molecular oxygen and ozone in the stratosphere reduces the solar radiation reaching the tropopause. Second, however, the RF value has to be adjusted to take account of the effects of any solar-induced changes within the stratosphere itself (e.g., temperature redistribution). Heating of the stratosphere by enhanced solar UV produces additional downward LW radiation at the tropopause, i.e., a positive feedback. Changes in ozone also impact the radiation fields: additional O_3 reduces the downward SW fluxes but increases the LW fluxes. Thus, a precise determination of solar RF depends on the response of stratospheric temperatures and ozone to the changes in solar irradiance. These are not well established (see section 3.1) so that published estimates of the ozone amplification of direct TSI forcing show a very wide range [*Haigh*, 2007; *Gray et al.*, 2009] with even the sign of the effect remaining uncertain.

6. SUMMARY AND FUTURE DIRECTIONS

[144] This paper presents a review of our present knowledge of solar influence on climate, including the physics of solar variability, information on direct and proxy observations of both solar variability and climate, and some of the suggested mechanisms by which solar variability might influence climate. Satellite and ground-based observations, together with advances in theory and modeling, have greatly advanced our knowledge of the Sun in recent decades. Observations have indicated that electromagnetic radiation from the Sun varies with the solar cycle so that the Sun emits more radiation at sunspot maximum when, paradoxically, it is most covered with dark sunspots. We now understand this to be a result of the dominance of the bright faculae, which also vary over the solar cycle (see section 2).

6.1. Solar Variability

[145] There have been great strides in understanding how the magnetic variability of the Sun is related to the variation of both the total and the spectrally resolved solar irradiance. Basically, the magnetic fields associated with the sunspots divert the convective upflow of energy so that the spots are dark, and although the greater portion of the blocked energy upflow is returned to the solar convection zone, some of it emerges in the areas surrounding the sunspots, leading to brightening there.

[146] Through observations of the life cycle of sunspot groups, together with theory, a quantitative understanding has emerged that allows the use of magnetic observations of the Sun to model the observed solar irradiance variability. Using these techniques, we can explain satellite observations of solar irradiance in terms of the magnetic behavior of the Sun. Progress in this field has been greatest in terms of understanding TSI variations on daily to decadal time scales, but recently, much progress has also been achieved in understanding and modeling variability in different spectral wavelength intervals.

[147] One complication is that satellite instruments measuring solar irradiance have a limited lifetime, and there has been insufficient commitment to ensure continuous, overlapping observations especially in the case of spectrally resolved irradiance. This has necessitated the reconstruction of multidecade variations of solar irradiance. There have been varied approaches to this. One approach takes the measurements to be inviolable, thus assuming that the native measurement precision is adequate so that overlaps between instruments serve only to establish continuity between instruments. The other approach is that instrument degradation is occurring, and this degradation must be determined and taken into account when constructing multidecade time series of solar irradiance. Our understanding of the connection between solar irradiance and the Sun's magnetic variability can be used to resolve these different approaches, and it has now become clear that the latter approach is more appropriate.

[148] Direct measurements of solar irradiance are only available for the last few decades. For the period before these direct observations, proxy measurements are required. Systematic sunspot measurements have been made for about 4 centuries. Additionally, neutron monitor data show that GCR fluxes vary inversely with the strength of the interplanetary magnetic field, which is modulated by the Sun. GCRs interact with the atmosphere producing cosmogenic radionuclides such as ^{10}Be and ^{14}C. Measuring ^{10}Be in ice cores and ^{14}C in tree rings provides information about the solar activity over at least the last 10,000 years.

[149] Reconstruction of the solar irradiance over the past few centuries is difficult since direct observations are not available from a Maunder Minimum type epoch when sunspots were virtually absent for decades, and some arbitrary assumptions must be made about what the Sun's

magnetic field looked like during such epochs. Thus, the estimated increase in TSI from the Maunder Minimum (~1645–1715) to present-day values is uncertain. Recent studies have converged on a probable increase of ~1.3 W m^{-2} with an uncertainty range of 0.9–1.6 W m^{-2}. This corresponds to an increase in the mean global top-of-atmosphere radiative forcing of only 0.16–0.28 W m^{-2}. Nevertheless, because of the complexity of the nonlinear climate system and the different physics involved, it is far from ideal to compare forcings by simply using mean global values in W m^{-2} or, indeed, to apply the concept of sensitivity which is defined for equilibrium conditions that are never reached.

6.2. Climate Observations

[150] The Sun's irradiance is approximately that of a blackbody at a temperature of about 5770 K. As such, about 50% of the Sun's output is in the visible and near-infrared wavelengths. Although very little of the Sun's output is in the UV, the Sun's variability is much greater at these shorter wavelengths. This shortwave solar radiation is mostly absorbed in the Earth's middle and upper atmosphere, so we expect to find the most obvious solar variability at these altitudes (see section 3).

[151] Direct influences on temperature and on ozone concentrations in the tropical and midlatitude upper stratosphere have been observed and are consistent with estimates due to the direct impact of irradiance changes, but a secondary maximum in the lower stratosphere in both fields remains to be explained. Solar influences on stratospheric temperatures result in changes in stratospheric winds, and studies show a wind response that is much larger than can be explained by direct effects of solar electromagnetic and corpuscular radiation.

[152] One of the best established solar-climate relations follows from the pioneering work of *Labitzke* [1987] and *Labitzke and van Loon* [1988], who found a clear SC influence on winter, NH stratospheric polar temperatures when the data were sorted according to the phase of the QBO. Subsequent research has established that similar correlations persist into the other seasons and into the Southern Hemisphere.

[153] Many studies have found solar influences in the ocean, troposphere, and land surface. In the troposphere, there is evidence of an intensification of the tropical precipitation maxima with a broadening of the Hadley circulation under S_{max} conditions and a strengthening of the Walker circulation in the equatorial Pacific in association with a La Niña–like SST response during peak solar forcing years, followed by an El Niño–like response a year or two later. There is also growing evidence for a solar modulation of the extratropical modes of variability, especially when the QBO phase is also taken into account.

[154] There have been reports of strong correlations between global low cloud amounts and GCRs, but the continued correlation into the 1990s is due to an adjustment to the satellite cloud data that is considered unjustifiable. We therefore conclude that the currently available data do not provide substantial support for the hypothesized global cloud cover linkage to cosmic rays. The SC-GCR-cloud-climate link continues to be an active area of investigation, however, with controversial aspects remaining. We also note that correlation studies cannot establish cause and effect as clouds will respond to changes in climate whatever their cause. Only quantitative treatments of GCR influence on cloud amounts through the clean air (ion-induced) mechanisms have been developed to the point where models can be tested against observations.

[155] At the Earth's surface, detection of a SC influence is difficult not only because it is so small but also because many other factors have influenced climate during the recent period for which we have accurate measurements, including increasing greenhouse gases, volcanoes, and aerosol changes. Nevertheless, studies of both ocean and land surface temperatures have detected signals. Variations in ocean temperatures have been found with both 11 and ~80 year periodicities, which correspond with cycles in solar activity. Typical global average amplitudes of approximately 0.08 ± 0.02 K have been found on ~11 year time scales, which is similar to estimates of direct heating of the oceans' mixed layer. There is also evidence of much larger responses in regional analyses which appear to share some similarities with the natural modes of variability, e.g., ENSO. Recent correlation studies between 11 year SC forcing and land surface temperature observations also appear to be robust but display similar patterns in geographical distribution to those from forcing due to greenhouse gases.

[156] There have been suggestions that twentieth century global and hemispheric mean surface temperature variations are correlated to longer-term solar variations. Advanced statistical detection and attribution methodologies confirm that solar forcing contributed to the increase in global temperatures in the early part of the century, but for the latter part of the twentieth century they consistently find that using realistic variations, solar forcing played only a minor role in global warming, in agreement with the practically constant mean solar forcing since 1980.

[157] On longer time scales, proxies are required both for estimates of the Sun's variations (e.g., sunspots) and for climate (e.g., tree rings). A solar influence has been identified during the last millennium, including the so-called Medieval Warm Period (~800–1200 A.D.) and the relatively cold Maunder Minimum (~1645–1715 A.D.). There has been some controversy about whether the latter was actually a global-scale cooling or was a more regional, i.e., European, effect. Recent modeling research suggests that it may have been a manifestation of a shift in the AO/NAO regime, but investigation of the mechanisms causing the observed European winter cooling remains a topic of active research.

[158] There have been many other investigations of connections of solar activity with changes in climate variables such as the location and intensity of the ITCZ, periods of midcontinent droughts, ocean currents, and monsoon strength using proxies for both solar activity and climate. A challenge is to model these patterns of regional climate response to solar forcing, work that is being actively pursued at present. It is clear that many of the observed correlations

between climate variables and solar activity are larger than would be expected from the direct influence of the Sun's observed variation over the past 3 decades, so the challenge has been to find viable mechanisms that give testable physical linkages between the Sun's variations and the observed variations in the climate variables.

6.3. Mechanisms

[159] Suggested mechanisms for solar influence on climate vary in their maturity: the most mature can be represented in climate models using well-established physics, and their impacts on the modeled climate can be examined. The less mature are based on hypotheses that may be credible but have not yet been put into physical models in order to test their influence.

[160] The most obvious mechanism for solar variations affecting the Earth's climate is due to the change in heating of the Earth system associated with varying TSI. These are found to partially explain the variations in the temperature of the oceanic mixed layer, but even in this case, it appears that modulations in the ocean-atmosphere sensible and latent heat fluxes are needed to explain the observations, suggesting a possible interaction with variations in the Hadley and Walker circulations. There has been recent progress in the development and testing of mechanisms to explain the observed solar signal in the Pacific which resembles the ENSO signal.

[161] The most mature Sun-climate mechanism at this time involves the direct effect of the observed variation in solar UV radiation affecting stratospheric ozone, leading to associated temperature variations. The resulting temperature gradients lead to changes in the zonal wind, which, in turn, changes planetary wave–mean flow interactions. Inclusion of these mechanisms in fully coupled chemistry-climate models has been achieved, and many of the observed features in stratospheric temperatures, winds, and ozone distributions have been reproduced, including the maximum in ozone in the lower stratosphere, which appears to be an indirect effect associated with changes in the global circulation. Progress has been made in understanding and modeling the observed SC-QBO interactions, but there are still aspects that are not well understood, including the lower stratospheric temperature maximum and the mechanism for SC-QBO influence on sudden warmings. The SC influences in summertime and in the SH also require further study.

[162] The inclusions in climate models of SC irradiance and ozone feedback mechanisms have also resulted in changes in the modeled troposphere, including modification to the Hadley circulation and changes in extratropical modes of variability (NAM and SAM). These have been achieved in models in which the SSTs are fixed, suggesting that these tropospheric changes are at least partly due to a top-down mechanism, i.e., stratosphere-troposphere coupling, which may be particularly helpful in explaining the observed regional signals. However, models that include the bottom-up coupled air-sea response mechanism also show these changes and indicate that the two mechanisms could be additive to produce the magnitude of the responses observed in the climate system. Since the nature of the exact mechanisms for this coupling is crucial for understanding solar-climate connections, there is much active research in this area.

[163] The solar modulation of GCRs or the global electric circuit has also been proposed as a mechanism for SC influence on climate, through their ability to influence cloud cover. However, as noted above, this mechanism has only just begun to be tested in physical models.

6.4. Climate Change

[164] Finally, the role of solar variability in climate change has received much public attention because reliable estimates of solar influence are needed to limit uncertainty in the importance of human activity as a potential explanation for global warming. Extensive climate model studies have indicated that the models can only reproduce the late twentieth century warming when anthropogenic forcing is included, in addition to the solar and volcanic forcings [*IPCC*, 2007]. The change in solar radiative forcing since 1750 was estimated in the *IPCC* [2007] report to be 0.12 W m^{-2}, corresponding to an increase in TSI of 0.69 W m^{-2}. A value of 0.24 W m^{-2} solar radiative forcing difference from Maunder Minimum to the present is currently considered to be more appropriate. Despite these uncertainties in solar radiative forcing, they are nevertheless much smaller than the estimated radiative forcing due to anthropogenic changes, and the predicted SC-related surface temperature change is small relative to anthropogenic changes.

[165] One thing that is very clear from this review is that enormous progress has been achieved in our knowledge and understanding over the past few decades. The topic has emerged from its beginnings of almost purely investigation of statistical relationships that were subject to substantial criticism to become a solid scientific field that involves both solar physicists and climate scientists. Indeed, even 20 years ago it would have been very unlikely that the collection of scientific fields represented by the authors of this paper would have collaborated on such a review.

6.5. Further Research

[166] Further observations and research are required to improve our understanding of solar forcing mechanisms and their impacts on the Earth's climate. In particular, it is necessary (1) to understand the recent SORCE SIM measurements of spectrally resolved irradiances and assess their implications for solar influence on climate (see section 2.2.2); (2) to determine an accurate value of the total and spectrally resolved solar irradiance during a grand solar minimum such as the Maunder Minimum, when the Sun was in a different mode than during the past few decades (see section 2.2.3); (3) to improve the characterization of the solar signal in surface and tropospheric observations as additional years of data becomes available (see sections 3.2 and 3.3); (4) to improve the characterization of the observed stratospheric temperature response to the 11 year solar cycle, particularly the vertical structure of the response at tropical latitudes so

that the differences between the estimated SC signals from the TOVS data and from reanalysis data can be fully understood, which will likely require future observations with improved vertical resolution (see section 3.1.2); and (5) to improve model simulations of the observed solar signals in climate observations and, in particular, assess the requirement to explicitly represent stratospheric mechanisms in future climate models, which will require fully coupled ocean-troposphere-stratosphere models with interactive chemistry so that the relative contribution and interactions of the top-down and bottom-up influences can be understood. We note that, there will still be a continuing role for simpler models to investigate and improve the simulation of specific mechanisms, including the development of models that investigate possible influences of galactic cosmic rays on cloud formation (see section 4.4).

NOTATION

[167] The interdisciplinary nature of this review introduces a great many acronyms and notations that are in common use in any one field but may not be so well known by scientists from another field. We therefore list them here.

Acronyms

ACRIM	Active Cavity Radiometer Irradiance Monitor.
AO	Arctic Oscillation.
B-D	Brewer-Dobson (circulation).
BSi	biogenic silica content.
CCN	cloud condensation nucleii.
CCM	chemistry climate models.
CZ	convection zone (solar).
D2	data set generated by ISCCP.
DIARAD	Differential Absolute Radiometer (part of the VIRGO instrument on SoHO).
DJF	December, January, and February.
ECMWF	European Centre for Medium Range Weather Forecasts.
ENSO	El Niño–Southern Oscillation.
ERA-40	ECMWF reanalysis data set for 1959–2001.
GHG	greenhouse gas.
HALOE	Halogen Occultation Experiment (instrument on UARS).
HF	Hickey-Frieden Radiometer (an instrument on the Nimbus 7 satellite).
IMF	interplanetary magnetic field.
IPCC	Intergovernmental Panel on Climate Change.
IR	infrared.
IRD	ice-rafted debris.
IRMB	Institut Royal Meteorologique Belgique.
ISCCP	International Satellite Cloud Climatology Project.
ITCZ	Intertropical Convergence Zone.
GCM	general circulation model.
GCR	galactic cosmic rays.
LCA	low cloud amount.
LOSU	level of scientific understanding.
LW	longwave radiation.
Ly-α	Lyman alpha emission line.
MDI	Michelson Doppler Interferometer (instrument on SoHO).
MODIS	Moderate Resolution Imaging Spectroradiometer (instruments on the Terra and Aqua satellites).
NAM	northern annular mode.
NAO	North Atlantic Oscillation.
NCEP	National Centers for Environmental Prediction (formerly NMC).
NH	Northern Hemisphere.
NO_x	nitrogen species NO + NO_2.
NP	North Pole.
NRC	National Research Council.
PMOD	Physikalisch-Meteorologisches Observatorium Davos (Switzerland).
PM6	a cavity radiometer (part of the VIRGO instrument on SoHO).
QBO	quasi-biennial oscillation.
QBO-E	easterly wind years of the QBO.
QBO-W	westerly wind years of the QBO.
RF	radiative forcing.
SAGE	Stratospheric Aerosol and Gas Experiments (satellite).
SAM	southern annular mode.
SATIRE	Spectral and Total Irradiance Reconstruction.
SC	solar cycle.
SEP	solar energetic particles.
SH	Southern Hemisphere.
SIM	Spectral Irradiance Monitor (instrument on the SORCE).
S_{max}	sunspot cycle maximum.
S_{min}	sunspot cycle minimum.
SoHO	Solar and Heliospheric Observatory (satellite).
SORCE	Solar Radiation and Climate Experiment.
SP	South Pole.
SPCZ	South Pacific Convergence Zone.
SPE	solar proton event.
SSI	spectral solar irradiance.
SST	sea surface temperature.
SSW	stratospheric sudden warming.
SW	shortwave radiation.
TIROS	Television Infrared Observation Satellites.
TOVS	TIROS Operational Vertical Sounder (infrared radiometers on TIROS satellites).
TSI	total solar irradiance.
UARS	Upper Atmosphere Research Satellite.
UCN	ultrafine condensation nuclei.
UV	ultraviolet.
VIRGO	Variability of Solar Irradiance and Gravity Oscillations (instrument on SoHO).
^{10}Be	beryllium-10 (cosmogenic isotope).
^{14}C	carbon-14 (cosmogenic isotope).

Parameters

A	Earth's SW albedo.
B_{QS}	average quiet Sun magnetic field during the Maunder Minimum.
aa	planetary index of geomagnetic activity.
Ap	planetary index of geomagnetic activity.
C	counts detected by the neutron monitor at Climax, Colorado.
$\nabla \cdot F$	Eliassen-Palm planetary flux divergence.
F_S	open solar magnetic flux.
$F_{10.7}$	10.7 cm solar radio flux (in W m^{-2} Hz^{-1}).
GCR	counts detected by the neutron monitor at McMurdo, Antarctica.
I	spectral solar irradiance (SSI).
I_{TS}	total solar irradiance (TSI).
L	solar cycle length.
M	heliospheric modulation parameter (of GCRs).
Mg ii	Mg ii line (280 nm) core-to-wing ratio.
$P[^{10}Be]$	global production rate of the cosmogenic ^{10}Be isotope.
R	sunspot number.
R_{11}	11 year running mean of sunspot number.
R_G	group sunspot number.
T	temperature.
T_S	global mean surface air temperature.
U	wind speed.
Z_{30}	30 hPa geopotential height.
λ	climate sensitivity parameter.
ΔF	change in forcing at the top of the atmosphere.
ΔT_S	change in global mean surface air temperature.
$\Delta^{14}C$	carbon-14 production rate.
ΔU	change in wind speed.
$\delta^{18}O$	a measure of the ratio of the oxygen-18 to oxygen-16 isotopes.

Non-SI Units

AU	astronomical distance.
DU	Dobson units (column ozone measurement).
R_E	Mean Earth radius.

[168] **ACKNOWLEDGMENTS.** The development of this review article has evolved from work carried out by an international team of the International Space Science Institute (ISSI), Bern, Switzerland, and from work carried out under the auspices of Scientific Committee on Solar Terrestrial Physics (SCOSTEP) Climate and Weather of the Sun-Earth System (CAWSES-1). The support of ISSI in providing workshop and meeting facilities is acknowledged, especially support from Y. Calisesi and V. Manno. SCOSTEP is acknowledged for kindly providing financial assistance to allow the paper to be published under an open access policy. L.J.G. was supported by the UK Natural Environment Research Council (NERC) through their National Centre for Atmospheric Research (NCAS) Climate program. K.M. was supported by a Marie Curie International Outgoing Fellowship within the 6th European Community Framework Programme. J.L. acknowledges support by the EU/FP7 program Assessing Climate Impacts on the Quantity and Quality of Water (ACQWA, 212250) and from the DFG Project Precipitation in the Past Millennium in Europe (PRIME) within the Priority Program INTERDYNAMIK. L.H. acknowledges support from the U.S. NASA Living With a Star program. G.M. acknowledges support from the Office of Science (BER), U.S. Department of Energy, Cooperative Agreement DE-FC02-97ER62402, and the National Science Foundation. We also wish to thank Karin Labitzke and Markus Kunze for supplying an updated Figure 13, Andrew Heaps for technical support, and Paul Dickinson for editorial support. Part of the research was carried out under the SPP CAWSES funded by GFG. J.B. was financially supported by NCCR Climate–Swiss Climate Research.

[169] The Editor for this manuscript was Pete Riley. He wishes to thank an anonymous reviewer.

REFERENCES

Allan, R. J. (2000), ENSO and climatic variability in the last 150 years, in *El Nino and the Southern Oscillation: Multiscale Variability, Global and Regional Impacts*, edited by H. F. Diaz and V. Markgraf, pp. 3–35, Cambridge Univ. Press, Cambridge, U. K.

Ammann, C. M. (2005), Solar signals in records and simulations of past climates, *Mem. Soc. Astron. Ital.*, *76*, 802–804.

Ammann, C. M., G. A. Meehl, W. M. Washington, and C. A. Zender (2003), A monthly and latitudinally varying volcanic forcing dataset in simulations of 20th century climate, *Geophys. Res. Lett.*, *30*(12), 1657, doi:10.1029/2003GL016875.

Ammann, C. M., F. Joos, D. S. Schimel, B. L. Otto-Bliesner, and R. A. Tomas (2007), Solar influence on climate during the past millennium: Results from transient simulations with the NCAR Climate System Model, *Proc. Natl. Acad. Sci. U. S. A.*, *104*, 3713–3718, doi:10.1073/pnas.0605064103.

Aplin, K. L. (2008), Composition and measurement of charged atmospheric clusters, *Space Sci. Rev.*, *137*, 213–224, doi:10.1007/s11214-008-9397-1.

Arnold, N. F., and T. R. Robinson (2000), Amplification of the influence of solar flux variations on the winter stratosphere by planetary waves, *Space Sci. Rev.*, *94*, 279–286, doi:10.1023/A:1026783609783.

Austin, J., L. L. Hood, and B. E. Soukharev (2007), Solar cycle variations of stratospheric ozone and temperature in simulations with a coupled chemistry-climate model, *Atmos. Chem. Phys.*, *7*, 1693–1706, doi:10.5194/acp-7-1693-2007.

Austin, J., et al. (2008), Coupled chemistry climate model simulations of the solar cycle in ozone and temperature, *J. Geophys. Res.*, *113*, D11306, doi:10.1029/2007JD009391.

Balachandran, N., and D. Rind (1995), Modelling the effects of UV variability and the QBO on the troposphere-stratosphere system. Part I: The middle atmosphere, *J. Clim.*, *8*, 2058–2079, doi:10.1175/1520-0442(1995)008<2058:MTEOUV>2.0.CO;2.

Balachandran, N. K., D. Rind, P. Lonergan, and D. T. Shindell (1999), Effects of solar cycle variability on the lower stratosphere and the troposphere, *J. Geophys. Res.*, *104*, 27,321–27,339, doi:10.1029/1999JD900924.

Baldwin, M. P., and T. J. Dunkerton (2001), The solar cycle and stratosphere-troposphere dynamical coupling, *Science*, *294*, 581–584, doi:10.1126/science.1063315.

Baldwin, M. P., et al. (2001), The quasi biennial oscillation, *Rev. Geophys.*, *39*, 179–229, doi:10.1029/1999RG000073.

Baliunas, S., and R. Jastrow (1990), Evidence for long-term brightness changes of solar-type stars, *Nature*, *348*, 520–523, doi:10.1038/348520a0.

Bard, E., G. Raisbeck, F. Yiou, and J. Jouzel (2000), Solar irradiance during the last 1200 years based on cosmogenic nuclides, *Tellus, Ser. B*, *52*, 985–992.

Barriopedro, D., R. García-Herrera, and R. Huth (2008), Solar modulation of Northern Hemisphere winter blocking, *J. Geophys. Res.*, *113*, D14118, doi:10.1029/2008JD009789.

Bates, J. R. (1981), A dynamical mechanism through which variations in solar ultra violet radiation can influence tropospheric climate, *Sol. Phys.*, *74*, 399–415, doi:10.1007/BF00154526.

Beer, J., and B. van Geel (2008), Holocene climate change and the evidence for solar and other forcings, in *Natural Climate Variability and Global Warming: A Holocene Perspective*, edited by R. W. Batterbee and H. A. Binney, pp. 138–162, Wiley-Blackwell, Oxford, U. K.

Beer, J., W. Mende, and R. Stellmacher (2000), The role of the Sun in climate forcing, *Quat. Sci. Rev.*, *19*, 403–415, doi:10.1016/S0277-3791(99)00072-4.

Beer, J., M. Vonmoos, and R. Muscheler (2006), Solar variability over the past several millennia, *Space Sci. Rev.*, *125*, 67–79, doi:10.1007/s11214-006-9047-4.

Bennett, A. J., and R. G. Harrison (2008), Surface measurement system for the atmospheric electrical vertical conduction current density, with displacement current correction, *J. Atmos. Sol. Terr. Phys.*, *70*, 1373–1381, doi:10.1016/j.jastp.2008.04.014.

Bennett, A. J., and R. G. Harrison (2009), Evidence for global circuit current flow through water droplet layers, *J. Atmos. Sol. Terr. Phys.*, *71*(12), 1219–1221, doi:10.1016/j.jastp.2009.04.011.

Bhatnagar, A., K. Jain, and S. C. Tripathy (2002), Variation of solar irradiance and mode frequencies during Maunder Minimum, *Astrophys. Space Sci.*, *281*, 761–764, doi:10.1023/A:1016325824515.

Björck, S., et al. (2001), High-resolution analyses of an early Holocene climate event may imply decreased solar forcing as an important climate trigger, *Geology*, *29*, 1107–1110, doi:10.1130/0091-7613(2001)029<1107:HRAOAE>2.0.CO;2.

Blaauw, M., G. B. M. Heuvelink, D. Mauquoy, J. van der Plicht, and B. van Geel (2003), A numerical approach to ^{14}C wiggle-match dating of organic deposits: Best fits and confidence intervals, *Quat. Sci. Rev.*, *22*, 1485–1500, doi:10.1016/S0277-3791(03)00086-6.

Black, D. E., R. C. Thunell, A. Kaplan, L. C. Peterson, and E. J. Tappa (2004), A 2000-year record of Caribbean and tropical North Atlantic hydrographic variability, *Paleoceanography*, *19*, PA2022, doi:10.1029/2003PA000982.

Black, R. X. (2002), Stratospheric forcing of surface climate in the Arctic oscillation, *J. Clim.*, *15*, 268–277, doi:10.1175/1520-0442(2002)015<0268:SFOSCI>2.0.CO;2.

Boberg, F., and H. Lundstedt (2002), Solar wind variations related to fluctuations of the North Atlantic Oscillation, *Geophys. Res. Lett.*, *29*(15), 1718, doi:10.1029/2002GL014903.

Bond, G., B. Kromer, J. Beer, R. Muscheler, M. N. Evans, W. Showers, S. Hoffmann, R. Lotti-Bond, I. Hajdas, and G. Bonani (2001), Persistent solar influence on North Atlantic climate during the Holocene, *Science*, *294*, 2130–2136, doi:10.1126/science.1065680.

Briffa, K. R., P. D. Jones, F. H. Schweingruber, and T. J. Osborn (1998), Influence of volcanic eruptions on northern hemisphere summer temperature over the past 600 years, *Nature*, *393*, 450–455, doi:10.1038/30943.

Brönnimann, S., T. Ewen, T. Griesser, and R. Jenne (2007), Multi-decadal signal of solar variability in the upper troposphere during the 20th century, *Space Sci. Rev.*, *125*, 305–317, doi:10.1007/s11214-006-9065-2.

Brown, B. H. (2008), Short-term changes in global cloud cover and in cosmic radiation, *J. Atmos. Sol. Terr. Phys.*, *70*(7), 1122–1131, doi:10.1016/j.jastp.2008.02.003.

Burke, H. K., and A. A. Few (1978), Direct measurements of the atmospheric conduction current, *J. Geophys. Res.*, *83*(C6), 3093–3098, doi:10.1029/JC083iC06p03093.

Calbó, J., J.-A. Gonzalez, and D. Pagès (2001), A method for sky-condition classification from ground-based solar radiation measurements, *J. Appl. Meteorol.*, *40*, 2193–2199, doi:10.1175/1520-0450(2001)040<2193:AMFSCC>2.0.CO;2.

Calisesi, Y., R.-M. Bonnet, L. Gray, J. Langen, and M. Lockwood (2006), *Solar Variability and Planetary Climate*, Springer, Dordrecht, Netherlands.

Callis, L. B., D. N. Baker, M. Natarajan, J. B. Bernard, R. A. Mewaldt, R. S. Selesnick, and J. R. Cummings (1996), A 2-D model simulation of downward transport of NO_y into the stratosphere: Effects on the 1994 austral spring $O_3$and NO_y, *Geophys. Res. Lett.*, *23*(15), 1905–1908, doi:10.1029/96GL01788.

Callis, L. B., M. Natarajan, and J. D. Lambeth (2000), Calculated upper stratospheric effects of solar UV flux and NO_y variations during the 11-year solar cycle, *Geophys. Res. Lett.*, *27*, 3869–3872, doi:10.1029/2000GL011622.

Callis, L. B., M. Natarajan, and J. D. Lambeth (2001), Solar-atmospheric coupling by electrons (SOLACE): 3. Comparisons of simulations and observations, 1979–1997, issues and implications, *J. Geophys. Res.*, *106*, 7523–7539, doi:10.1029/2000JD900615.

Calogovic, J., C. Albert, F. Arnold, J. Beer, L. Desorgher, and E. O. Flueckiger (2010), Sudden cosmic ray decreases: No change of global cloud cover, *Geophys. Res. Lett.*, *37*, L03802, doi:10.1029/2009GL041327.

Camp, C. D., and K. K. Tung (2007), The influence of the solar cycle and QBO on the late winter stratospheric polar vortex, *J. Atmos. Sci.*, *64*, 1267–1283, doi:10.1175/JAS3883.1.

Castanheira, J. M., and H.-F. Graf (2003), North Pacific–North Atlantic relationships under stratospheric control?, *J. Geophys. Res.*, *108*(D1), 4036, doi:10.1029/2002JD002754.

Chalmers, J. A. (1967), *Atmospheric Electricity*, 2nd ed., Pergamon, Oxford, U. K.

Chandra, S., and R. D. McPeters (1994), The solar cycle variation of ozone in the stratosphere inferred from Nimbus 7 and NOAA 11 satellites, *J. Geophys. Res.*, *99*, 20,665–20,671, doi:10.1029/94JD02010.

Chapman, G. A., A. M. Cookson, J. J. Dobias, and S. R. Walton (2001), An improved determination of the area ratio of faculae to sunspots, *Astrophys. J.*, *555*, 462–465, doi:10.1086/321466.

Chipperfield, M. P., et al. (2007), Global ozone past and present, in *Scientific Assessment of Ozone Depletion: 2006*, *Global Ozone Res. Monit. Proj. Rep.*, *50*, chap. 3, pp. 3.1–3.58, World Meteorol. Organ., Geneva, Switzerland.

Clement, A. C., R. Seager, M. A. Cane, and S. E. Zebiak (1996), An ocean dynamical thermostat, *J. Clim.*, *9*, 2190–2196, doi:10.1175/1520-0442(1996)009<2190:AODT>2.0.CO;2.

Cook, E. R., J. G. Palmer, and R. D. D'Arrigo (2002), Evidence for a 'Medieval Warm Period' in a 1,100 year tree-ring reconstruction of past austral summer temperatures in New Zealand, *Geophys. Res. Lett.*, *29*(14), 1667, doi:10.1029/2001GL014580.

Cordero, E. C., and T. R. Nathan (2005), A new pathway for communicating the 11-year solar cycle signal to the QBO, *Geophys. Res. Lett.*, *32*, L18805, doi:10.1029/2005GL023696.

Crommelynck, D., A. Fichot, R. B. Lee III, and J. Romero (1995), First realisation of the Space Absolute Radiometric Reference (SARR) during the ATLAS 2 flight period, *Adv. Space Res.*, *16*, 17–23, doi:10.1016/0273-1177(95)00261-C.

Crooks, S. A., and L. J. Gray (2005), Characterisation of the 11-year solar signal using a multiple regression analysis of the ERA-40 dataset, *J. Clim.*, *18*, 996–1015, doi:10.1175/JCLI-3308.1.

Crowley, T. J. (2000), Causes of climate change over the past 1000 years, *Science*, *289*, 270–277, doi:10.1126/science.289.5477.270.

Cubasch, U., and R. Voss (2000), The influence of total solar irradiance on climate, *Space Sci. Rev.*, *94*, 185–198, doi:10.1023/A:1026719322987.

Cubasch, U., R. Voss, G. C. Hegerl, J. Waszkewitz, and T. C. Crowley (1997), Simulation with an O-AGCM of the influence of variations of the solar constant on the global climate, *Clim. Dyn.*, *13*, 757–767, doi:10.1007/s003820050196.

Cubasch, U., E. Zorita, F. Kaspar, J. F. Gonzales-Rouco, H. von Storch, and K. Prommel (2006), Simulation of the role of solar

and orbital forcing on climate, *Adv. Space Res.*, *37*, 1629–1634, doi:10.1016/j.asr.2005.04.076.

Damiani, A., M. Storini, M. Laurenza, C. Rafanelli, E. Piervitali, and E. G. Cordero (2006), Southern ozone variations induced by solar particle events during 15 January–5 February 2005, *J. Atmos. Sol. Terr. Phys.*, *68*(17), 2042–2052, doi:10.1016/j.jastp.2006.03.010.

Damon, P. E., and P. Laut (2004), Pattern of strange errors plagues solar activity and terrestrial climate data, *Eos Trans. AGU*, *85*, 370, doi:10.1029/2004EO390005.

de Jager, C., and I. Usoskin (2006), On possible drivers of Sun-induced climate changes, *J. Atmos. Sol. Terr. Phys.*, *68*, 2053–2060, doi:10.1016/j.jastp.2006.05.019.

Dengel, S., D. Aeby, and J. Grace (2009), A relationship between galactic cosmic radiation and tree rings, *New Phytol.*, *184*, 545–551, doi:10.1111/j.1469-8137.2009.03026.x.

de Putter, T., M.-F. Loutre, and G. Wansard (1998), Decadal periodicities of Nile river historical discharge (A.D. 622–1470) and climatic implications, *Geophys. Res. Lett.*, *25*, 3193–3196, doi:10.1029/98GL02250.

Dewitte, S., D. Crommelynck, S. Mekaoui, and A. Joukoff (2004), Measurement and uncertainty of the long-term total solar irradiance trend, *Sol. Phys.*, *224*, 209–216, doi:10.1007/s11207-005-5698-7.

Dickinson, R. E. (1975), Solar variability and the lower atmosphere, *Bull. Am. Meteorol. Soc.*, *56*, 1240–1248, doi:10.1175/1520-0477(1975)056<1240:SVATLA>2.0.CO;2.

Duchon, C. E., and M. S. O'Malley (1999), Estimating cloud type from pyranometer observations, *J. Appl. Meteorol.*, *38*, 132–141, doi:10.1175/1520-0450(1999)038<0132:ECTFPO>2.0.CO;2.

Duplissy, J., et al. (2009), Results from the CERN pilot CLOUD experiment, *Atmos. Chem. Phys. Discuss.*, *9*, 18,235–18,270, doi:10.5194/acpd-9-18235-2009.

Dykoski, C. A., R. L. Edwards, H. Cheng, D. Yuan, Y. Cai, M. Zhang, Y. Lin, J. Qing, Z. An, and J. Revenaugh (2005), A high-resolution, absolute dated Holocene and deglacial Asian monsoon record from Dongge Cave, China, *Earth Planet. Sci. Lett.*, *233*, 71–86, doi:10.1016/j.epsl.2005.01.036.

Eddy, J. A. (1976), The Maunder Minimum, *Science*, *192*, 1189–1202, doi:10.1126/science.192.4245.1189.

Egorova, T., E. Rozanov, E. Manzini, M. Haberreiter, W. Schmutz, V. Zubov, and T. Peter (2004), Chemical and dynamical response to the 11-year variability of the solar irradiance simulated with a chemistry-climate model, *Geophys. Res. Lett.*, *31*, L06119, doi:10.1029/2003GL019294.

Eichkorn, S., S. Wilhelm, H. Aufmhoff, K. H. Wohlfrom, and F. Arnold (2002), Cosmic ray-induced aerosol-formation: First observational evidence from aircraft-based ion mass spectrometer measurements in the upper troposphere, *Geophys. Res. Lett.*, *29*(14), 1698, doi:10.1029/2002GL015044.

Eltahir, E. A. B., and G. Wang (1999), Nilometers, El Nino, and climate variability, *Geophys. Res. Lett.*, *26*, 489–492, doi:10.1029/1999GL900013.

Emile-Geay, J., M. Cane, R. Seager, A. Kaplan, and P. Almasi (2007), El Nino as a mediator of the solar influence on climate, *Paleoceanography*, *22*, PA3210, doi:10.1029/2006PA001304.

Evan, A. T., A. K. Heidinger, and D. J. Vimon (2007), Arguments against a physical long-term trend in global ISCCP cloud amounts, *Geophys. Res. Lett.*, *34*, L04701, doi:10.1029/2006GL028083.

Field, C. V., G. A. Schmidt, D. Koch, and C. Salyk (2006), Modeling production and climate-related impacts on ^{10}Be concentrations in ice cores, *J. Geophys. Res.*, *111*, D15107, doi:10.1029/2005JD006410.

Fischer, P., and K. K. Tung (2008), A reexamination of the QBO period modulation by the solar cycle, *J. Geophys. Res.*, *113*, D07114, doi:10.1029/2007JD008983.

Fleitmann, D., S. J. Burns, M. Mudelsee, U. Neff, J. Kramers, A. Mangini, and A. Matter (2003), Holocene forcing of the Indian monsoon recorded in a stalagmite from southern Oman, *Science*, *300*, 1737–1739, doi:10.1126/science.1083130.

Fligge, M., and S. K. Solanki (1998), Long-term behaviour of emissions from solar faculae: Steps towards a robust index, *Astron. Astrophys.*, *332*, 1082–1086.

Foster, S. S. (2004), Reconstruction of solar irradiance variations, for use in studies of global climate change: Application of recent SoHO observations with historic data from the Greenwich observations, Ph.D. thesis, Sch. of Phys. and Astron., Univ. of Southampton, Southampton, U. K.

Foukal, P., K. Harvey, and F. Hill (1991), Do changes in the photospheric magnetic network cause the 11-year variation of total solar irradiance?, *Astrophys. J.*, *383*, L89–L92, doi:10.1086/186249.

Foukal, P., G. North, and T. Wigley (2004), A stellar view on solar variations and climate, *Science*, *306*, 68–69, doi:10.1126/science.1101694.

Fraedrich, K., and C. Bantzer (1991), A note on fluctuations of the Nile river flood levels (715–1470), *Theor. Appl. Climatol.*, *44*, 167–171, doi:10.1007/BF00868171.

Frame, T. H. A., and L. J. Gray (2010), The 11-year solar cycle in ERA-40 data: An update to 2008, *J. Clim.*, *23*, 2213–2222, doi:10.1175/2009JCLI3150.1

Friis-Christensen, E., and K. Lassen (1991), Length of the solar cycle: An indicator of solar activity closely associated with climate, *Science*, *254*, 698–700, doi:10.1126/science.254.5032.698.

Fröhlich, C. (2002), Total solar irradiance variations since 1978, *Adv. Space Res.*, *29*, 1409–1416, doi:10.1016/S0273-1177(02)00203-X.

Fröhlich, C. (2006), Solar irradiance variability since 1978: Revision of the PMOD composite during solar cycle 21, *Space Sci. Rev.*, *125*, 53–65, doi:10.1007/s11214-006-9046-5.

Funke, B., M. López-Puertas, S. Gil-López, T. von Clarmann, G. P. Stiller, H. Fischer, and S. Kellman (2005), Downward transport of upper atmospheric NO_x into the polar stratosphere and lower mesosphere during the Antarctic 2003 and Arctic 2002/2003 winters, *J. Geophys. Res.*, *110*, D24308, doi:10.1029/2005JD006463.

Ganguly, N. D. (2010), Influence of solar proton events during the declining phase of solar cycle 23 on the total ozone concentration in India, *Int. J. Remote Sens.*, *31*(2), 313–322, doi:10.1080/01431160902882678.

Geller, M. A. (1988), Solar cycles and the atmosphere, *Nature*, *332*, 584–585, doi:10.1038/332584a0.

Geller, M. A., and J. C. Alpert (1980), Planetary wave coupling between the troposphere and the middle atmosphere as a possible Sun-weather mechanism, *J. Atmos. Sci.*, *37*, 1197–1215, doi:10.1175/1520-0469(1980)037<1197:PWCBTT>2.0.CO;2.

Giampapa, M. (2004), Stellar analogs of solar activity: The Sun in a stellar context, in *The Sun, Solar Analogs and the Climate*, edited by I. Redi, M. Güdel, and W. Schmutz, pp. 305–423, Springer, Berlin.

Gleisner, H., and P. Thejll (2003), Patterns of tropospheric response to solar variability, *Geophys. Res. Lett.*, *30*(13), 1711, doi:10.1029/2003GL017129.

Goosse, H., O. Arzel, J. Luterbacher, M. E. Mann, H. Renssen, N. Riedwyl, A. Timmermann, E. Xoplaki, and H. Wanner (2006), The origin of the European 'Medieval Warm Period,' *Clim. Past*, *2*, 99–113, doi:10.5194/cp-2-99-2006.

Graham, N. E., and W. B. White (1988), The El Niño cycle: A natural oscillator of the Pacific Ocean atmosphere system, *Science*, *240*(4857), 1293–1302, doi:10.1126/science.240.4857.1293.

Graham, N. E., et al. (2007), Tropical Pacific mid-latitude teleconnections in medieval times, *Clim. Change*, *83*, 241–285, doi:10.1007/s10584-007-9239-2.

Gray, L. J. (2003), The influence of the equatorial upper stratosphere on stratospheric sudden warmings, *Geophys. Res. Lett.*, *30*(4), 1166, doi:10.1029/2002GL016430.

Gray, L. J. (2010), Equatorial dynamics, in *The Stratosphere: Dynamics, Transport, and Chemistry*, *Geophys. Monogr. Ser.*, vol. 190, edited by L. M. Polvani, A. H. Sobel, and D. W. Waugh, AGU, Washington, D. C., in press.

Gray, L. J., S. J. Phipps, T. J. Dunkerton, M. P. Baldwin, E. F. Drysdale, and M. R. Allen (2001), A data study of the influence of the equatorial upper stratosphere on Northern Hemisphere stratospheric sudden warmings, *Q. J. R. Meteorol. Soc.*, *127*, 1985–2003, doi:10.1002/qj.49712757607.

Gray, L. J., S. Crooks, C. Pascoe, S. Sparrow, and M. Palmer (2004), Solar and QBO influences on the timing of stratospheric sudden warmings, *J. Atmos. Sci.*, *61*, 2777–2796, doi:10.1175/JAS-3297.1.

Gray, L. J., S. A. Crooks, M. A. Palmer, C. L. Pascoe, and S. Sparrow (2006), A possible transfer mechanism for the 11-year solar cycle to the lower stratosphere, *Space Sci. Rev.*, *125*, 357–370, doi:10.1007/s11214-006-9069-y.

Gray, L. J., S. T. Rumbold, and K. P. Shine (2009), Stratospheric temperature and radiative forcing response to 11-year solar cycle changes in irradiance and ozone, *J. Atmos. Sci.*, *66*, 2402–2417, doi:10.1175/2009JAS2866.1.

Gunn, R. (1965), The hyperelectrification of raindrops by electric fields, *J. Meteorol.*, *13*, 283–288.

Haigh, J. D. (1994), The role of stratospheric ozone in modulating the solar radiative forcing of climate, *Nature*, *370*, 544–546, doi:10.1038/370544a0.

Haigh, J. D. (1996), The impact of solar variability on climate, *Science*, *272*, 981–984, doi:10.1126/science.272.5264.981.

Haigh, J. D. (1999), A GCM study of climate change in response to the 11-year solar cycle, *Q. J. R. Meteorol. Soc.*, *125*, 871–892, doi:10.1002/qj.49712555506.

Haigh, J. D. (2003), The effects of solar variability on the Earth's climate, *Philos. Trans. R. Soc. London, Ser. A*, *361*, 95–111, doi:10.1098/rsta.2002.1111.

Haigh, J. D. (2007), The Sun and the Earth's climate, *Living Rev. Sol. Phys.*, *4*, lrsp-2007-2.

Haigh, J. D., and M. Blackburn (2006), Solar influences on dynamical coupling between the stratosphere and troposphere, *Space Sci. Rev.*, *125*, 331–344, doi:10.1007/s11214-006-9067-0.

Haigh, J. D., and H. K. Roscoe (2009), The final warming date of the Antarctic polar vortex and influences on its interannual variability, *J. Clim.*, *22*, 5809–5819, doi:10.1175/2009JCLI2865.1.

Haigh, J. D., M. Blackburn, and R. Day (2005), The response of tropospheric circulation to perturbations in lower-stratospheric temperature, *J. Clim.*, *18*, 3672–3685, doi:10.1175/JCLI3472.1.

Haigh, J. D., A. R. Winning, R. Toumi, and J. W. Harder (2010), An influence of solar spectral variations on radiative forcing of climate, *Nature*, in press.

Hall, J. C., and G. W. Lockwood (2004), The chromospheric activity and variability of cycling and flat activity solar-analog stars, *Astrophys. J.*, *614*(2), 942–946, doi:10.1086/423926.

Hamilton, K. (2002), On the quasi decadal modulation of the stratospheric QBO period, *J. Clim.*, *15*, 2562–2565, doi:10.1175/1520-0442(2002)015<2562:OTQDMO>2.0.CO;2.

Hannon, G. E., R. H. W. Bradshaw, and S. Wastegard (2003), Rapid vegetation change during the early Holocene in the Faroe Islands detected in terrestrial and aquatic ecosystems, *J. Quat. Sci.*, *18*, 615–619, doi:10.1002/jqs.783.

Hansen, J., M. Sato, and R. Reudy (1997), Radiative forcing and climate response, *J. Geophys. Res.*, *102*, 6831–6864, doi:10.1029/96JD03436.

Harder, J. W., J. M. Fontenla, P. Pilewskie, E. C. Richard, and T. N. Woods (2009), Trends in solar spectral irradiance variability in the visible and infrared, *Geophys. Res. Lett.*, *36*, L07801, doi:10.1029/2008GL036797.

Hardiman, S. C., and P. H. Haynes (2008), Dynamical sensitivity of the stratospheric circulation and downward influence of upper level perturbations, *J. Geophys. Res.*, *113*, D23103, doi:10.1029/2008JD010168.

Harris, R. N., and D. S. Chapman (2005), Borehole temperatures and tree rings: Seasonality and estimates of extratropical northern hemispheric warming, *J. Geophys. Res.*, *110*, F04003, doi:10.1029/2005JF000303.

Harrison, R. G. (2000), Cloud formation and the possible significance of charge for atmospheric condensation and ice nuclei, *Space Sci. Rev.*, *94*, 381–396, doi:10.1023/A:1026708415235.

Harrison, R. G. (2008), Discrimination between cosmic ray and solar irradiance effects on clouds and evidence for geophysical modulation of cloud thickness, *Proc. R. Soc. A*, *464*, 2575–2590.

Harrison, R. G., and M. H. P. Ambaum (2008), Enhancement of cloud formation by droplet charging, *Proc. R. Soc. A*, *464*, 2561–2573, doi:10.1098/rspa.2008.0009.

Harrison, R. G., and M. H. P. Ambaum (2009), Observed atmospheric electricity effect on clouds, *Environ. Res. Lett.*, *4*, 014003, doi:10.1088/1748-9326/4/1/014003.

Harrison, R. G., and W. J. Ingram (2005), Air-Earth current measurements at Kew, London, 1909–1979, *Atmos. Res.*, *76*, 49–64, doi:10.1016/j.atmosres.2004.11.022.

Harrison, R. G., and D. B. Stephenson (2005), Empirical evidence for a nonlinear effect of galactic cosmic rays on clouds, *Proc. R. Soc. A*, *462*, 1221–1233, doi:10.1098/rspa.2005.1628.

Harrison, R. G., and I. Usoskin (2010), Solar modulation in surface atmospheric electricity, *J. Atmos. Sol. Terr. Phys.*, *72*, 176–182, doi:10.1016/j.jastp.2009.11.006.

Harrison, R. G., N. Chalmers, and R. J. Hogan (2008), Retrospective cloud determinations from surface solar radiation measurements, *Atmos. Res.*, *90*, 54–62, doi:10.1016/j.atmosres.2008.04.001.

Hartley, D. E., J. T. Villarin, R. X. Black, and C. A. Davis (1998), A new perspective on the dynamical link between the stratosphere and troposphere, *Nature*, *391*, 471–474, doi:10.1038/35112.

Hartmann, D. L., J. M. Wallace, V. Limpasuvan, D. W. J. Thompson, and J. R. Holton (2000), Can ozone depletion and global warming interact to produce rapid climate change?, *Proc. Natl. Acad. Sci. U. S. A.*, *97*, 1412–1417, doi:10.1073/pnas.97.4.1412.

Harvey, K. L. (1992), The cyclic behavior of solar activity, in *The Solar Cycle: Proceedings of the National Solar Observatory/Sacramento Peak 12th Summer Workshop, Sunspot, NM, Oct. 15–18, 1991*, *ASP Conf. Ser.*, vol. 27, edited by K. L. Harvey, pp. 335–367, Astron. Soc. of the Pac., San Francisco, Calif.

Haug, G. H., K. A. Hughen, D. M. Sigman, L. C. Peterson, and U. Röhl (2001), Southward migration of the Intertropical Convergence Zone trough in the Holocene, *Science*, *293*, 1304–1308, doi:10.1126/science.1059725.

Haynes, P. (2005), Stratospheric dynamics, *Annu. Rev. Fluid Mech.*, *37*, 263–293, doi:10.1146/annurev.fluid.37.061903.175710.

Hegerl, G. C., H. von Storch, K. Hasselmann, B. D. Santer, U. Cubasch, and P. D. Jones (1996), Detecting greenhouse-gas-induced climate change with an optimal fingerprint method, *J. Clim.*, *9*(10), 2281–2306, doi:10.1175/1520-0442(1996)009<2281:DGGICC>2.0.CO;2.

Hegerl, G. C., T. J. Crowley, S. K. Baum, K. Y. Kim, and W. T. Hyde (2003), Detection of volcanic, solar and greenhouse gas signals in paleo-reconstructions of Northern Hemispheric temperature, *Geophys. Res. Lett.*, *30*(5), 1242, doi:10.1029/2002GL016635.

Heikkilä, U., J. Beer, and J. Feichter (2008), Modeling cosmogenic radionuclides ^{10}Be and ^{7}Be during the Maunder Minimum using the ECHAM5-HAM General Circulation Model, *Atmos. Chem. Phys.*, *8*, 2797–2809, doi:10.5194/acp-8-2797-2008.

Heikkilä, U., J. Beer, and J. Feichter (2009), Meridional transport and deposition of atmospheric ^{10}Be, *Atmos. Chem. Phys.*, *9*, 515–527, doi:10.5194/acp-9-515-2009.

Herman, J. R., and R. A. Goldberg (1978), Sun, weather and climate, *NASA Spec. Publ.*, *426*.

Herschel, W. (1801), Observations tending to investigate the nature of the Sun, in order to find the causes or symptoms of its variable emission of light and heat: With remarks on the use that may possibly be drawn from solar observations, *Philos. Trans. R. Soc. London*, *91*, 265–318, doi:10.1098/rstl.1801.0015.

Hines, C. O. (1974), A possible mechanism for the production of Sun-weather correlations, *J. Atmos. Sci.*, *31*, 589–591, doi:10.1175/1520-0469(1974)031<0589:APMFTP>2.0.CO;2.

Hofmann, D. J., J. H. Butler, and P. P. Tans (2008), A new look at atmospheric carbon dioxide, *Atmos. Environ.*, *43*, 2084–2086, doi:10.1016/j.atmosenv.2008.12.028.

Holton, J. R., and H.-C. Tan (1980), The influence of the equatorial Quasi-Biennial Oscillation on the global circulation at 50 mb, *J. Atmos. Sci.*, *37*, 2200–2208, doi:10.1175/1520-0469(1980)037<2200:TIOTEQ>2.0.CO;2.

Holton, J. R., and H.-C. Tan (1982), The Quasi-Biennial Oscillation in the Northern Hemisphere lower stratosphere, *J. Meteorol. Soc. Jpn.*, *60*, 140–148.

Hong, Y. T., Z. G. Wang, H. B. Jiang, Q. H. Lin, B. Hong, Y. X. Zhu, Y. Wang, L. S. Xu, X. T. Leng, and H. D. Li (2001), A 6000-year record of changes in drought and precipitation in northeast China based on a δ^{13}C time series from peat cellulose, *Earth Planet. Sci. Lett.*, *185*(1–2), 111–119, doi:10.1016/S0012-821X(00)00367-8.

Hood, L. (2004), Effects of solar UV variability on the stratosphere, in *Solar Variability and Its Effect on the Earth's Atmosphere and Climate System*, *Geophys. Monogr. Ser.*, vol. 14, edited by J. Pap et al., pp. 283–303, AGU, Washington, D. C.

Hood, L. L., and B. E. Soukharev (2003), Quasi-decadal variability of the tropical lower stratosphere: The role of extratropical wave forcing, *J. Atmos. Sci.*, *60*, 2389–2403, doi:10.1175/1520-0469(2003)060<2389:QVOTTL>2.0.CO;2.

Hood, L. L., and B. E. Soukharev (2010), Decadal variability of the tropical stratosphere: Secondary influence of the El Niño–Southern Oscillation, *J. Geophys. Res.*, *115*, D11113, doi:10.1029/2009JD012291.

Hood, L. L., J. L. Jirikowic, and J. P. McCormack (1993), Quasi decadal variability of the stratosphere: Influence of long-term solar ultraviolet variations, *J. Atmos. Sci.*, *50*, 3941–3958, doi:10.1175/1520-0469(1993)050<3941:QDVOTS>2.0.CO;2.

Hõrrak, U., J. Salm, and H. Tammet (1998), Bursts of intermediate ions in atmospheric air, *J. Geophys. Res.*, *103*(D12), 13,909–13,915, doi:10.1029/97JD01570.

Hoyt, D. V., and K. H. Schatten (1993), A discussion of plausible solar irradiance variations 1700–1992, *J. Geophys. Res.*, *98*, 18,895–18,906, doi:10.1029/93JA01944.

Hoyt, D. V., and K. H. Schatten (1997), *The Role of the Sun in Climate Change*, 279 pp., Oxford Univ. Press, Oxford, U. K.

Hu, F. S., D. Kaufman, S. Yoneji, D. Nelson, A. Shemesh, Y. Huang, J. Tian, G. Bond, B. Clegg, and T. Brown (2003), Cyclic variation and solar forcing of Holocene climate in the Alaskan subarctic, *Science*, *301*, 1890–1893, doi:10.1126/science.1088568.

Intergovernmental Panel on Climate Change (IPCC) (2007), *Climate Change 2007: The Physical Science Basis—Contribution of Working Group I to the Fourth Assessment Report of the Intergovernmental Panel on Climate Change*, edited by S. Solomon et al., pp. 663–745, Cambridge Univ. Press, Cambridge, U. K.

Jackman, C. H., M. T. DeLand, G. J. Labow, E. I. Fleming, and M. López-Puertas (2006), Satellite measurements of middle atmospheric impacts by solar proton events in solar cycle 23, *Space Sci. Rev.*, *125*, 381–391, doi:10.1007/s11214-006-9071-4.

Jackman, C. H., et al. (2008), Short- and medium-term atmospheric constituent effects of very large solar proton events, *Atmos. Chem. Phys.*, *8*, 765–785, doi:10.5194/acp-8-765-2008.

Jones, P. D., and M. E. Mann (2004), Climate over past millennia, *Rev. Geophys.*, *42*, RG2002, doi:10.1029/2003RG000143.

Jones, P. D., K. R. Briffa, and T. J. Osborn (2003), Changes in the Northern Hemisphere annual cycle: Implications for paleoclimatology?, *J. Geophys. Res.*, *108*(D18), 4588, doi:10.1029/2003JD003695.

Jones, P. D., et al. (2009), High resolution paleoclimatology of the last millennium: A review of current status and future prospects, *Holocene*, *19*(1), 3–49, doi:10.1177/0959683608098952.

Kazil, J., and E. R. Lovejoy (2004), Tropospheric ionization and aerosol production: A model study, *J. Geophys. Res.*, *109*, D19206, doi:10.1029/2004JD004852.

Kazil, J., E. R. Lovejoy, M. C. Barth, and K. O'Brien (2006), Aerosol nucleation over oceans and the role of galactic cosmic rays, *Atmos. Chem. Phys.*, *6*, 4905–4924, doi:10.5194/acp-6-4905-2006.

Keigwin, L. D., and R. S. Pickart (1999), Slope water current over the Laurentian Fan on interannual to millennial time scales, *Science*, *286*, 520–523, doi:10.1126/science.286.5439.520.

Kernthaler, S. C., R. Toumi, and J. D. Haigh (1999), Some doubts concerning a link between cosmic ray fluxes and global cloudiness, *Geophys. Res. Lett.*, *26*(7), 863–865, doi:10.1029/1999GL900121.

Khain, A., V. Arkhipov, M. Pinsky, Y. Feldman, and Y. Ryabov (2004), Rain enhancement and fog elimination by seeding with charged droplets. Part I: Theory and numerical simulations, *J. Appl. Meteorol.*, *43*, 1513–1529, doi:10.1175/JAM2131.1.

Kilian, M. R., J. van der Plicht, and B. van Geel (1995), Dating raised bogs: New aspects of AMS ^{14}C wiggle matching, a reservoir effect and climatic change, *Quat. Sci. Rev.*, *14*, 959–966, doi:10.1016/0277-3791(95)00081-X.

Klein, S. A., and D. L. Hartmann (1993), Spurious changes in the ISCCP dataset, *Geophys. Res. Lett.*, *20*, 455–458, doi:10.1029/93GL00211.

Kniveton, D. R., B. A. Tinsley, G. B. Burns, E. A. Bering, and O. A. Troshichev (2008), Variations in global cloud cover and the fair-weather vertical electric field, *J. Atmos. Sol. Terr. Phys.*, *70*, 1633–1642, doi:10.1016/j.jastp.2008.07.001.

Knutson, T. R., T. L. Delworth, K. W. Dixon, I. M. Held, J. Lu, V. Ramaswamy, M. D. Schwarzkopf, G. Stenchikov, and R. J. Stouffer (2006), Assessment of twentieth-century regional surface temperature trends using the GFDL CM2 coupled models, *J. Clim.*, *19*, 1624–1651, doi:10.1175/JCLI3709.1.

Kodera, K. (1995), On the origin and nature of the interannual variability of the winter stratospheric circulation in the Northern Hemisphere, *J. Geophys. Res.*, *100*, 14,077–14,087, doi:10.1029/95JD01172.

Kodera, K. (2002), Solar cycle modulation of the North Atlantic Oscillation: Implications in the spatial structure of the NAO, *Geophys. Res. Lett.*, *29*(8), 1218, doi:10.1029/2001GL014557.

Kodera, K. (2004), Solar influence on the Indian Ocean Monsoon through dynamical processes, *Geophys. Res. Lett.*, *31*, L24209, doi:10.1029/2004GL020928.

Kodera, K., and Y. Kuroda (2002), Dynamical response to the solar cycle: Winter stratopause and lower stratosphere, *J. Geophys. Res.*, *107*(D24), 4749, doi:10.1029/2002JD002224.

Kodera, K., and K. Shibata (2006), Solar influence on the tropical stratosphere and troposphere in the northern summer, *Geophys. Res. Lett.*, *33*, L19704, doi:10.1029/2006GL026659.

Kodera, K., and K. Yamazaki (1990), Long-term variation of upper stratospheric circulation in the Northern Hemisphere in December, *J. Meteorol. Soc. Jpn.*, *68*, 101–105.

Kodera, K., M. Chiba, and K. Shibata (1991), A general circulation model study of the solar and QBO modulation of the stratospheric

circulation during Northern Hemisphere winter, *Geophys. Res. Lett.*, *18*, 1209–1212, doi:10.1029/91GL01610.

Kodera, K., K. Matthes, K. Shibata, U. Langematz, and Y. Kuroda (2003), Solar impact on the lower mesospheric subtropical jet in winter: A comparative study with general circulation model simulations, *Geophys. Res. Lett.*, *30*(6), 1315, doi:10.1029/2002GL016124.

Kodera, K., K. Coughlin, and O. Arakawa (2007), Possible modulation of the connection between the Pacific and Indian Ocean variability by the solar cycle, *Geophys. Res. Lett.*, *34*, L03710, doi:10.1029/2006GL027827.

Kondrashov, D., V. Feliks, and M. Ghil (2005), Oscillatory modes of extended Nile River records (A. D. 622–1922), *Geophys. Res. Lett.*, *32*, L10702, doi:10.1029/2004GL022156.

Kopp, G., G. Lawrence, and G. Rottman (2005), The Total Irradiance Monitor (TIM): Science results, *Sol. Phys.*, *230*(1–2), 129–139.

Kristjánsson, J. E., and J. Kristiansen (2000), Is there a cosmic ray signal in recent variations in global cloudiness and cloud radiative forcing?, *J. Geophys. Res.*, *105*(D9), 11,851–11,863, doi:10.1029/2000JD900029.

Kristjánsson, J. E., A. Staple, J. Kristiansen, and E. Kaas (2002), A new look at possible connections between solar activity, clouds and climate, *Geophys. Res. Lett.*, *29*(23), 2107, doi:10.1029/2002GL015646

Kristjánsson, J. E., C. W. Stjern, F. Stordal, A. M. Fjaeraa, G. Myhre, and K. Jonasson (2008), Cosmic rays, cloud condensation nuclei and clouds—A reassessment using MODIS data, *Atmos. Chem. Phys.*, *8*(24), 7373–7387.

Krivova, N. A., and S. K. Solanki (2005), Reconstruction of solar UV irradiance, *Adv. Space Res.*, *35*, 361–364, doi:10.1016/j.asr.2004.12.027.

Krivova, N. A., S. K. Solanki, M. Fligge, and Y. C. Unruh (2003), Reconstruction of solar irradiance variations in cycle 23: Is solar surface magnetism the cause?, *Astron. Astrophys.*, *399*, L1–L4, doi:10.1051/0004-6361:20030029.

Krivova, N. A., L. Balmaceda, and S. K. Solanki (2007), Reconstruction of solar total irradiance since 1700 from the surface magnetic flux, *Astron. Astrophys.*, *467*, 335–346, doi:10.1051/0004-6361:20066725.

Kuhn, J. R., and K. G. Libbrecht (1991), Non-facular solar luminosity variations, *Astrophys. J.*, *381*, L35–L37, doi:10.1086/186190.

Kuroda, Y., and K. Kodera (1999), Role of planetary waves in the stratosphere troposphere coupled variability in the Northern Winter, *Geophys. Res. Lett.*, *26*, 2375–2378, doi:10.1029/1999GL900507.

Kuroda, Y., and K. Kodera (2004), Role of the Polar-night Jet Oscillation on the formation of the Arctic Oscillation in the Northern Hemisphere winter, *J. Geophys. Res.*, *109*, D11112, doi:10.1029/2003JD004123.

Kuroda, Y., and K. Kodera (2005), Solar cycle modulation of the Southern Annular Mode, *Geophys. Res. Lett.*, *32*, L13802, doi:10.1029/2005GL022516.

Kuroda, Y., M. Deushi, and K. Shibata (2007), Role of solar activity in the troposphere-stratosphere coupling in the Southern Hemisphere winter, *Geophys. Res. Lett.*, *34*, L21704, doi:10.1029/2007GL030983.

Kushner, P. J., and L. M. Polvani (2004), Stratosphere-troposphere coupling in a relatively simple AGCM: The role of eddies, *J. Clim.*, *17*, 629–639, doi:10.1175/1520-0442(2004)017<0629:SCIARS>2.0.CO;2.

Kushner, P. J., and L. M. Polvani (2006), Stratosphere-troposphere coupling in a relatively simple AGCM: Impact of the seasonal cycle, *J. Clim.*, *19*, 5721–5727, doi:10.1175/JCLI4007.1.

Labitzke, K. (1987), Sunspots, the QBO and the stratospheric temperature in the north polar region, *Geophys. Res. Lett.*, *14*, 535–537, doi:10.1029/GL014i005p00535.

Labitzke, K. (2003), The global signal of the 11-year solar cycle in the atmosphere: When do we need the QBO?, *Meteorol. Z.*, *12*, 209–216, doi:10.1127/0941-2948/2003/0012-0211.

Labitzke, K., and H. van Loon (1988), Associations between the 11-year solar cycle, the QBO and the atmosphere. Part I: The troposphere and stratosphere in the northern hemisphere in winter, *J. Atmos. Terr. Phys.*, *50*, 197–206, doi:10.1016/0021-9169(88)90068-2.

Labitzke, K., and H. van Loon (1995), Connections between the troposphere and stratosphere on a decadal scale, *Tellus, Ser. A*, *47*, 275–286, doi:10.1034/j.1600-0870.1995.t01-1-00008.x.

Labitzke, K., J. Austin, N. Butchart, J. Knight, M. Takahashi, M. Nakamoto, T. Nagashima, J. Haigh, and V. Williams (2002), The global signal of the 11-year solar cycle in the stratosphere: Observations and model results, *J. Atmos. Terr. Phys.*, *64*, 203–210, doi:10.1016/S1364-6826(01)00084-0.

Labitzke, K., M. Kunze, and S. Bronnimann (2006), Sunspots, the QBO and the stratosphere in the north polar region—20 years later, *Meteorol. Z.*, *15*, 355–363, doi:10.1127/0941-2948/2006/0136.

Langematz, U., J. L. Grenfell, K. Matthes, P. Mieth, M. Kunze, B. Steil, and C. Brühl (2005), Chemical effects in 11-year solar cycle simulations with the Freie Universität Berlin Climate Middle Atmosphere Model with online chemistry (FUB-CMAM-CHEM), *Geophys. Res. Lett.*, *32*, L13803, doi:10.1029/2005GL022686.

Larkin, A., J. D. Haigh, and S. Djavidnia (2000), The effect of solar UV radiation variations on the Earth's atmosphere, *Space Sci. Rev.*, *94*, 199–214, doi:10.1023/A:1026771307057.

Laut, P. (2003), Solar activity and terrestrial climate: An analysis of some purported correlations, *J. Atmos. Sol. Terr. Phys.*, *65*, 801–812, doi:10.1016/S1364-6826(03)00041-5.

Lean, J. (1991), Variations in the Suns radiative output, *Rev. Geophys.*, *29*(4), 505–535, doi:10.1029/91RG01895.

Lean, J. (2000a), Evolution of the Sun's spectral irradiance since the Maunder Minimum, *Geophys. Res. Lett.*, *27*, 2425–2428, doi:10.1029/2000GL000043.

Lean, J. L. (2000b), Short term, direct indices of solar variability, *Space Sci. Rev.*, *94*, 39–51, doi:10.1023/A:1026726029831.

Lean, J. L. (2006), Comment on "Estimated solar contribution to the global surface warming using the ACRIM TSI satellite composite" by N. Scafetta and B. J. West, *Geophys. Res. Lett.*, *33*, L15701, doi:10.1029/2005GL025342.

Lean, J., J. Beer, and R. Bradley (1995), Reconstruction of solar irradiance since 1610: Implications for climate change, *Geophys. Res. Lett.*, *22*, 3195–3198, doi:10.1029/95GL03093.

Lean, J. L., Y.-M. Wang, and N. R. Sheeley Jr. (2002), The effect of increasing solar activity on the Sun's total and open magnetic flux during multiple cycles: Implications for solar forcing of climate, *Geophys. Res. Lett.*, *29*(24), 2224, doi:10.1029/2002GL015880.

Lee, J. N., and S. Hameed (2007), The Northern Hemisphere annular mode in summer: Its physical significance and its relation to solar activity variations, *J. Geophys. Res.*, *112*, D15111, doi:10.1029/2007JD008394.

Lee, H., and A. K. Smith (2003), Simulation of the combined effects of solar cycle, quasi-biennial oscillation, and volcanic forcing on stratospheric ozone changes in recent decades, *J. Geophys. Res.*, *108*(D2), 4049, doi:10.1029/2001JD001503.

Lee, J. N., S. Hameed, and D. T. Shindell (2008), Northern annular mode in summer and its relation to solar activity variations in the GISS Model E, *J. Atmos. Sol. Terr. Phys.*, *70*, 730–741, doi:10.1016/j.jastp.2007.10.012.

Lee, J. N., D. T. Shindell, and S. Hameed (2009), The influence of solar forcing on tropical circulation, *J. Clim.*, *22*, 5870–5885, doi:10.1175/2009JCLI2670.1.

Lockwood, M. (2002), An evaluation of the correlation between open solar flux and total solar irradiance, *Astron. Astrophys.*, *382*, 678–687, doi:10.1051/0004-6361:20011666.

Lockwood, M. (2004), Solar outputs, their variations and their effects on Earth, in *The Sun, Solar Analogs and the Climate*, *Proc. Saas Fee Adv. Course*, vol. 34, edited by I. Redi, M. Güdel, and W. Schmutz, pp. 107–304, Springer, Berlin.

Lockwood, M. (2006), What do cosmogenic isotopes tell us about past solar forcing of climate?, *Space Sci. Rev.*, *125*, 95–109, doi:10.1007/s11214-006-9049-2.

Lockwood, M. (2010), Solar change and climate: An update in the light of the current exceptional solar minimum, *Proc. R. Soc. A*, *466*(2114), 303–329, doi:10.1098/rspa.2009.0519.

Lockwood, M., and C. Fröhlich (2007), Recent oppositely directed trends in solar climate forcings and the global mean surface air temperature, *Proc. R. Soc. A*, *463*(2086), 2447–2460.

Lockwood, M., and C. Fröhlich (2008), Recent oppositely directed trends in solar climate forcings and the global mean surface air temperature: II. Different reconstructions of the total solar irradiance variation and dependence on response time scale, *Proc. R. Soc.*, *464*, 1367–1385.

Lockwood, M., and R. Stamper (1999), Long-term drift of the coronal source magnetic flux and the total solar irradiance, *Geophys. Res. Lett.*, *26*, 2461–2464, doi:10.1029/1999GL900485.

Lockwood, M., R. Stamper, and M. N. Wild (1999), A doubling of the Sun's coronal magnetic field during the last 100 years, *Nature*, *399*, 437–439, doi:10.1038/20867.

Long, C. N., and T. P. Ackerman (2000), Identification of clear skies from broadband pyranometer measurements and calculation of downwelling shortwave cloud effects, *J. Geophys. Res.*, *105*, 15,609–15,626, doi:10.1029/2000JD900077.

Lu, H., M. A. Clilverd, A. Seppala, and L. L. Hood (2008), Geomagnetic perturbations on stratospheric circulation in late winter and spring, *J. Geophys. Res.*, *113*, D16106, doi:10.1029/2007JD008915.

Luterbacher, J., C. Schmutz, D. Gyalistras, E. Xoplaki, and H. Wanner (1999), Reconstruction of monthly NAO and EU indices back to 1675, *Geophys. Res. Lett.*, *26*, 2745–2748, doi:10.1029/1999GL900576.

Luterbacher, J., R. Rickli, E. Xoplaki, C. Tinguely, C. Beck, C. Pfister, and H. Wanner (2001), The late Maunder Minimum (1675–1715)—A key period for studying decadal scale climatic change in Europe, *Clim. Change*, *49*, 441–462, doi:10.1023/A:1010667524422.

Luterbacher, J., et al. (2002), Extending North Atlantic Oscillation reconstructions back to 1500, *Atmos. Sci. Lett.*, *2*, 114–124, doi:10.1006/asle.2002.0047.

Luterbacher, J., D. Dietrich, E. Xoplaki, M. Grosjean, and H. Wanner (2004), European seasonal and annual temperature variability, trends and extremes since 1500, *Science*, *303*, 1499–1503, doi:10.1126/science.1093877.

Mangini, A., C. Spötl, and P. Verdes (2005), Reconstruction of temperature in the Central Alps during the past 2000 yr from a $\delta^{18}O$ stalagmite record, *Earth Planet. Sci. Lett.*, *235*, 741–750, doi:10.1016/j.epsl.2005.05.010.

Mann, M. E., R. S. Bradley, and M. K. Hughes (1999), Northern hemisphere temperatures during the past millennium: Inferences, uncertainties, and limitations, *Geophys. Res. Lett.*, *26*, 759–762, doi:10.1029/1999GL900070.

Mann, M. E., Z. Zhang, S. Rutherford, R. S. Bradley, M. K. Hughes, D. Shindell, C. Ammann, G. Faluvegi, and F. Ni (2009), Global signatures of the Little Ice Age and Medieval climate anomaly and plausible dynamical origins, *Science*, *326*, 1256–1260, doi:10.1126/science.1177303.

Markson, R. (1981), Modulation of the Earth's electric field by cosmic radiation, *Nature*, *291*, 304–308, doi:10.1038/291304a0.

Markson, R., and M. Muir (1980), Solar wind control of the Earth's electric field, *Science*, *208*(4447), 979–990, doi:10.1126/science.208.4447.979.

Marsh, D. R., and R. R. Garcia (2007), Attribution of decadal variability in lower-stratospheric tropical ozone, *Geophys. Res. Lett.*, *34*, L21807, doi:10.1029/2007GL030935.

Marsh, N., and H. Svensmark (2000), Cosmic rays, clouds, and climate, *Space Sci. Rev.*, *94*, 215–230, doi:10.1023/A:1026723423896.

Marsh, N., and H. Svensmark (2003), Galactic cosmic ray and El Nino Southern Oscillation trends in International Satellite Cloud Climatology Project D2 low-cloud properties, *J. Geophys. Res.*, *108*(D6), 4195, doi:10.1029/2001JD001264.

Marsh, N., and H. Svensmark (2004), Comment on "Solar influences on cosmic rays and cloud formation: A reassessment" by Bomin Sun and Raymond S. Bradley, *J. Geophys. Res.*, *109*, D14205, doi:10.1029/2003JD004063.

Marsh, D. R., R. R. Garcia, D. E. Kinnison, B. A. Boville, F. Sassi, S. C. Solomon, and K. Matthes (2007), Modeling the whole atmosphere response to solar cycle changes in radiative and geomagnetic forcing, *J. Geophys. Res.*, *112*, D23306, doi:10.1029/2006JD008306.

Masarik, J., and J. Beer (2009), An updated simulation of particle fluxes and cosmogenic nuclide production in the Earth's atmosphere, *J. Geophys. Res.*, *114*, D11103, doi:10.1029/2008JD010557.

Mason, B. J. (1971), *The Physics of Clouds*, Pergamon, New York.

Matthes, K., K. Kodera, J. D. Haigh, D. T. Shindell, K. Shibata, U. Langematz, E. Rozanov, and Y. Kuroda (2003), GRIPS solar experiments intercomparison project: Initial results, *Pap. Meteorol. Geophys.*, *54*, 71–90, doi:10.2467/mripapers.54.71.

Matthes, K., U. Langematz, L. J. Gray, K. Kodera, and K. Labitzke (2004), Improved 11-year solar signal in the Freie Universität Berlin Climate Middle Atmosphere Model (FUB-CMAM), *J. Geophys. Res.*, *109*, D06101, doi:10.1029/2003JD004012.

Matthes, K., Y. Kuroda, K. Kodera, and U. Langematz (2006), Transfer of the solar signal from the stratosphere to the troposphere: Northern winter, *J. Geophys. Res.*, *111*, D06108, doi:10.1029/2005JD006283.

Matthes, K., K. Kodera, L. Gray, J. Austin, A. Kubin, U. Langematz, D. Marsh, J. McCormack, K. Shibata, and D. Shindell (2007), Report on the first SOLARIS workshop 4–6 October 2006, *SPARC Newsl., 28*, Sci. Policy Assess. and Res. on Clim., Boulder, Colo.

Matthes, K., D. Marsh, R. Garcia, F. Sassi, and S. Walters (2010), Role of the QBO in modulating the influence of the 11 year solar cycle on the atmosphere using constant forcings, *J. Geophys. Res.*, *115*, D18110, doi:10.1029/2009JD013020.

Mauquoy, D., B. van Geel, M. Blaauw, and J. van der Plicht (2002), Evidence from northwest European bogs shows 'Little Ice Age' climatic changes driven by variations in solar activity, *Holocene*, *12*, 1–6, doi:10.1191/0959683602hl514rr.

Mayr, H. G., J. G. Mengel, C. L. Wolff, and H. S. Porter (2006), QBO as potential amplifier of solar cycle influence, *Geophys. Res. Lett.*, *33*, L05812, doi:10.1029/2005GL025650.

McCormack, J. (2003), The influence of the 11-year solar cycle on the quasi-biennial oscillation, *Geophys. Res. Lett.*, *30*(22), 2162, doi:10.1029/2003GL018314.

McCormack, J. P., and L. L. Hood (1996), Apparent solar cycle variations of upper stratospheric ozone and temperature: Latitude and seasonal dependences, *J. Geophys. Res.*, *101*, 20,933–20,944, doi:10.1029/96JD01817.

McCormack, J. P., D. E. Siskind, and L. L. Hood (2007), Solar-QBO interaction and its impact on stratospheric ozone in a zonally averaged photochemical transport model of the middle atmosphere, *J. Geophys. Res.*, *112*, D16109, doi:10.1029/2006JD008369.

Meehl, G. A., and J. M. Arblaster (2009), A lagged warm event-like response to peaks in solar forcing in the Pacific region, *J. Clim.*, *22*(13), 3647–3660.

Meehl, G. A., W. M. Washington, T. M. L. Wigley, J. M. Arblaster, and A. Dai (2003), Solar and greenhouse gas forcing and climate response in the 20th century, *J. Clim.*, *16*, 426–444, doi:10.1175/1520-0442(2003)016<0426:SAGGFA>2.0.CO;2.

Meehl, G. A., W. M. Washington, C. M. Amman, J. M. Arblaster, T. M. L. Wigley, and C. Tebaldi (2004), Combinations of natural and anthropogenic forcings and 20th century climate, *J. Clim.*, *17*, 3721–3727, doi:10.1175/1520-0442(2004)017<3721:CONAAF>2.0.CO;2.

Meehl, G. A., J. M. Arblaster, G. Branstator, and H. van Loon (2008), A coupled air-sea response mechanism to solar forcing in the Pacific region, *J. Clim.*, *21*, 2883–2897, doi:10.1175/2007JCLI1776.1.

Meehl, G. A., J. M. Arblaster, K. Matthes, F. Sassi, and H. van Loon (2009), Amplifying the Pacific climate system response to a small 11 year solar cycle forcing, *Science*, *325*, 1114–1118, doi:10.1126/science.1172872.

Mendoza, B. (1997), Estimations of Maunder Minimum solar irradiance and Ca II H and K fluxes using rotation rates and diameters, *Astrophys. J.*, *483*, 523–526, doi:10.1086/304210.

Moore, J., A. Grinsted, and S. Jevrejeva (2006), Is there evidence for sunspot forcing of climate at multi-year and decadal periods?, *Geophys. Res. Lett.*, *33*, L17705, doi:10.1029/2006GL026501.

Muscheler, R., F. Joos, J. Beer, S. A. Müller, M. Vonmoos, and I. Snowball (2007), Solar activity during the last 1000 yr inferred from radionuclide records, *Quat. Sci. Rev.*, *26*, 82–97, doi:10.1016/j.quascirev.2006.07.012.

Naito, Y., and I. Hirota (1997), Interannual variability of the northern winter stratospheric circulation related to the QBO and the solar cycle, *J. Meteorol. Soc. Jpn.*, *75*, 925–937.

Nathan, T. R., and E. C. Cordero (2007), An ozone-modified refractive index for vertically propagating planetary waves, *J. Geophys. Res.*, *112*, D02105, doi:10.1029/2006JD007357.

National Research Council (NRC) (1994), *Natural Climate Variability on Decade-to-Century Timescales*, 81 pp., Natl. Acad., Washington, D. C.

Neff, U., S. J. Burns, A. Mangini, M. Mudelsee, D. Fleitmann, and A. Matter (2001), Strong coherence between solar variability and the monsoon in Oman between 9 and 6 kyr ago, *Nature*, *411*, 290–293, doi:10.1038/35077048.

Nesje, A., and S. O. Dahl (2003), The Little Ice Age—Only temperature?, *Holocene*, *13*, 139–145, doi:10.1191/0959683603hl603fa.

Nesme-Ribes, E., E. N. Ferreira, R. Sadournay, H. Le Truet, and Z. X. Li (1993), Solar dynamics and its impact on solar irradiance and terrestrial climate, *J. Geophys. Res.*, *98*, 18,923–18,935.

Ney, E. P. (1959), Cosmic radiation and the weather, *Nature*, *183*, 451–452, doi:10.1038/183451a0.

Nicoll, K. A., and R. G. Harrison (2009), Vertical current flow through extensive layer clouds, *J. Atmos. Sol. Terr. Phys.*, *71*(12), 1219–1221.

North, G. R., and M. J. Stevens (1998), Detecting climate signals in the surface temperature record, *J. Clim.*, *11*(4), 563–577.

Palmer, M. A., L. J. Gray, M. R. Allen, and W. A. Norton (2004), Solar forcing of climate: Model results, *Adv. Space Res.*, *34*, 343–348, doi:10.1016/j.asr.2003.02.039.

Pascoe, C. L., L. J. Gray, S. A. Crooks, M. N. Juckes, and M. P. Baldwin (2005), The quasi biennial oscillation: Analysis using ERA-40 data, *J. Geophys. Res.*, *110*, D08105, doi:10.1029/2004JD004941.

Pauling, A., J. Luterbacher, C. Casty, and H. Wanner (2006), Five hundred years of gridded high resolution precipitation reconstructions over Europe and the connection to large-scale circulation, *Clim. Dyn.*, *26*, 387–405, doi:10.1007/s00382-005-0090-8.

Perlwitz, J., and N. Harnik (2003), Observational evidence of a stratospheric influence on the troposphere by planetary wave reflection, *J. Clim.*, *16*, 3011–3026, doi:10.1175/1520-0442(2003)016<3011:OEOASI>2.0.CO;2.

Pierce, J. R., and P. J. Adams (2009), Can cosmic rays affect cloud condensation nuclei by altering new particle formation rates?, *Geophys. Res. Lett.*, *36*, L09820, doi:10.1029/2009GL037946.

Pittock, A. B. (1978), A critical look at long-term Sun-weather relationships, *Rev. Geophys.*, *16*, 400–420, doi:10.1029/RG016i003p00400.

Plumb, R. A., and K. Semeniuk (2003), Downward migration of extratropical zonal wind anomalies, *J. Geophys. Res.*, *108*(D7), 4223, doi:10.1029/2002JD002773.

Polissar, P. J., M. B. Abbott, A. P. Wolfe, M. Bezada, V. Rull, and R. S. Bradley (2006), Solar modulation of Little Ice Age climate in the tropical Andes, *Proc. Natl. Acad. Sci. U. S. A.*, *103*, 8937–8942, doi:10.1073/pnas.0603118103.

Polvani, L. M., and P. J. Kushner (2002), Tropospheric response to stratospheric perturbations in a relatively simple general circulation model, *Geophys. Res. Lett.*, *29*(7), 1114, doi:10.1029/2001GL014284.

Poore, R. Z., T. M. Quinn, and S. Verardo (2004), Century-scale movement of the Atlantic Intertropical Convergence Zone linked to solar variability, *Geophys. Res. Lett.*, *31*, L12214, doi:10.1029/2004GL019940.

Pulkkinen, T. I., H. Nevanlinna, P. J. Pulkkinen, and M. Lockwood (2001), The Earth-Sun connection in time scales from years to decades to centuries, *Space Sci. Rev.*, *95*(1–2), 625–637, doi:10.1023/A:1005299314802.

Ramaswamy, V., J. W. Hurrell, and G. A. Meehl (2006), Why do temperatures vary vertically (from the surface to the stratosphere) and what do we understand about why they might vary and change over time?, in *Temperature Trends in the Lower Atmosphere: Steps for Understanding and Reconciling Difference*, edited by T. R. Karl et al., pp. 15–28, U.S. Clim. Change Sci. Program, Washington, D. C.

Randall, C. E., D. W. Rusch, R. M. Bevilacqua, K. W. Hoppel, and J. D. Lumpe (1998), Polar Ozone and Aerosol Measurement (POAM) II stratospheric NO_2, 1993–1996, *J. Geophys. Res.*, *103*, 28,361–28,371, doi:10.1029/98JD02092.

Randall, C. E., et al. (2005), Stratospheric effects of energetic particle precipitation in 2003–2004, *Geophys. Res. Lett.*, *32*, L05802, doi:10.1029/2004GL022003.

Randall, C. E., V. L. Harvey, C. S. Singleton, P. F. Bernath, C. D. Boone, and J. U. Kozyra (2006), Enhanced NO_x in 2006 linked to strong upper stratospheric arctic vortex, *Geophys. Res. Lett.*, *33*, L18811, doi:10.1029/2006GL027160.

Randall, C. E., V. L. Harvey, C. S. Singleton, S. M. Bailey, P. F. Bernath, M. Codrescu, H. Nakajima, and J. M. Russell III (2007), Energetic particle precipitation effects on the Southern Hemisphere stratosphere in 1992–2005, *J. Geophys. Res.*, *112*, D08308, doi:10.1029/2006JD007696.

Randel, W. J., and F. Wu (2007), A stratospheric ozone profile data set for 1979–2005: Variability, trends and comparisons with column ozone data, *J. Geophys. Res.*, *112*, D06313, doi:10.1029/2006JD007339.

Randel, W. J., et al. (2009), An update of observed stratospheric temperature trends, *J. Geophys. Res.*, *114*, D02107, doi:10.1029/2008JD010421.

Reames, D. V. (1999), Particle acceleration at the Sun and in the heliosphere, *Space Sci. Rev.*, *90*, 413–491, doi:10.1023/A:1005105831781.

Reid, G. C. (1997), Solar forcing and the global climate change since the mid-17th century, *Clim. Change*, *37*, 391–405, doi:10.1023/A:1005307009726.

Reid, G. C. (2000), Solar variability and the Earth's climate: Introduction and overview, *Space Sci. Rev.*, *94*, 1–11, doi:10.1023/A:1026797127105.

Rind, D. (2002), The Sun's role in climate variations, *Science*, *296*, 673–677, doi:10.1126/science.1069562.

Rind, D., J. Lean, and R. Healy (1999), Simulated time-dependent climate response to solar radiative forcing since 1600, *J. Geophys. Res.*, *104*, 1973–1990, doi:10.1029/1998JD200020.

Rind, D., P. Lonergan, N. K. Balachandran, and D. Shindell (2002), 2 × CO_2 and solar variability influences on the troposphere through wave-mean flow interactions, *J. Meteorol. Soc. Jpn.*, *80*, 863–876, doi:10.2151/jmsj.80.863.

Rind, D., D. Shindell, J. Perlwitz, J. Lerner, P. Lonergan, J. Lean, and C. McLinden (2004), The relative importance of solar and anthropogenic forcing of climate change between the Maunder Minimum and the present, *J. Clim.*, *17*, 906–929, doi:10.1175/1520-0442(2004)017<0906:TRIOSA>2.0.CO;2.

Rind, D., J. Lean, J. Lerner, P. Lonergan, and A. Leboissitier (2008), Exploring the stratospheric/tropospheric response to solar forcing, *J. Geophys. Res.*, *113*, D24103, doi:10.1029/2008JD010114.

Rouillard, A., and M. Lockwood (2004), Oscillations in the open solar magnetic flux with period 1.68 years: Imprint on galactic cosmic rays and implications for heliospheric shielding, *Ann. Geophys.*, *22*, 4381–4395, doi:10.5194/angeo-22-4381-2004.

Roy, I., and J. D. Haigh (2010), Solar cycle signals in sea level pressure and sea surface temperature, *Atmos. Chem. Phys.*, *100*, 3147–3153.

Rozanov, E. V., M. E. Schlesinger, T. A. Egorova, B. Li, N. Andronova, and V. A. Zubov (2004), Atmospheric response to the observed increase of solar UV radiation from solar minimum to solar maximum simulated by the University of Illinois at Urbana-Champaign climate-chemistry model, *J. Geophys. Res.*, *109*, D01110, doi:10.1029/2003JD003796.

Rozanov, E. V., L. Callis, E. Schlesinger, F. Yang, N. Andronova, and V. A. Zubov (2005), Atmospheric response to NO_y source due to energetic electron precipitation, *Geophys. Res. Lett.*, *32*, L14811, doi:10.1029/2005GL023041.

Russell, J. M., and T. C. Johnson (2007), Little Ice Age drought in equatorial Africa: Intertropical Convergence Zone migrations and El Niño–Southern Oscillation variability, *Geology*, *35*, 21–24, doi:10.1130/G23125A.1.

Ruzmaikin, A., and J. Feynman (2002), Solar influence on a major mode of atmospheric variability, *J. Geophys. Res.*, *107*(D14), 4209, doi:10.1029/2001JD001239.

Ruzmaikin, A., J. Feynman, and Y. L. Yung (2006), Is solar variability reflected in the Nile River?, *J. Geophys. Res.*, *111*, D21114, doi:10.1029/2006JD007462.

Rycroft, M. J., S. Israelsson, and C. Price (2000), The global atmospheric electric circuit, solar activity and climate change, *J. Atmos. Sol. Terr. Phys.*, *62*, 1563–1576, doi:10.1016/S1364-6826(00)00112-7.

Rycroft, M. J., R. G. Harrison, K. A. Nicoll, and E. A. Mareev (2008), An overview of Earth's global electric circuit and atmospheric conductivity, *Space Sci. Rev.*, *137*, 83–105, doi:10.1007/s11214-008-9368-6.

Salby, M., and P. Callaghan (2000), Connection between the solar cycle and the QBO: The missing link?, *J. Clim.*, *13*, 2652–2662, doi:10.1175/1520-0442(1999)012<2652:CBTSCA>2.0.CO;2.

Salby, M. L., and P. F. Callaghan (2005), Interaction between the Brewer-Dobson circulation and the Hadley circulation, *J. Clim.*, *18*, 4303–4316, doi:10.1175/JCLI3509.1.

Salby, M. L., and P. F. Callaghan (2006), Relationship of the quasi-biennial oscillation to the stratospheric signature of the solar cycle, *J. Geophys. Res.*, *111*, D06110, doi:10.1029/2005JD006012.

Santer, B. D., et al. (1996), A search for human influences on the structure of the atmosphere, *Nature*, *382*, 39–46, doi:10.1038/382039a0.

Santer, B. D., et al. (2003), Behavior of tropopause height and atmospheric temperature in models, reanalyses, and observations: Decadal changes, *J. Geophys. Res.*, *108*(D1), 4002, doi:10.1029/2002JD002258.

Scaife, A. A., J. Austin, N. Butchart, S. Pawson, M. Keil, J. Nash, and I. N. James (2000), Seasonal and interannual variability of the stratosphere diagnosed from UKMO TOVS analyses, *Q. J. R. Meteorol. Soc.*, *126*, 2585–2604, doi:10.1002/qj.49712656812.

Schmidt, H., and G. P. Brasseur (2006), The response of the middle atmosphere to solar cycle forcing in the Hamburg Model of the Neutral and Ionized Atmosphere, *Space Sci. Rev.*, *125*, 345–356, doi:10.1007/s11214-006-9068-z.

Schopf, P. S., and M. J. Suarez (1988), Vacillations in a coupled ocean-atmosphere model, *J. Atmos. Sci.*, *45*, 549–566.

Shepherd, T. G. (2002), Issues in stratosphere-troposphere coupling, *J. Meteorol. Soc. Jpn.*, *80*, 769–792, doi:10.2151/jmsj.80.769.

Shibata, K., and M. Deushi (2008), Long-term variations and trends in the simulation of the middle atmosphere 1980–2004 by the chemistry-climate model of the Meteorological Research Institute, *Ann. Geophys.*, *26*, 1299–1326, doi:10.5194/angeo-26-1299-2008.

Shibata, K., and K. Kodera (2005), Simulation of radiative and dynamical responses of the middle atmosphere to the 11-year solar cycle, *J. Atmos. Sol. Terr. Phys.*, *67*, 125–143, doi:10.1016/j.jastp.2004.07.022.

Shindell, D., D. Rind, N. Balachandran, J. Lean, and P. Lonergan (1999), Solar cycle variability, ozone and climate, *Science*, *284*, 305–308, doi:10.1126/science.284.5412.305.

Shindell, D. T., G. A. Schmidt, R. L. Miller, and D. Rind (2001), Northern Hemisphere winter climate response to greenhouse gas, ozone, solar, and volcanic forcing, *J. Geophys. Res.*, *106*, 7193–7210, doi:10.1029/2000JD900547.

Shindell, D. T., G. A. Schmidt, R. L. Miller, and M. E. Mann (2003), Volcanic and solar forcing of climate change during the preindustrial era, *J. Clim.*, *16*, 4094–4107, doi:10.1175/1520-0442(2003)016<4094:VASFOC>2.0.CO;2.

Shindell, D. T., G. A. Schmidt, M. E. Mann, and G. Faluvegi (2004), Dynamic winter climate response to large tropical volcanic eruptions since 1600, *J. Geophys. Res.*, *109*, D05104, doi:10.1029/2003JD004151.

Shindell, D. T., G. Faluvegi, R. L. Miller, G. A. Schmidt, J. E. Hansen, and S. Sun (2006), Solar and anthropogenic forcing of tropical hydrology, *Geophys. Res. Lett.*, *33*, L24706, doi:10.1029/2006GL027468.

Shiogama, H., N. Christidis, J. Caesar, T. Yokohata, T. Nozawa, and S. Emori (2006), Detection of greenhouse gas and aerosol influences on changes in temperature extremes, *SOLA*, *2*, 152–155, doi:10.2151/sola.2006-039.

Simpson, I., M. Blackburn, and J. D. Haigh (2009), The role of eddies in driving the tropospheric response to stratospheric heating perturbations, *J. Atmos. Sci.*, *66*, 1347–1365.

Siskind, D. E., and J. M. Russell III (1996), Coupling between middle and upper atmospheric NO: Constraints from HALOE observations, *Geophys. Res. Lett.*, *23*, 137–140, doi:10.1029/95GL03782.

Siskind, D. E., G. E. Nedoluha, C. E. Randall, M. Fromm, and J. M. Russell III (2000), An assessment of Southern Hemisphere stratospheric NOx enhancements due to transport from the upper atmosphere, *Geophys. Res. Lett.*, *27*, 329–332, doi:10.1029/1999GL010940.

Sloan, T., and A. W. Wolfendale (2008), Testing the proposed causal link between cosmic rays and cloud cover, *Environ. Res. Lett.*, *3*, 024001, doi:10.1088/1748-9326/3/2/024001.

Slonosky, V. C., P. D. Jones, and T. D. Davies (2001), Instrumental pressure observation from the 17th and 18th centuries: London and Paris, *Int. J. Climatol.*, *21*, 285–298, doi:10.1002/joc.611.

Smith, A. K., and K. Matthes (2008), Decadal-scale periodicities in the stratosphere associated with the solar cycle and the QBO, *J. Geophys. Res.*, *113*, D05311, doi:10.1029/2007JD009051.

Solanki, S. K. (2002), Solar variability and climate change: Is there a link?, *Astron. Geophys.*, *43*, 5.9–5.13.

Solanki, S. K., and M. Fligge (1999), A reconstruction of total solar irradiance since 1700, *Geophys. Res. Lett.*, *26*, 2465–2468, doi:10.1029/1999GL900370.

Solanki, S. K., and M. Fligge (2000), Reconstruction of past solar irradiance, *Space Sci. Rev.*, *94*, 127–138, doi:10.1023/A:1026754803423.

Solanki, S. K., M. Schüssler, and M. Fligge (2002), Secular evolution of the Suns magnetic flux, *Astron. Astrophys.*, *383*, 706–712, doi:10.1051/0004-6361:20011790.

Solanki, S. K., I. G. Usoskin, B. Kromer, M. Schüssler, and J. Beer (2004), Unusual activity of the Sun during recent decades compared to the previous 11,000 years, *Nature*, *431*, 1084–1087, doi:10.1038/nature02995.

Solanki, S. K., N. A. Krivova, and T. Wenzler (2005), Irradiance models, *Adv. Space Res.*, *35*, 376–383, doi:10.1016/j.asr.2004.12.077.

Solomon, S., P. J. Crutzen, and R. G. Roble (1982), Photochemical coupling between the thermosphere and the lower atmosphere: 1. Odd nitrogen from 50 to 120 km, *J. Geophys. Res.*, *87*, 7206–7220, doi:10.1029/JC087iC09p07206.

Song, Y., and W. A. Robinson (2004), Dynamical mechanisms for stratospheric influences on the troposphere, *J. Atmos. Sci.*, *61*, 1711–1725, doi:10.1175/1520-0469(2004)061<1711:DMFSIO>2.0.CO;2.

Soukharev, B. E., and L. L. Hood (2006), Solar cycle variation of stratospheric ozone: Multiple regression analysis of long-term satellite data sets and comparisons with models, *J. Geophys. Res.*, *111*, D20314, doi:10.1029/2006JD007107.

Speranza, A., B. van Geel, and J. van der Plicht (2002), Evidence for solar forcing of climate change at ca. 850 cal BC from a Czech peat sequence, *Global Planet. Change*, *35*, 51–65, doi:10.1016/S0921-8181(02)00091-7.

Spruit, H. (2000), Theory of solar irradiance variations, *Space Sci. Rev.*, *94*, 113–126, doi:10.1023/A:1026742519353.

Steinhilber, F., J. A. Abreu, and J. Beer (2008), Solar modulation during the Holocene, *Astrophys. Space Sci. Trans.*, *4*, 1–6, doi:10.5194/astra-4-1-2008.

Steinhilber, F., J. Beer, and C. Fröhlich (2009), Total solar irradiance during the Holocene, *Geophys. Res. Lett.*, *36*, L19704, doi:10.1029/2009GL040142.

Steinhilber, F., J. A. Abreu, J. Beer, and K. G. McCracken (2010), Interplanetary magnetic field during the past 9300 years inferred from cosmogenic radionuclides, *J. Geophys. Res.*, *115*, A01104, doi:10.1029/2009JA014193.

Stendel, M., I. A. Mogensen, and J. H. Christensen (2006), Influence of various forcings on global climate in historical times using a coupled atmosphere-ocean general circulation model, *Clim. Dyn.*, *26*(1), 1–15, doi:10.1007/s00382-005-0041-4.

Stott, P. A., S. F. B. Tett, G. S. Jones, M. R. Allen, J. F. B. Mitchell, and G. J. Jenkins (2000), External control of 20th century temperature variations by natural and anthropogenic forcings, *Science*, *290*, 2133–2137, doi:10.1126/science.290.5499.2133.

Stott, P. A., G. S. Jones, and J. F. B. Mitchell (2003), Do models underestimate the solar contribution to recent climate change?, *J. Clim.*, *16*(24), 4079–4093, doi:10.1175/1520-0442(2003)016<4079:DMUTSC>2.0.CO;2.

Stott, P. A., J. F. B. Mitchell, M. R. Allen, T. L. Delworth, J. M. Gregory, G. A. Meehl, and B. D. Santer (2006), Observational constraints on past attributable warming and predictions of future global warming, *J. Clim.*, *19*, 3055–3069, doi:10.1175/JCLI3802.1.

Sun, B., and R. S. Bradley (2002), Solar influences on cosmic rays and cloud formation: A reassessment, *J. Geophys. Res.*, *107*(D14), 4211, doi:10.1029/2001JD000560.

Sun, B., and R. S. Bradley (2004), Reply to comment by N. D. Marsh and H. Svensmark on "Solar influences on cosmic rays and cloud formation: A reassessment," *J. Geophys. Res.*, *109*, D14206, doi:10.1029/2003JD004479.

Svensmark, H., and E. Friis-Christensen (1997), Variations of cosmic ray flux and global cloud coverage—A missing link in solar-climate relationships, *J. Atmos. Terr. Phys.*, *59*, 1225–1232, doi:10.1016/S1364-6826(97)00001-1.

Svensmark, H., T. Bondo, and J. Svensmark (2009), Cosmic ray decreases affect atmospheric aerosols and clouds, *Geophys. Res. Lett.*, *36*, L15101, doi:10.1029/2009GL038429.

Tett, S. F. B., et al. (2002), Estimation of natural and anthropogenic contributions to twentieth century temperature change, *J. Geophys. Res.*, *107*(D16), 4306, doi:10.1029/2000JD000028.

Thejll, P., and K. Lassen (2000), Solar forcing of the Northern Hemisphere land air temperature: New data, *J. Atmos. Sol. Terr. Phys.*, *62*, 1207–1213, doi:10.1016/S1364-6826(00)00104-8.

Thejll, P., B. Christiansen, and H. Gleisner (2003), On correlations between the North Atlantic Oscillation, geopotential heights and geomagnetic activity, *Geophys. Res. Lett.*, *30*(6), 1347, doi:10.1029/2002GL016598.

Thomas, B. C., C. H. Jackman, and A. L. Melott (2007), Modeling atmospheric effects of the September 1859 solar flare, *Geophys. Res. Lett.*, *34*, L06810, doi:10.1029/2006GL029174.

Thompson, D. W. J., M. P. Baldwin, and S. Solomon (2005), Stratosphere-troposphere coupling in the Southern Hemisphere, *J. Atmos. Sci.*, *62*, 708–715, doi:10.1175/JAS-3321.1.

Tinsley, B. A. (2000), Influence of solar wind on the global electric circuit, and inferred effects on cloud microphysics, temperature, and dynamics in the troposphere, *Space Sci. Rev.*, *94*, 231–258, doi:10.1023/A:1026775408875.

Tinsley, B. A., G. M. Brown, and P. H. Scherrer (1989), Solar variability influences on weather and climate: Possible connections through cosmic ray-fluxes and storm intensification, *J. Geophys. Res.*, *94*, 14,783–14,792, doi:10.1029/JD094iD12p14783.

Tinsley, B. A., R. P. Rohrbaugh, M. Hei, and K. V. Beard (2000), Effects of image charges on the scavenging of aerosol particles by cloud droplets and on droplet charging and possible ice nucleation processes, *J. Atmos. Sci.*, *57*, 2118–2134, doi:10.1175/1520-0469(2000)057<2118:EOICOT>2.0.CO;2.

Tinsley, B. A., R. P. Rohrbaugh, and M. Hei (2001), Electroscavenging in clouds with broad droplet size distributions and weak electrification, *Atmos. Res.*, *59–60*, 115–135, doi:10.1016/S0169-8095(01)00112-0.

Topka, K. P., T. D. Tarbell, and A. M. Title (1997), Smallest solar magnetic elements. II. Observations versus hot wall models of faculae, *Astrophys. J.*, *484*, 479–486, doi:10.1086/304295.

Tourpali, K., C. J. E. Schuurmans, R. van Dorland, B. Steil, and C. Bruehl (2003), Stratospheric and tropospheric response to enhanced solar UV radiation: A model study, *Geophys. Res. Lett.*, *30*(5), 1231, doi:10.1029/2002GL016650.

Tripathi, S. N., and R. G. Harrison (2002), Enhancement of contact nucleation by scavenging of charged aerosol particles, *Atmos. Res.*, *62*, 57–70, doi:10.1016/S0169-8095(02)00020-0.

Tripathi, S. N., S. Vishnoi, S. Kumar, and R. G. Harrison (2006), Computationally efficient expressions for the collision efficiency between electrically charged aerosol particles and cloud droplets, *Q. J. R. Meteorol. Soc.*, *132*, 1717–1731, doi:10.1256/qj.05.125.

Trouet, V., J. Esper, N. E. Graham, A. Baker, J. D. Scourse, and D. C. Frank (2009), Persistent positive North Atlantic Oscillation mode dominated the Medieval climate anomaly, *Science*, *324*, 78–80, doi:10.1126/science.1166349.

Tung, K. K., and C. D. Camp (2008), Solar cycle warming at the Earth's surface in NCEP and ERA-40 data: A linear discriminant analysis, *J. Geophys. Res.*, *113*, D05114, doi:10.1029/2007JD009164.

Udelhofen, P. M., and R. D. Cess (2001), Cloud cover variations over the United States: An influence of cosmic rays or solar variability?, *Geophys. Res. Lett.*, *28*(13), 2617–2620, doi:10.1029/2000GL012659.

Unruh, Y. C., S. K. Solanki, and M. Fligge (1999), The spectral dependence of facular contrast and solar irradiance variations, *Astron. Astrophys.*, *345*(2), 635–642.

Unruh, Y. C., N. A. Krivova, S. K. Solanki, J. W. Harder, and G. Kopp (2008), Spectral irradiance variations: Comparison between observations and the SATIRE model on solar rotation

time scales, *Astron. Astrophys.*, *486*, 311–323, doi:10.1051/0004-6361:20078421.

Usoskin, I. G., S. K. Solanki, M. Schüssler, K. Mursula, and K. Alanko (2003), Millennium-scale sunspot number reconstruction: Evidence for an unusually active Sun since the 1940s, *Phys. Rev. Lett.*, *91*, 211101, doi:10.1103/PhysRevLett.91.211101.

Usoskin, I. G., K. Mursula, S. Solanki, M. Schüssler, and K. Alanko (2004), Reconstruction of solar activity for the last millennium using ^{10}Be data, *Astron. Astrophys.*, *413*, 745–751, doi:10.1051/0004-6361:20031533.

Usoskin, I. G., M. Schüssler, S. K. Solanki, and K. Mursula (2005), Solar activity, cosmic rays, and Earth's temperature: A millennium-scale comparison, *J. Geophys. Res.*, *110*, A10102, doi:10.1029/2004JA010946.

van der Plicht, J., B. van Geel, S. J. P. Bohncke, J. A. A. Bos, M. Blaauw, A. O. M. Speranza, R. Muscheler, and S. Björck (2004), The Preboreal climate reversal and a subsequent solar-forced climate shift, *J. Quat. Sci.*, *19*, 263–269, doi:10.1002/jqs.835.

van Geel, B., and W. G. Mook (1989), High-resolution ^{14}C dating of organic deposits using natural atmospheric ^{14}C variations, *Radiocarbon*, *31*, 151–156.

van Geel, B., J. Buurman, and H. T. Waterbolk (1996), Archaeological and palaeoecological indications for an abrupt climate change in the Netherlands and evidence for climatological teleconnections around 2650 BP, *J. Quat. Sci.*, *11*, 451–460, doi:10.1002/(SICI)1099-1417(199611/12)11:6<451::AID-JQS275>3.0.CO;2-9.

van Geel, B., J. van der Plicht, M. R. Kilian, E. R. Klaver, J. H. M. Kouwenberg, H. Renssen, I. Reynaud-Farrera, and H. T. Waterbolk (1998), The sharp rise of Δ^{14}C ca. 800 cal BC: Possible causes, related climatic teleconnections and the impact on human environments, *Radiocarbon*, *40*, 535–550.

van Loon, H., and G. A. Meehl (2008), The response in the Pacific to the Sun's decadal peaks and contrasts to cold events in the Southern Oscillation, *J. Atmos. Sol. Terr. Phys.*, *70*, 1046–1055, doi:10.1016/j.jastp.2008.01.009.

van Loon, H., and D. J. Shea (2000), The global 11-yr solar signal in July–August, *Geophys. Res. Lett.*, *27*, 2965–2968, doi:10.1029/2000GL003764.

van Loon, H., G. A. Meehl, and J. M. Arblaster (2004), A decadal solar effect in the tropics in July–August, *J. Atmos. Sol. Terr. Phys.*, *66*, 1767–1778, doi:10.1016/j.jastp.2004.06.003.

van Loon, H., G. A. Meehl, and D. Shea (2007), The effect of the decadal solar oscillation in the Pacific troposphere in northern winter, *J. Geophys. Res.*, *112*, D02108, doi:10.1029/2006JD007378.

Verschuren, D., K. R. Laird, and B. F. Cumming (2000), Rainfall and drought in equatorial east Africa during the past 1100 years, *Nature*, *403*, 410–414, doi:10.1038/35000179.

Voiculescu, M., I. G. Usoskin, and K. Mursula (2006), Different response of clouds to solar input, *Geophys. Res. Lett.*, *33*, L21802, doi:10.1029/2006GL027820.

Vonmoos, M., J. Beer, and R. Muscheler (2006), Large variations in Holocene solar activity: Constraints from ^{10}Be in the Greenland Ice Core Project ice core, *J. Geophys. Res.*, *111*, A10105, doi:10.1029/2005JA011500.

Wagner, G., D. M. Livingstone, J. Masarik, R. Muscheler, and J. Beer (2001), Some results relevant to the discussion of a possible link between cosmic rays and the Earth's climate, *J. Geophys. Res.*, *106*(D4), 3381–3387, doi:10.1029/2000JD900589.

Walton, S. R., D. G. Preminger, and G. A. Chapman (2003), The contribution of faculae and network to long-term changes in the total solar irradiance, *Astrophys. J.*, *590*10881094, doi:10.1086/375022.

Wang, Y.-M., J. L. Lean, and N. R. Sheeley Jr. (2005), Modeling the Sun's magnetic field and irradiance since 1713, *Astrophys. J.*, *625*(1), 522–538, doi:10.1086/429689.

Wanner, H., C. Pfister, R. Brázdil, P. Frich, K. Frydendahl, T. Jónsson, J. Kington, H. H. Lamb, S. Rosenørn, and E. Wishman (1995), Wintertime European circulation patterns during the late Maunder Minimum cooling period (1675–1704), *Theor. Appl. Climatol.*, *51*, 167–175, doi:10.1007/BF00867443.

Wanner, H., et al. (2008), Mid- to Late Holocene climate change: An overview, *Quat. Sci. Rev.*, *27*, 1791–1828, doi:10.1016/j.quascirev.2008.06.013.

Waple, A. M., M. E. Mann, and R. S. Bradley (2002), Long-term patterns of solar irradiance forcing in model experiments and proxy-based surface temperature reconstructions, *Clim. Dyn.*, *18*, 563–578.

Weber, S. L. (2005), A timescale analysis of the Northern Hemisphere temperature response to volcanic and solar forcing, *Clim. Past*, *1*, 9–17, doi:10.5194/cp-1-9-2005.

Wenzler, T., S. K. Solanki, N. A. Krivova, and C. Fröhlich (2006), Reconstruction of solar irradiance variations in cycles 21–23 based on surface magnetic fields, *Astron. Astrophys*, *460*, 583–595.

Wetherald, R. T., and S. Manabe (1975), The effects of changing the solar constant on the climate of a general circulation model, *J. Atmos. Sci.*, *32*, 2044–2059, doi:10.1175/1520-0469(1975)032<2044:TEOCTS>2.0.CO;2.

White, W. B. (2006), Response of tropical global ocean temperature to the Sun's quasi-decadal UV radiative forcing of the stratosphere, *J. Geophys. Res.*, *111*, C09020, doi:10.1029/2004JC002552.

White, W. B., and Z. Liu (2008a), Resonant response of the quasi-decadal oscillation to the 11-yr period signal in the Sun's irradiance, *J. Geophys. Res.*, *113*, C01002, doi:10.1029/2006JC004057.

White, W. B., and Z. Liu (2008b), Non-linear alignment of El Nino to the 11-yr solar cycle, *Geophys. Res. Lett.*, *35*, L19607, doi:10.1029/2008GL034831.

White, W. B., and Y. M. Tourre (2003), Global SST/SLP waves during the 20th century, *Geophys. Res. Lett.*, *30*(12), 1651, doi:10.1029/2003GL017055.

White, W. B., J. Lean, D. R. Cayan, and M. D. Dettinger (1997), Response of global upper ocean temperature to changing solar irradiance, *J. Geophys. Res.*, *102*, 3255–3266, doi:10.1029/96JC03549.

White, W. B., D. R. Cayan, and J. Lean (1998), Global upper ocean heat storage response to radiative forcing from changing solar irradiance and increasing greenhouse gas/aerosol concentrations, *J. Geophys. Res.*, *103*, 21,355–21,366.

White, W. B., M. D. Dettinger, and D. R. Cayan (2003), Sources of global warming in the upper-ocean on decadal period scales, *J. Geophys. Res.*, *108*(C8), 3248, doi:10.1029/2002JC001396.

Wiles, G. C., R. D. D'Arrigo, R. Villalba, P. E. Calkin, and D. J. Barclay (2004), Century-scale solar variability and Alaskan temperature change over the past millennium, *Geophys. Res. Lett.*, *31*, L15203, doi:10.1029/2004GL020050.

Willson, R. C., and A. V. Mordvinov (2003), Secular total solar irradiance trend during solar cycles 21–23, *Geophys. Res. Lett.*, *30*(5), 1199, doi:10.1029/2002GL016038.

Wilson, C. T. R. (1906), On the measurement of the Earth-air current and on the origin of atmospheric electricity, *Proc. Cambridge Philos. Soc.*, *13*(6), 363–382.

World Meteorological Organization (2007), Scientific assessment of ozone depletion: 2006, *Global Ozone Res. Monit. Proj. Rep., 50*, 527 pp., Geneva, Switzerland.

Xoplaki, E., P. Maheras, and J. Luterbacher (2001), Variability of climate in meridional Balkans during the periods 1675–1715 and 1780–1830 and its impact on human life, *Clim. Change*, *48*, 581–615, doi:10.1023/A:1005616424463.

Xoplaki, E., J. Luterbacher, H. Paeth, D. Dietrich, N. Steiner, M. Grosjean, and H. Wanner (2005), European spring and autumn temperature variability and change of extremes over

the last half millennium, *Geophys. Res. Lett.*, *32*, L15713, doi:10.1029/2005GL023424.

Yu, F. (2002), Altitude variations of cosmic ray induced production of aerosols: Implications for global cloudiness and climate, *J. Geophys. Res.*, *107*(A7), 1118, doi:10.1029/2001JA000248.

Yu, F., and E. Ito (1999), Possible solar forcing of century-scale drought frequency in the northern Great Plains, *Geology*, *27*, 263–266, doi:10.1130/0091-7613(1999)027<0263:PSFOCS>2.3.CO;2.

Zebiak, S. E., and M. A. Cane (1987), A model El Niño–Southern Oscillation, *Mon. Weather Rev.*, *115*, 2262–2278.

Zerefos, C. W., K. Tourpali, B. R. Bojkov, D. S. Balis, B. Rognerund, and I. S. A. Isaksen (1997), Solar activity-total ozone relationships: Observations and model studies with heterogeneous chemistry, *J. Geophys. Res.*, *102*, 1561–1569, doi:10.1029/96JD02395.

Zhang, P., et al. (2008), A test of climate, Sun and culture relationships from an 1810-year Chinese cave record, *Science*, *322*, 940–942, doi:10.1126/science.1163965.

Zhang, Q., W. H. Soon, S. L. Baliunas, G. W. Lockwood, B. A. Skiff, and R. R. Raddick (1994), A method of determining possible brightness variations of the Sun in past centuries from observations of solar-type stars, *Astrophys. J.*, *427*, L111–L114, doi:10.1086/187377.

Zhou, L., and B. A. Tinsley (2007), Production of space charge at the boundaries of layer clouds, *J. Geophys. Res.*, *112*, D11203, doi:10.1029/2006JD007998.

Zorita, E., H. von Storch, F. Gonzalez-Rouco, U. Cubasch, J. Luterbacher, S. Legutke, I. Fischer-Bruns, and U. Schlese (2004), Climate evolution in the last five centuries simulated by an atmosphere-ocean model: Global temperatures, the North Atlantic Oscillation and the late Maunder Minimum, *Meteorol. Z.*, *13*, 271–289.

J. Beer, Swiss Federal Institute for Environmental Science and Technology, CH-8600 Dubendorf, Switzerland.

U. Cubasch, Institut für Meteorologie, Freie Universität Berlin, D-14195 Berlin, Germany.

D. Fleitmann, Oeschger Centre for Climate Change Research, University of Bern, CH-3012 Bern, Switzerland.

M. Geller, Institute for Terrestrial and Planetary Atmosphere, State University of New York at Stony Brook, Stony Brook, NY 11794-5000, USA.

L. J. Gray, National Centre for Atmospheric Sciences, Department of Atmospheric, Oceanic and Planetary Physics, University of Oxford, Parks Road, Oxford OX1 3PU, UK. (gray@atm.ox.ac.uk)

J. D. Haigh, Physics Department, Imperial College London, London SW7 2AZ, UK.

G. Harrison, Department of Meteorology, University of Reading, Reading RG6 6BB, UK.

L. Hood, Lunar and Planetary Laboratory, University of Arizona, Tucson, AZ 85721, USA.

M. Lockwood, Meteorology Department, University of Reading, Reading RG6 6AH, UK.

J. Luterbacher, Department of Geography, Justus Liebig University Giessen, D-35390 Giessen, Germany.

K. Matthes, Section 1.3: Earth System Modeling, Deutsches GeoForschungsZentrum Potsdam, D-14473 Potsdam, Germany.

G. A. Meehl, National Center for Atmospheric Research, Boulder, CO 80307, USA.

D. Shindell, NASA Goddard Institute for Space Studies, New York, NY 10025, USA.

B. van Geel, Institute for Biodiversity and Ecosystem Dynamics, Research Group Paleoecology and Landscape Ecology, Faculty of Science, Universiteit van Amsterdam, Kruislaan 318, NL-1098 SM Amsterdam, Netherlands.

W. White, Scripps Institution of Oceanography, University of California, San Diego, La Jolla, CA 92093, USA.